Scientific Report S-23
April 15, 1972
CR-123710

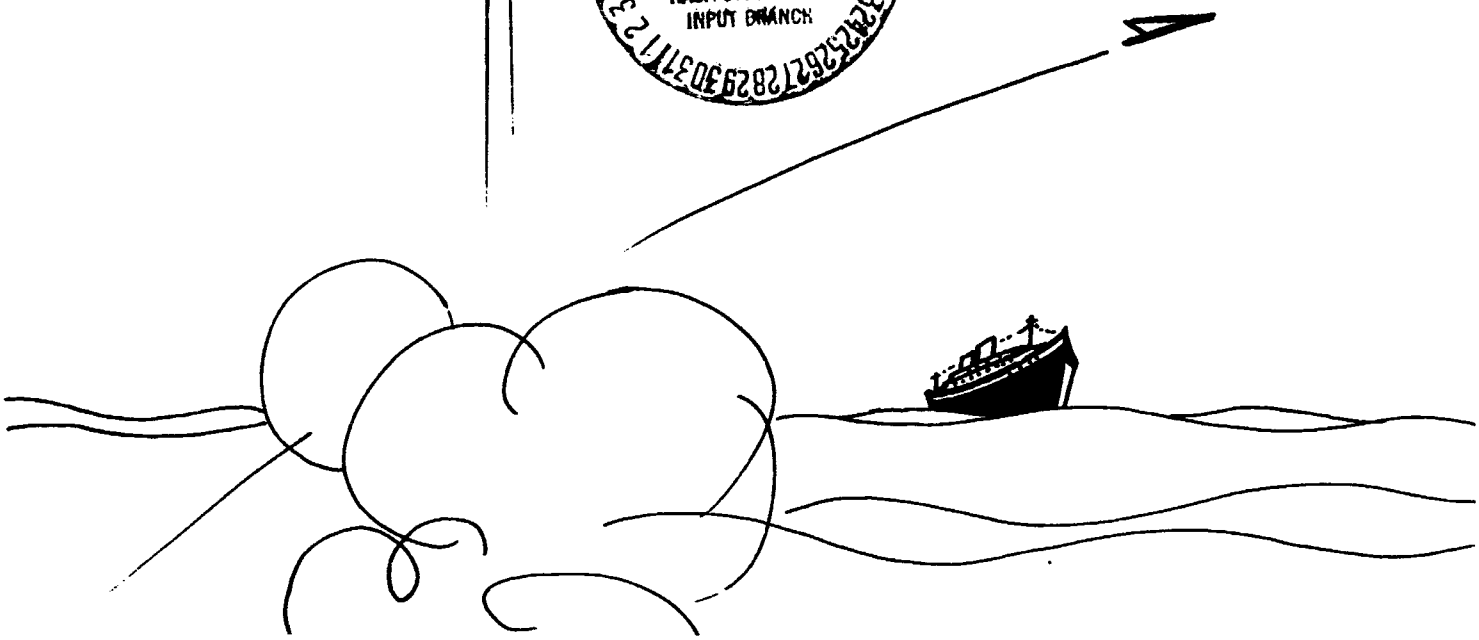

A STUDY OF STRAPDOWN PLATFORM TECHNOLOGY

Prepared for George C. Marshall Space Flight Center, National Aeronautics and Space Administration under Contract NAS8-27296/DCN 1-1-40-10230

THE UNIVERSITY OF TENNESSEE
DEPARTMENT OF ELECTRICAL ENGINEERING

Scientific Report S-23
April 15, 1972

A STUDY OF STRAPDOWN PLATFORM TECHNOLOGY

(Technical Report)

Prepared for
George C. Marshall Space Flight Center
National Aeronautics and Space Administration
Under Contract NAS8-27296/DCN 1-1-40-10230

Principal Investigator: James C. Hung

Department of Electrical Engineering
The University of Tennessee
Knoxville, Tennessee 37916

ACKNOWLEDGMENT

The research results presented in this report are produced by the combined effort of the faculty members at The University of Tennessee and the staff members at the NASA Marshall Space Flight Center. The progress of this study was made possible by the generous assistance of Dr. G.B. Doane, III, Mr. B.J. Doran and Mr. E.H. Berry, all of the Astrionics Laboratory, MSFC.

The contributors to the project activity from UT are:

Dr. J.C. Hung, Professor and Principal Investigator

Dr. T.V. Blalock, Associate Professor

Dr. E.J. Kennedy, Associate Professor

Mr. H.I. Brock, Graduate Research Assistant

Mr. LeSi Han, Graduate Research Assistant

Mr. W.L. Rowe, Graduate Research Assistant

Mr. Y. Yeh, Graduate Research Assistant

The skillful preparation of the manuscript by Mrs. Susan Storey is appreciated.

TABLE OF CONTENTS

CHAPTER PAGE

CHAPTER PAGE

CHAPTER PAGE

CHAPTER PAGE

LIST OF FIGURES

FIGURE PAGE

FIGURE PAGE

LIST OF TABLES

TABLE PAGE

CHAPTER 1

INTRODUCTION

J.C. Hung

This is a technical report on a study of strapdown platform technology. The study was initiated by the National Aeronautics and Space Administration, George C. Marshall Space Flight Center, and was performed by the University of Tennessee under Contract NAS8-27296 over a period of one year, beginning April 16, 1971.

Strapdown Principle

Strapdown navigation platforms have emerged as a new generation of navigation equipment. The basic principle involves 1) the mounting of several gyros and accelerometers directly on the vehicle body and 2) performing the equivalent function of a stabilized platform by maintaining the coordinate reference in a computer.[1] Three-axis body angular rates can be sensed by a set of gyros and/or accelerometers. This information can then be integrated over a short period of time to provide angular increments in the body's coordinate system. If the increments are sufficiently small and if the associated digital computer can perform sufficiently rapid computations, then an accurate angular reference can be maintained.[2]

There are several important advantages in using a strapdown system, as compared to a stabilized system. First, the nonexistence of a gimbaled platform eliminates all errors associated with the platform stabilization. Secondly, being free from gimbal lock allows an all attitude operation. Thirdly, because of the absence of mechanical platform gimbals, the system

can be smaller in size, lighter, more rugged, and easier to maintain. The last advantage, but probably the most important one, is the ease of the strapdown system to provide redundancy, which allows for an increase in system reliability. These advantages are achieved at the expense of a more complex electronic unit and a more stringent computer requirement. However, the progress of integrated circuit technology has made this trade-off worthwhile.

In general, the development of strapdown technology can be divided into two levels, namely, the platform system level and the sensor subsystem level. At the platform system level, the main consideration is how to use a set of sensors in a manner which will yield the maximum hardware reliability and give the best information accuracy. At the sensor subsystem level, the ultimate goal is to achieve the most accurate and reliable sensor, which depends on the sensor's principle of operation, its mechanical construction, and the associated electronic circuitry.

Rebalance Loop

The crux of a strapdown sensor system is the use of rebalance torques to continuously restore the position of sensor output axes. The rebalance feature results in a much simpler computation requirement, reduces the effect of nonlinearity, and avoids the occurrence of gimbal lock. Fig. 1-1 is a schematic of a rebalance gyro loop. An input body rate causes a precession about the gyro output axis. Motion of the output axis is sensed by a pickoff which passes this information to an electronic unit. A train of current pulses is generated by the electronic unit and the shape of these pulses is determined by the input signal. The sign of each pulse is determined by the sign of the angle of gyro output axis while the amplitude and the width of each pulse is accurately maintained. Thus, each pulse represents an incremental change of the output angle. These pulses are used for two different but related purposes: 1) as the current input to the gyro torquer to rebalance the output axis, and 2) as the discrete-data input to the computer for maintaining an attitude reference in the computer memory.

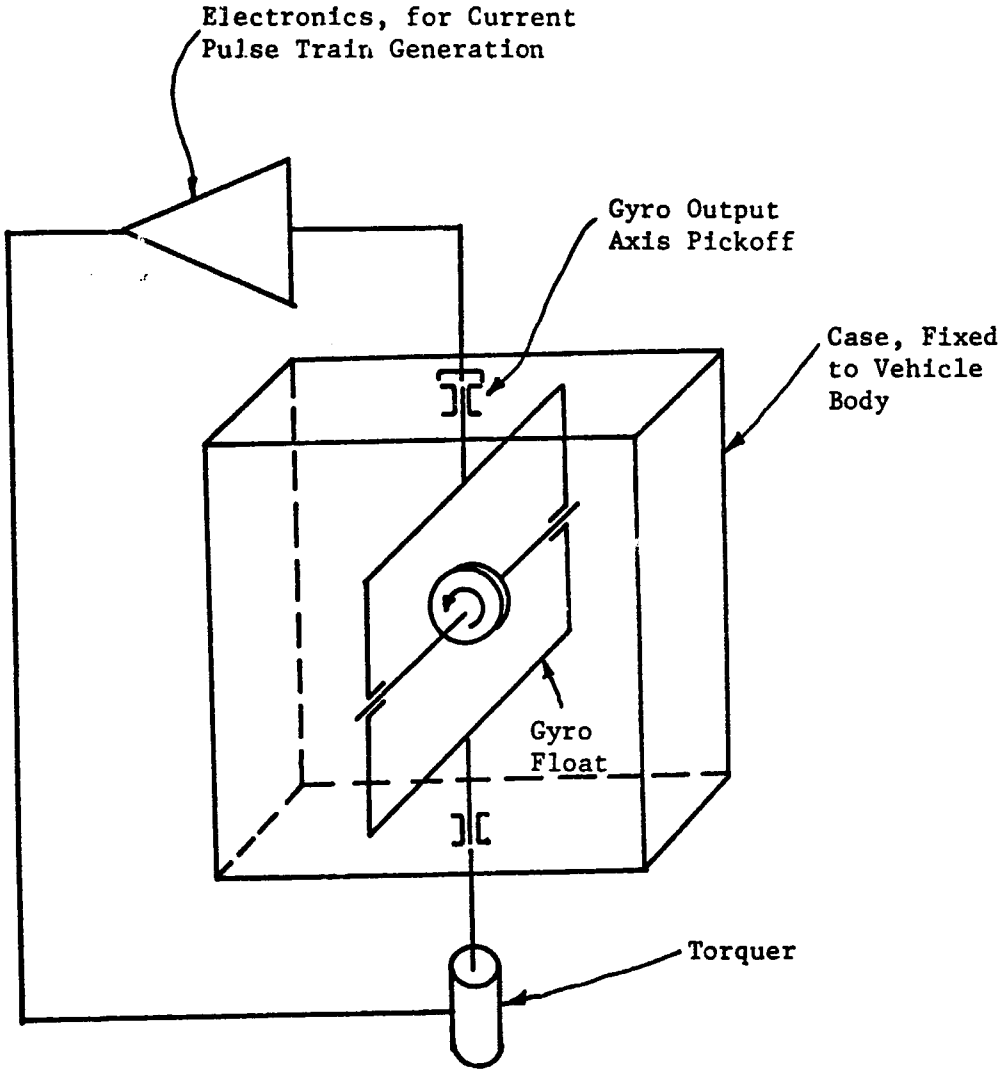

Figure 1-1. SDF Gyro Rebalance Loop.

There are four major requirements which dictate the design of a rebalance loop. The first is the stiffness and the stability of the rebalance loop, which governs the dynamic error introduced by the sensor. The loop must provide a sufficiently large maximum torque capable of rebalancing the largest probable sustained angular rate or linear acceleration input. Thus, it calls for a well compensated high gain feedback loop. The second requirement is placed on the characteristics of the generated current pulses. To achieve a good output resolution, a small pulse width is necessary. However, the strength of each pulse must be sufficiently large to produce an effective rebalance torque. Third, the pulse frequency must be capable with the frequency response characteristics of the torquer to obtain good linearity over its entire dynamic range. The fourth requirement is that the shape of each current pulse must be sufficiently insensitive to the unavoidable variations of electronic components to avoid the "scale factor error". This assumes that the signal which the computer receives from the sensor will match the rebalanced mechanical angular motion of the sensor output axis. By an intelligent choice of rebalance technique, a careful design of electronic circuitry, and a properly compensated rebalance loop, this requirement can be achieved.

High Reliability via Redundancy

One of the significant advantages of a strapdown system is the ease with which sensor redundancy may be implemented. The system must be capable of sensor performance management which includes the functions of failure detection, faulty sensor identification, system reconfiguration and, possibly, sensor recalibration. A number of sensor redundancy configurations have been developed using simple-degree-of-freedom sensors.[3-6] Continued research in this area is still needed to improve the system reliability and accuracy. In principle, two-degree-of-freedom gyros can also be used in a strapdown system where each gyro will provide attitude information along two coordinate axes. It is important to know to implement this class of strapdown systems and how they will compare with other classes of systems in performance, reliability, and complexity.

Attitude Algorithms

Two main difficulties of a strapdown navigation system, not shared by a stabilized navigation system, are the scale factor errors and the coordinate transformation errors. The former was mentioned in the previous section. Three factors which cause coordinate transformation errors are: 1) insufficient speed of computation, 2) truncation errors, and 3) round-off errors. The most obvious approach would be to use a fast and large computer; but these errors can also be reduced by the use of a more efficient computation algorithm. Several transformation algorithms are known;[7-11] however, at the present there are no guidelines which can be used for the selection of the best algorithm.

Rebalance Electronics

To have an accurate and reliable overall system, it is necessary that the rebalancing torquer be driven by very precise current pulses of well defined duration, amplitude, and shape. Therefore, the electronic pulse generator must provide such an output over the range of environment expected. Because of the stringent performance demanded of the electronic pulse generator, well designed electronic circuitry, which makes use of the best electronic components and novel circuit concepts, is needed.

Report Organization

Chapter 2 of this report presents the analysis of the pulse rebalance loop. Chapter 3 is devoted to the development of a new concept of high reliability strapdown systems using two-degree-of-freedom gyros for attitude sensing. Chapter 4 reviews the foundation of various transformation algorithms and presents their realizations by digital differential analyzers. Chapter 5 contains results of rebalance electronics analysis. Chapter 6, the last chapter, proposes problems for further study. A reference section is included at the end of each chapter except Chapters 1 and 6.

Related Publications

Several other publications reporting the partial results of the study conducted under this contract are listed below.

1. W.L. Rowe, "Analysis of Effects of Electronically Induced Errors in Strapdown Sensor Rebalance Loop", A Master of Science Thesis, The University of Tennessee, December, 1971.
2. W.L. Rowe and J.C. Hung, "Error Analysis for Strapdown Sensor Rebalance Loop", Proceedings of the Fourth Southeastern Symposium on System Theory, University of Kentucky, April 3-4, 1972.
3. Y. Yeh and J.C. Hung, "DDA Realizations of Attitude Algorithms", Proceedings of the Fifth Hawaii International Conference on System Science, University of Hawaii, January 11-13, 1972.
4. Lesi Han, "Redundancy Configurations and Reliability of Strapdown Navigation Platform Using Two-Degree-of-Freedom Gyros", A Master of Science Thesis, The University of Tennessee, March, 1972.

References

1. R.M. Bumstead and W.E. Vander Velde, "Navigation and Guidance Systems Employing a Gimballess IMU", Guidance and Control, Vol. II, Edited by Langford and Mundo, Progress in Astronautics and Aeronautics Series, Vol. 13, Academic Press, 1963, pp. 391-419.
2. T.F. Wiener, "Theoretical Analysis of Gimballess Reference Equipment Using Delta-Modulated Instrument", A Doctoral Dissertation, MIT, March, 1962.
3. U.S. Navy, "Polaris-Fleet Ballistic Missile Weapon System Fact Sheet", January, 1965.
4. B. Miller, "SST Avionics to Combine Proven Systems with Growth in Technology", Aviation Week and Space Technology, October, 1966.
5. A. Grammatikos, "Gimballess Inertial Systems for Space Navigation", A Doctoral Disseration, University of Pennsylvania, 1965.
6. J.P. Gilmore, "A Non-Orthogonal Gyro Configuration", A Master of Science Thesis, MIT, 1967.
7. J.E. Bortz, "A New Concept in Strapdown Inertial Navigation", A Doctoral Dissertation, MIT, 1969. (Also NASA TR-R-329)
8. United Aircraft Corporation, "A Study of the Critical Computation Problems Associated with Strapdown Inertial Navigation Systems", NASA CR-968, April, 1968.

9. J.W. Jordan, "Direction Cosine Computational Error", NASA TR R-304, March, 1969.

10. J.W. Jordan, "An Accurate Strapdown Direction Cosine Algorithm", NASA TN D-5384, September, 1969.

11. R.A. McKern, "A Study of Transformation Algorithm for Use in a Digital Computer", A Master of Science Thesis, MIT, 1968.

CHAPTER 2

REBALANCE LOOP ANALYSIS

J.C. Hung and W.L. Rowe

ABSTRACT

This chapter presents the analysis of the pulse rebalance loop where the pulses are of constant amplitude type. Properties of such systems will be discussed. Sensor errors caused by the distortion of the pulse shape, the dc bias, and the sampling process will be analyzed.

INTRODUCTION

The function of the sensor rebalance loop is to continuously restore the sensor axis from any variations to its aligned position. These variations are caused by changing attitude conditions of the vehicle. By properly measuring the rebalancing signal, the vehicle attitude can be determined.

While several different types of signals may be used to rebalance the sensor, the needed measurement accuracy of the attitude change requires a calibrated digital signal in such a form that each pulse has a definite weight associated with it. Such a rebalance loop is shown in Fig. 2-1. The purpose of the pulse generator is to analyze the continuous signal from the pickoff and provide a number of pulses to rebalance the sensor and at the same time provide highly calibrated information for the computer.

According to the form of rebalancing pulse stream, there are several different pulse-rebalance techniques as shown in Fig. 2-2. The binary technique has pulses of constant frequency and amplitude. Essentially, the problem

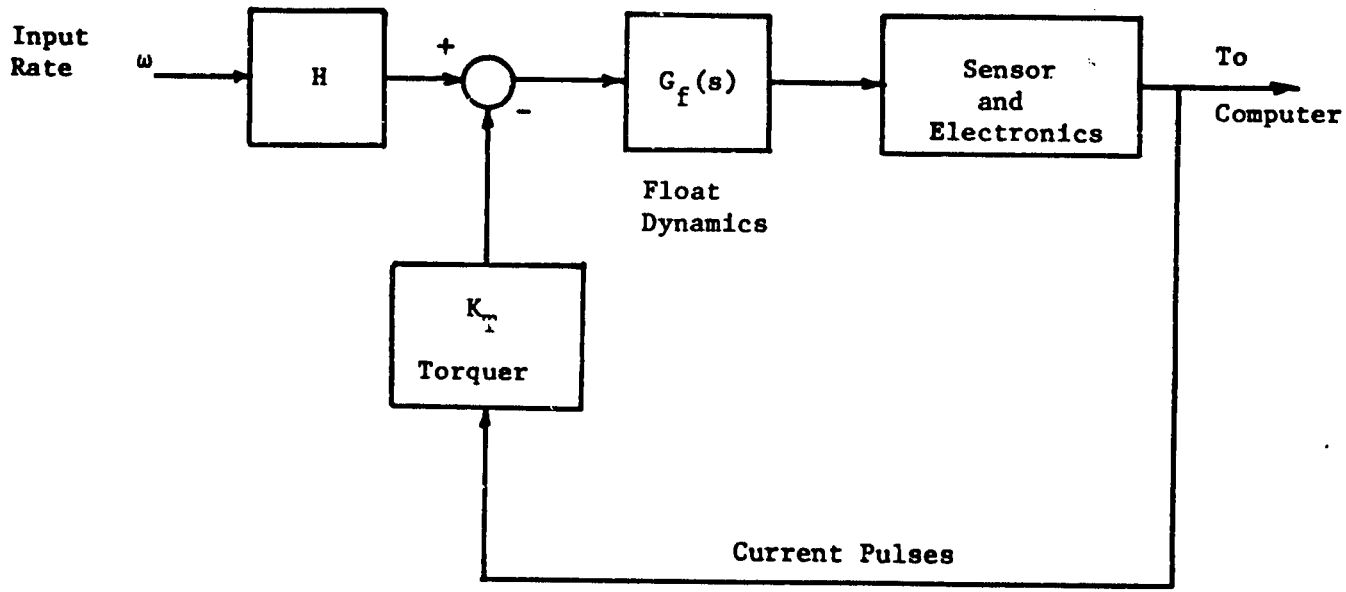

Figure 2-1. Basic Rebalancing Loop.

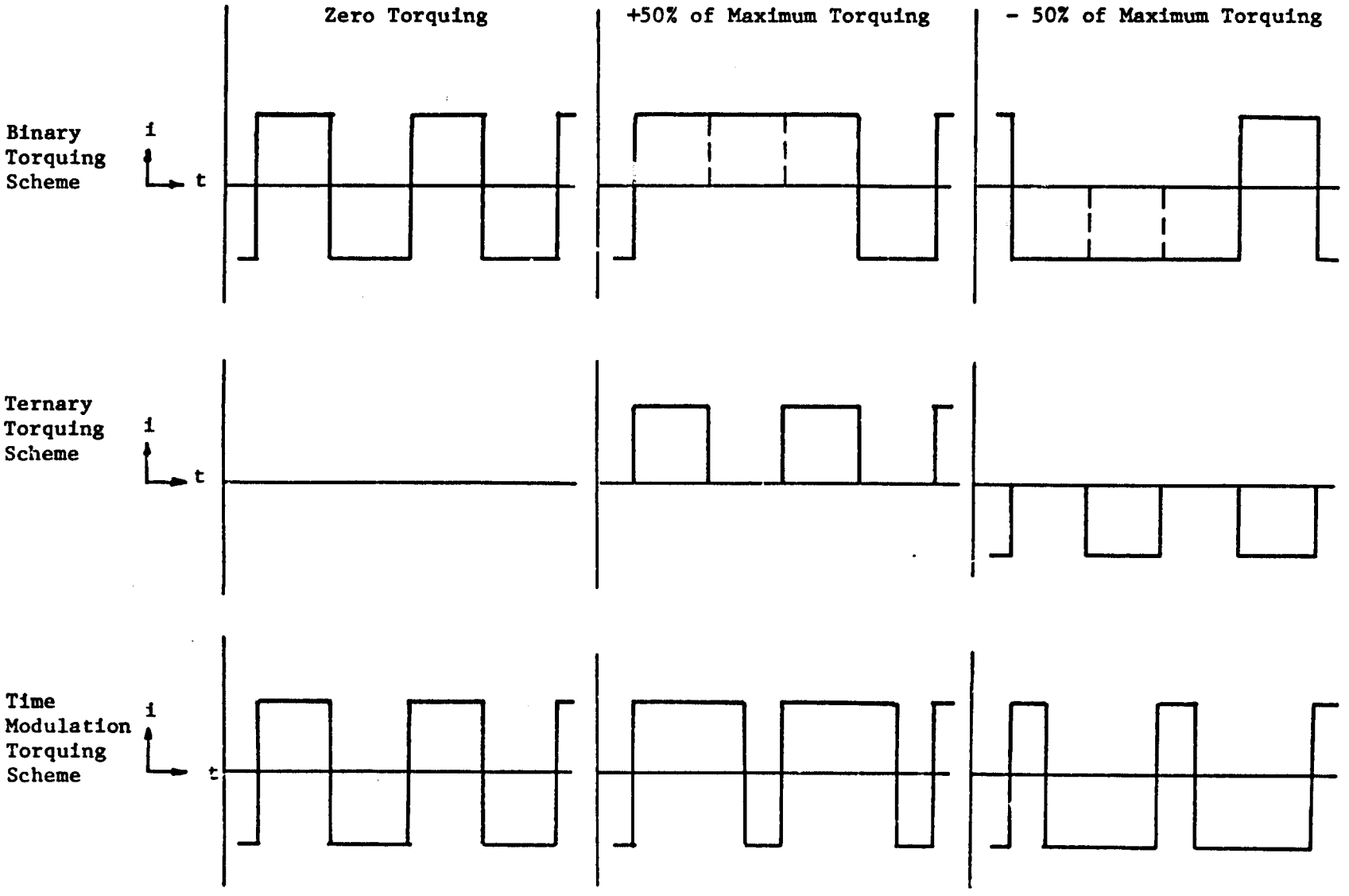

Figure 2-2. Torquing Pulses for Various Torquing Methods.

posed to the pulse generator is the choice of proper polarity of the pulse. The width-modulated binary technique follows the same concept, yet adds to the pulse generator the problem of determining the width of the pulse within certain limits. The variable pulse width also creates problems in providing the computer with quantized information since a simple counting technique would not differentiate between pulses of like polarity but different widths. The ternary technique is casual, with a pulse occurring only when the pickoff amplitude exceeds some value. Both constant and variable width pulses can be used in the ternary method. Obviously, as the function of the pulse generator becomes more sophisticated, the circuit itself becomes larger and more complex.

The purpose of this chapter is the analysis of possible errors in the strapdown sensor loop. Various errors due to the pulse generator are examined. Since the pulse generator is not ideal, one must consider errors such as the bias signal generated by the electronics and errors caused by the nonzero rise time of the torquing pulses. Knowing these errors and their effects, possible schemes of improvement are then considered. The effects of bias and of the shape of current pulses will be analyzed separately in the following sections.

EFFECT OF BIAS ERROR

Bias Error

To produce the torque needed to rebalance the sensor, an electronic network is used to generate current pulses to drive the torquer, which is essentially an electromagnetic device. Ideally, the properties of this network include (1) a linear input-output relationship and (2) a precise calibration. In order to have these properties, it is necessary that the shape of the current pulses be maintained and the net output current be zero when the input is zero.

Effect of Bias Error on Sensor Accuracy

From a knowledge of the system, which contains an integrator, it

is apparent that the error due to bias drift is cumulative and will require a number of pulses per unit time to null output variations. The accumulation of these error pulses occurs in the computer which records all pulses as attitude variations seen by the sensor. It is the purpose of this section to analyze this effect and to define the period of these error pulses, t_o, as a function of the drift magnitude.

The general system for the analysis of bias effect can be represented by Fig. 2-3, where the bias is assumed to have a constant magnitude. A. Two types of analysis will be discussed in the solution for t_o. If the electronic network or pickoff has a threshold, T_e, a pulse will occur whenever the response of the sensor due to the bias drift becomes equal to the threshold. A second method of analysis is to assume zero input condition with bias drift, such that the effective area under the output axis waveform is zero at t_o.

Method One. Given an initial response equal to the threshold, a pulse will occur which will torque the magnitude of the sensor response back within the limits of the detector, as shown in Fig. 2-4. Therefore, the time when the response due to the pulse and the bias drift again equals T_e corresponds to t_o. That is, the time t_o satisfying the following equation is the period of the error pulses due to bias error.

$$T_e + A * g_g(t) + B\,[u(t) - u(t - \tau)] * g_g(t) = T_e \quad , \qquad (2\text{-}1)$$

where "*" represents the real convolution operation and B is the pulse height. Eq. (2-1) may be reduced to

$$A * g_g(t) - B\,[u(t) - u(t - \tau)] * g_g(t) = 0 \quad , \qquad (2\text{-}2)$$

The equation describing the threshold case can now be reduced to

$$\frac{A}{as^2} - \frac{b\,(1 - \varepsilon^{-s\tau})}{s^2\,(s + a)} = 0 \Bigg|_{t=t_o} \quad , \qquad (2\text{-}3)$$

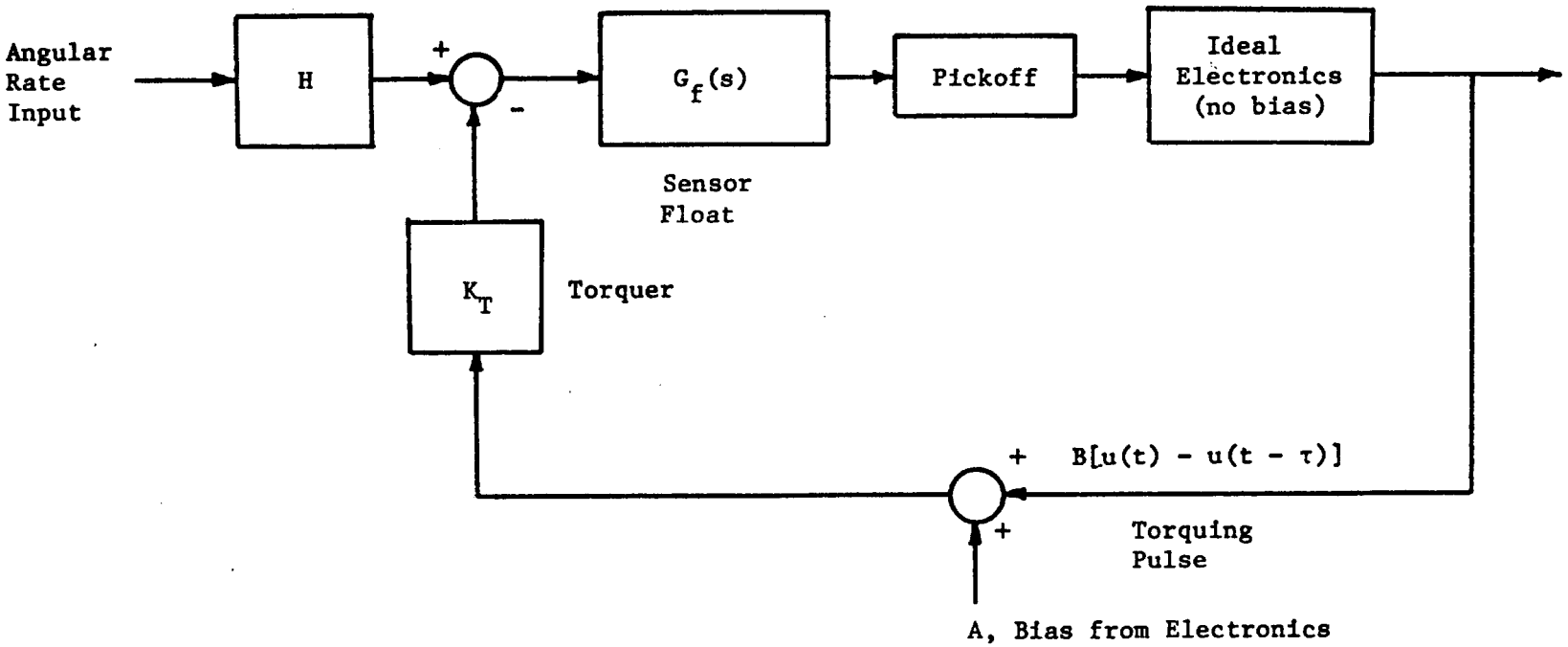

Figure 2-3. Rebalance Loop with Bias Error.

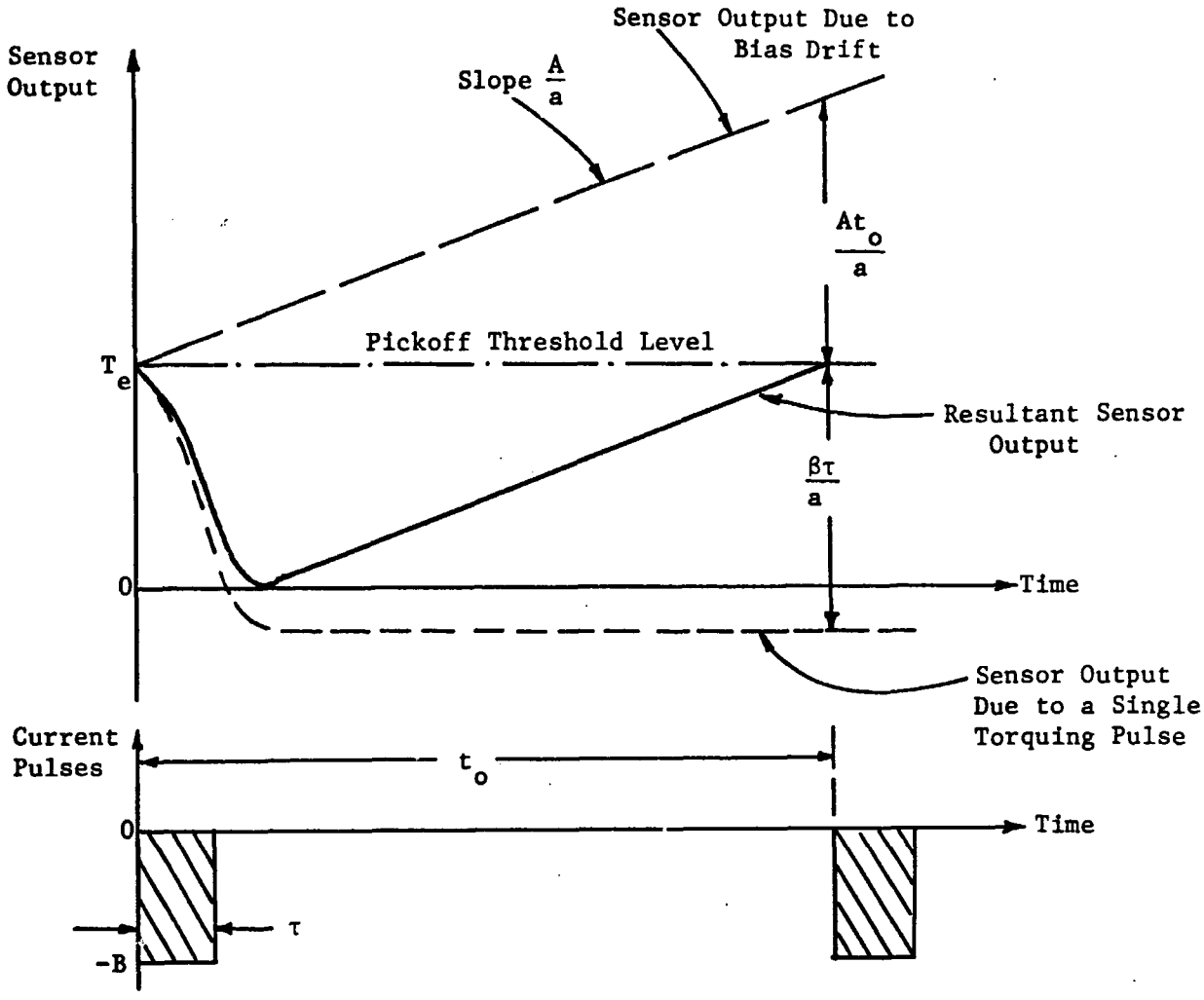

Figure 2-4. Quiescent Sensor Output.

which in the time domain yields

$$\frac{At}{a} - \left[\frac{B}{a} t - \frac{B}{a^2} + \frac{B}{a^2} \varepsilon^{-a\tau}\right] u(t) + \left[\frac{B}{a} (t - \tau)\right.$$

$$\left. - \frac{B}{a^2} + \frac{B}{a^2} \varepsilon^{-a(t-\tau)}\right] u(t - \tau) = 0 \Big|_{t=t_o} . \qquad (2\text{-}4)$$

Neglecting the transient terms and writing Eq. (2-5) at time t_o,

$$\frac{A}{a} t_o - \frac{B}{a} t_o + \frac{B}{a} (t_o - \tau) = 0 \quad . \qquad (2\text{-}5)$$

Solving Eq. (2-6) for t_o yields

$$t_o = \frac{B \tau}{A} \qquad (2\text{-}6)$$

Assuming that the torquing pulse does not drive the sensor past the opposite threshold of the detector, the period of the error pulse, t_o, is given by (2-6). Even if the system is torqued past the opposite threshold, a net summation of positive and negative pulses will yield one net error pulse every t_o seconds. An illustration of the relation of bias amplitude, A, the period of the error pulses, t_o, and the frequency of the error pulses, N_o, is shown in Table 2-1 and Fig. 2-5 for a pulse width and system time constant of one millisecond.

Method Two. The second method of analysis involves observing the result of the bias drift and the pulse inputs to the system. If the pulse is applied at a time such that the sum of the positive and negative areas is zero, then the time when the cancellation occurs corresponds to t_o. Since the output at t_o is zero, the net effects of the bias drift and pulse inputs at this time are also zero. Fig. 2-6 illustrates this idea.

TABLE 2-1

EFFECT OF BIAS ERROR ON PULSE OUTPUT OF THE SYSTEM

Drift Magnitude Pulse Height, $A/\lvert B\rvert$, units	Period of Error Pulses, t_o, seconds	Frequency of Error Pulses, N_o, pulses/second
10^{-6}	10^{3}	10^{-3}
2×10^{-6}	500	2×10^{-3}
4×10^{-6}	250	4×10^{-3}
8×10^{-6}	125	8×10^{-3}
10^{-5}	100	10^{-2}
2×10^{-5}	50	2×10^{-2}

Note: $a = 10^{-3}$, $\tau \cdot 10^{-3}$

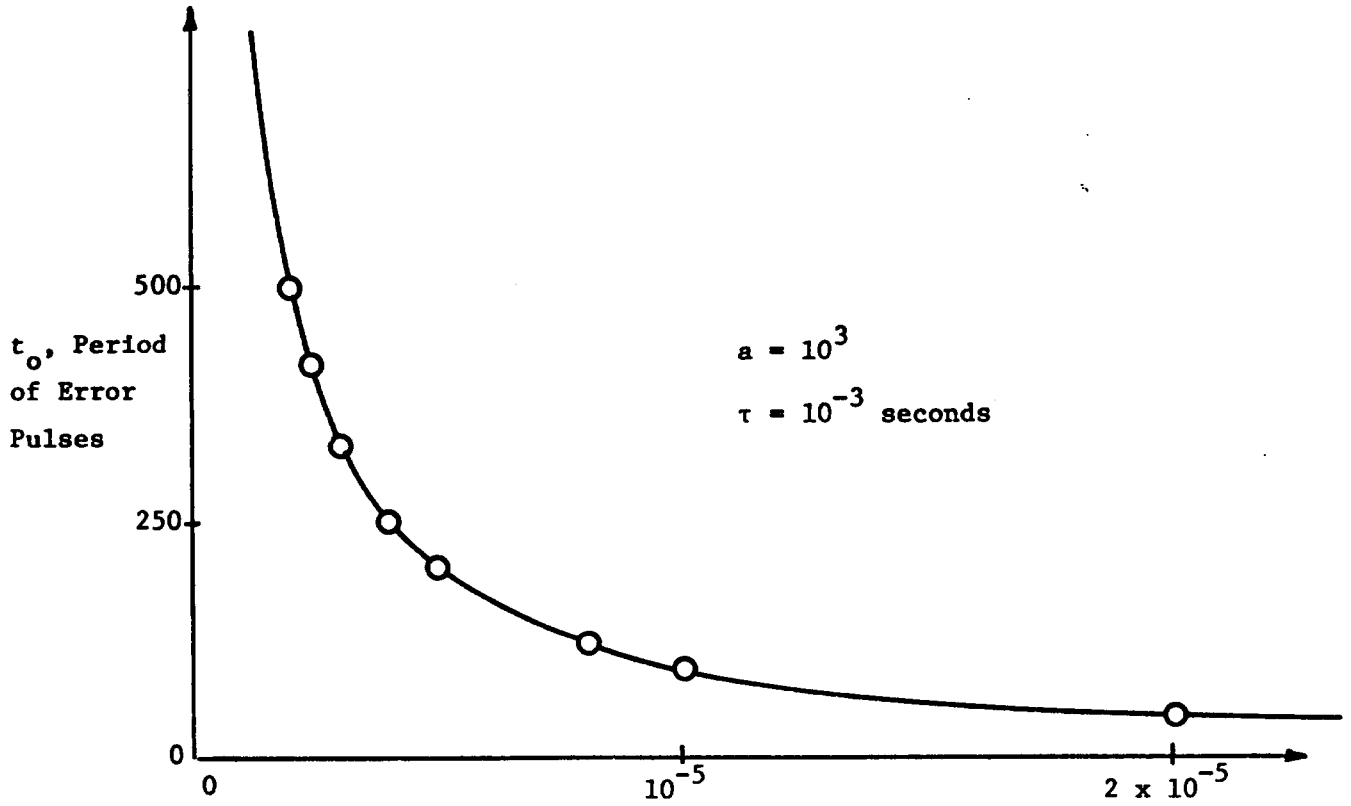

Figure 2-5. Period of Error Pulses Due to Bias Drift.

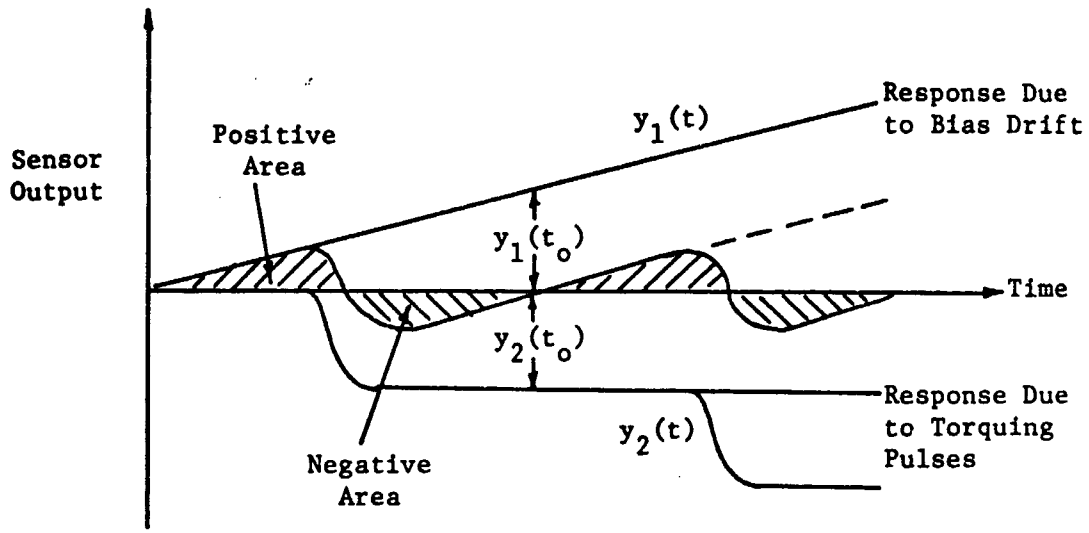

Figure 2-6. Equal Area Sensor Response.

The steady state response generated by the bias drift, $y_1(t)$ can be expressed as

$$y_1(t) = \left[\frac{A}{(s + a)} \Big|_{s=0} \right] t \quad , \tag{2-7}$$

or at time t_o

$$y_1(t) = \frac{At_o}{a} \quad . \tag{2-8}$$

Also, the steady state response due to the torquing pulse, $y_2(t)$, is

$$y_2(t) = -\left[\frac{B}{(s + a)} \Big|_{s=0} \right] t + \left[\frac{B}{(s + a)} \Big|_{s=0} \right] (t - \tau) \tag{2-9}$$

which at time t_o yields

$$y_2(t) = - \frac{B \tau}{a} \quad . \tag{2-10}$$

Since at time t_o the system output is zero, then

$$0 = y_1(t) + y_2(t) = \frac{At_o}{a} - \frac{B \tau}{a} \quad , \tag{2-11}$$

or

$$t_o = \frac{B \tau}{A} \quad , \tag{2-12}$$

which is identical to (2-6).

A More General Viewpoint. The identical result shown in (2-6) and (2-12) is not a coincidence. Examining (2-1) and (2-2), we see that the threshold T_e drops out from the analysis. That is why T_e does not appear in the expression for t_o. From the physical point of view, corresponding to each criterion for bias compensation, there is a threshold level as shown in Fig. 2-4. The period of the bias compensation pulses is simply

the time required for the ramp due to the bias drift to achieve the magnitude of the system response due to a single torquing pulse. At the instant of pulse application, we therefore have

$$\frac{A}{a} t_o = \frac{B}{a} \tau \tag{2-13}$$

$$t_o = \frac{B \tau}{A} \tag{2-14}$$

EFFECT OF WAVE SHAPE UPON SENSOR ACCURACY

In the previous chapter the bias error, which is generated by the electronics network under quiescent conditions, was examined. Under conditions of variations in attitude the additional error due to the nonideal shape of the torquing pulses will now be determined. Since the pulses must be calibrated so that the effect of each one upon the sensor will be precisely known, the sensitivity of the sensor to variations in the pulse shape is a prime consideration. Utilizing the effects of both ideal and realizable pulses upon the sensor, a comparison of the result as a function of pulse area forms the basis of this sensitivity analysis.

Property of Dynamic System with Staircase Output Response

In general, a system containing a pulse width modulator is nonlinear. However, it will be shown that, because of the way the output signal is fedback, the dynamics of the strapdown sensor rebalance loop is linear as long as the pulse width modulator is not driven beyond its saturation limit. Thus, linear analysis techniques can be applied for the study of the rebalance loop.

Consider a time invariant system G(s) with the associated impulse response g(t). The output y(t) and input u(t) are related by the real convolution integral

$$y(t) = \int_{-\infty}^{t} g(t - \tau)\, u(\tau)\, d\tau \quad . \tag{2-15}$$

Next, attaching a sampler and a zero order hold at the output of G(s) results in a new system G'(s) as shown in Fig. 2-7. This new system has a staircase shape output response. The impulse response of this system is given by

$$g'(t) = g(iT) , \qquad iT \leq t < (i + 1)T \quad . \tag{2-16}$$

Note that $g'(t) \to g(t)$ for $t \to o$. The general output y(t) responding to an input u(t) is

$$y'(t) = \int_{-\infty}^{t} g'(t - \tau)\, u(\tau)\, d\tau \quad . \tag{2-17}$$

At the discrete time $t = nT$, $n = 0, 1, 2, - - - -$ this now becomes

$$y'(t) = \int_{-\infty}^{t} g'(t - \tau)\, u(\tau)\, d\tau$$

$$= \sum_{i=-\infty}^{n} \int_{(i-1)T}^{iT} g'(nT - \tau)\, u(\tau)\, d\tau \quad .$$

But using (2-16), yields

$$y'(t) = \sum_{i=-\infty}^{n} \int_{(i-1)T}^{iT} g'(nT - \overline{i - 1}\, T)\, u(\tau)\, d\tau \quad .$$

Since g'(nT - i - 1T) does not involve the variable τ, it can be taken outside of the integral sign, i.e.,

$$y'(t) = \sum_{i=-\infty}^{n} g'(nT - \overline{i - 1T}) \int_{(i-1)T}^{iT} u(\tau)\, d\tau \tag{2-18}$$

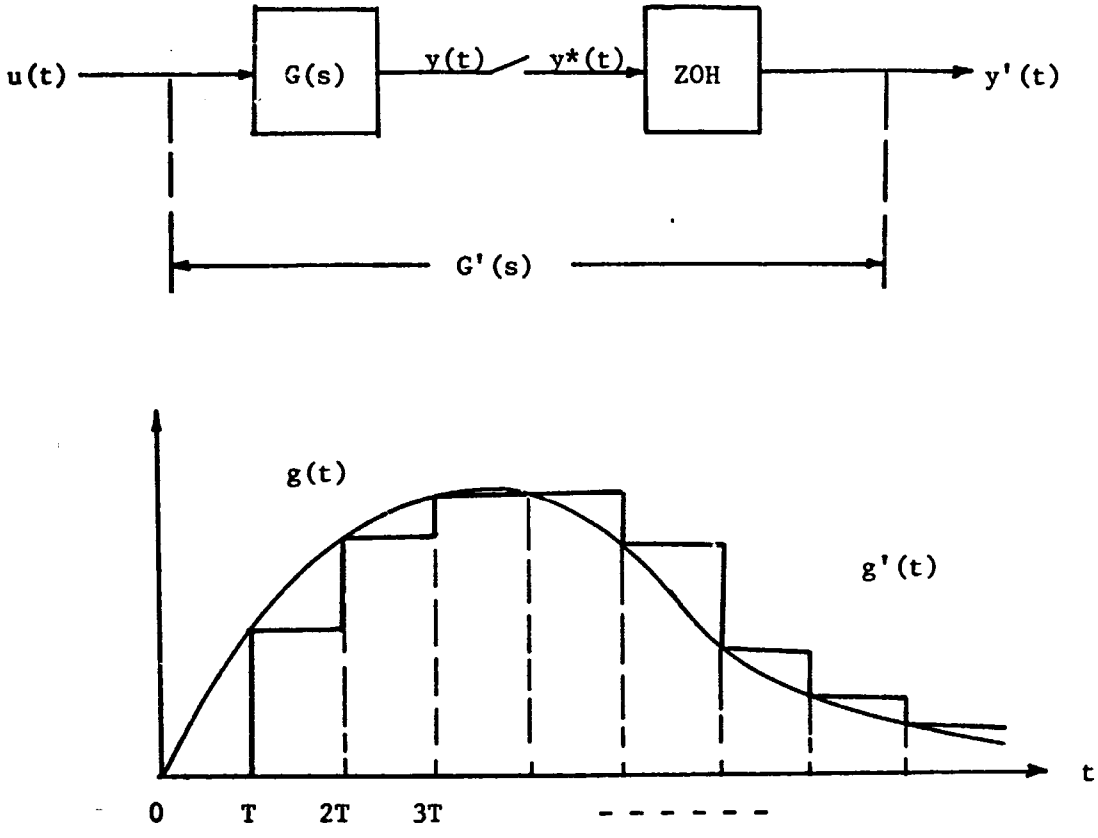

Figure 2-7. System With Staircase Output Response.

Now define

$$A(i) = \int_{(i-1)T}^{iT} u(\tau)\, d\tau \qquad (2\text{-}19)$$

which is the "input area" over the sampling period ending at t = iT. Then (2-18) becomes

$$y'(t) = \sum_{i=-\infty}^{n} g'(nT - \overline{i-1}T)\, A(i) \qquad (2\text{-}20)$$

Eq. (2-20) shows that "if the linear system has a staircase output response, then the response depends linearly on the input area over each sampling period, but not on the input wave shape during that period".

The Equivalent Rebalance Loop Configuration

Consider a typical pickoff-electronics block for width-modulated binary pulses. The input-output relationship is shown in Fig. 2-8a. This relationship can be represented by an equivalent block diagram shown in Fig. 2-8b. Therefore the overall dynamics of the rebalance loop can be represented by a configuration shown in Fig. 2-9 which is equivalent to Fig. 2-1. From the conclusion obtained in the last section and expressed in Eq. (2-20), the dynamics of this system is linear.

Effect of Time Constant on Pulse Area

Since pulse area is the determining factor in the system response, its sensitivity for the circuit parameter variations is important. Here we shall consider the variation in pulse area caused by a variation of the circuit time constant.

Let an ideal pulse be represented by

$$f(t) = u(t) - u(t - \frac{T}{2}) \qquad (2\text{-}21)$$

where u(t) is the unit step function and the pulse period is T. The area of

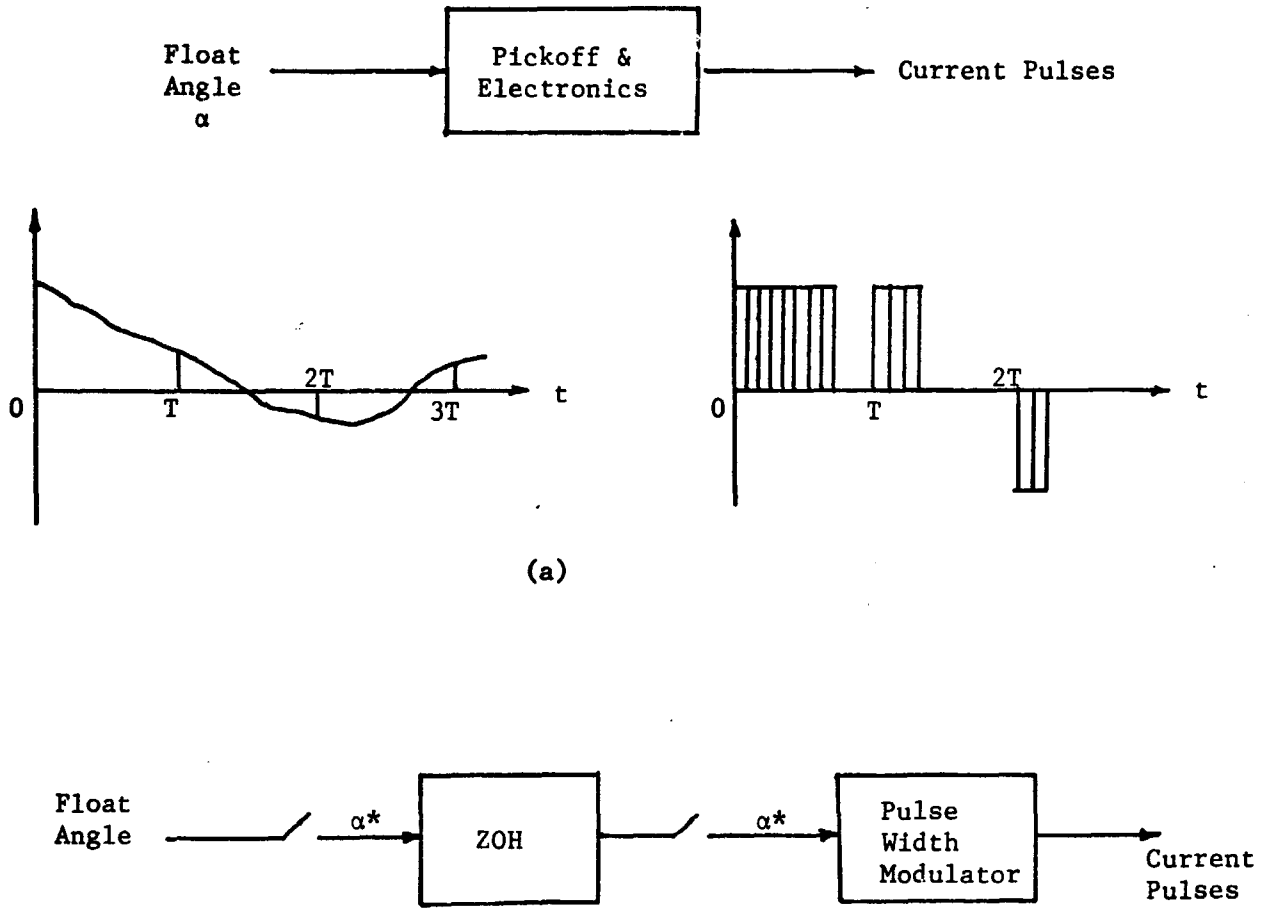

Figure 2-8. The Equivalent Pickoff-Electronics Block Diagrams

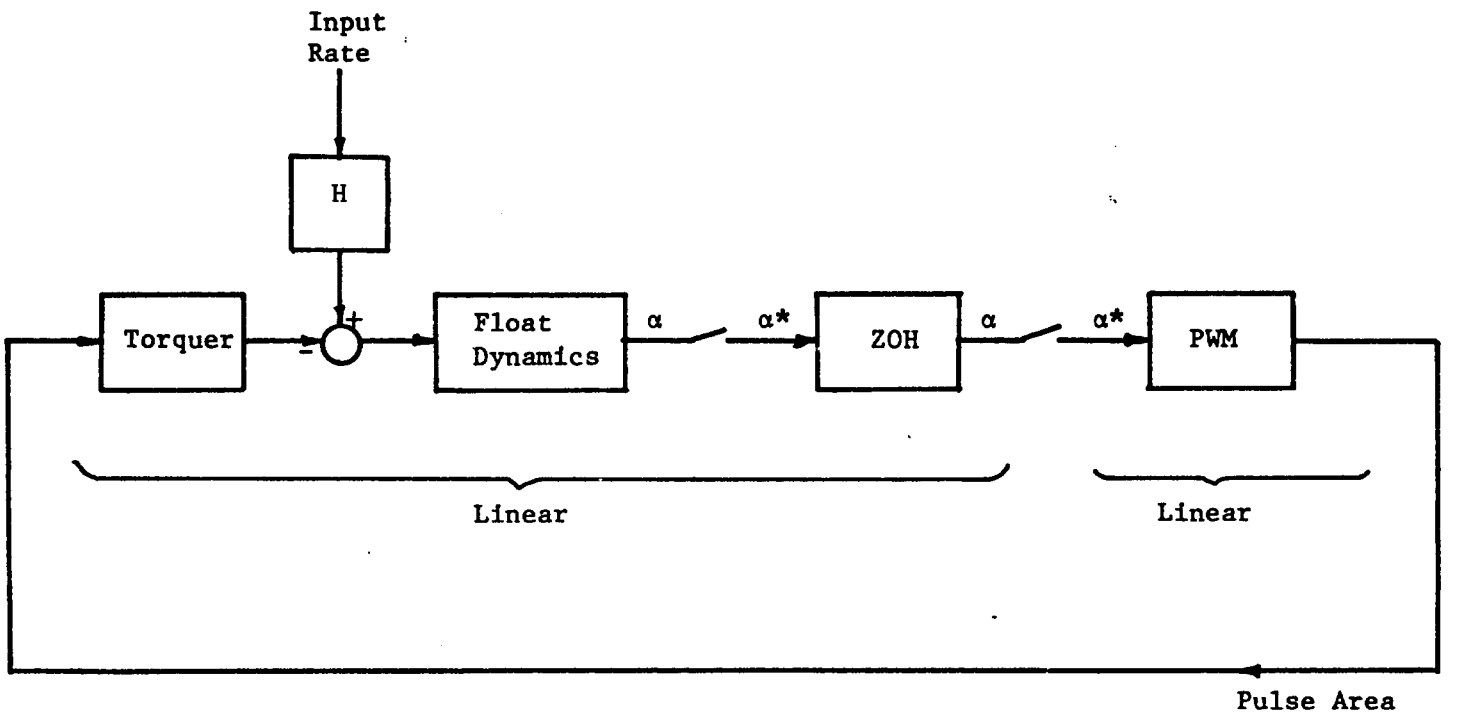

Figure 2-9. The Equivalent Rebalance Loop Configuration

this pulse is

$$A = \frac{T}{2} \quad . \tag{2-22}$$

Next, consider a pulse with finite and equal, but non-zero, rise and fall times as shown in Fig. 2-10. This pulse is represented by

$$f'(t) = \left[1 - e^{-\frac{t}{\tau}}\right]u(t) - \left[1 - e^{-\frac{1}{\tau}(t - \frac{T}{2})}\right]u(t - \frac{T}{2}) \tag{2-23}$$

where τ is the time constant, and its area over one period is given by

$$A' = \frac{T}{2} - \left[e^{-\frac{T}{2\tau}} - e^{-\frac{T}{\tau}}\right]\tau \quad . \tag{2-24}$$

Now define an "area ratio", A.R., as a measure of area deviation,

$$\text{A.R.} = \frac{\text{Actual area}}{\text{Ideal area}} \quad . \tag{2-25}$$

Then (2-22) and (2-24) give

$$\text{A.R.} = 1 - \frac{\tau\left[e^{-\frac{T}{2\tau}} - e^{-\frac{T}{\tau}}\right]}{\frac{T}{2}} \tag{2-26}$$

Table 2-2 shows the area ratios for different values of circuit time constants.

Table 2-2. Area Ratios

Time Constant τ sec.	Area Ratio
10^{-3}	0.52269
10^{-4}	0.99866
5×10^{-5}	0.99999
2×10^{-6}	.0000
10^{-6}	1.0000

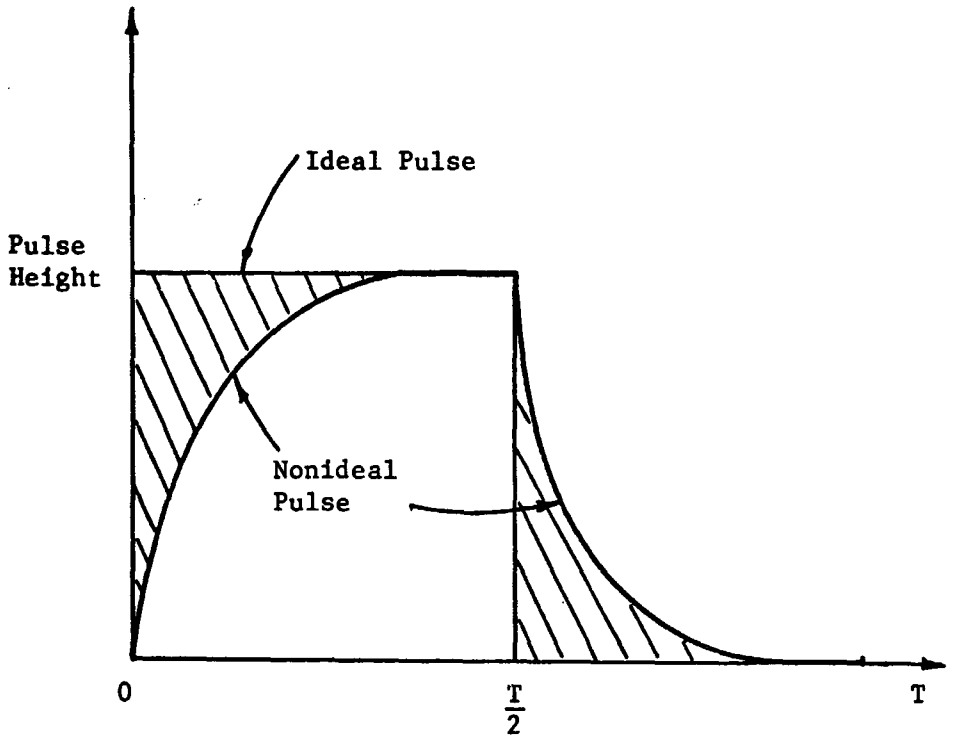

Figure 2-10. Waveforms of Ideal and Nonideal Torquing Pulses.

In order to form an effective measurement of area loss, the loss per unit time is used since this loss will be observed on each input pulse.

$$\text{Area Loss/second} = \frac{2(1-\text{Area Ratio})}{T} \quad . \tag{2-27}$$

For example, an Area Ratio of .99999 for a torquing pulse with a width of two milliseconds will yield an Area Loss of 0.01 pulse per second.

$$\text{Area Loss/second} = \frac{2(1. - .99999)}{2 \times 10^{-3}} = 10^{-2} \quad . \tag{2-28}$$

This loss will accumulate to the equivalent loss of one pulse in one hundred seconds, assuming full torquing of one polarity over that interval. This loss of one pulse for typical strapdown sensor loop resolution will result in errors on the order of 1 arc second.

Effect of Pulse Shape Upon the Output

Since the effects of rise and fall times upon the input pulse area are now known, the effect upon the output of the system is needed to complete the analysis. Using the system,

$$G(s) = \frac{1}{s(s + 10^3)} \tag{2-29}$$

and the ideal and nonideal pulse inputs which in Laplace notation are represented by

$$R(s) = \frac{(1 - e^{-Ts/2})}{s} \quad , \tag{2-30}$$

and

$$\hat{R}(s) = \frac{1}{s} - \frac{\tau}{1+\tau s} \quad (1 - e^{-Ts/2}) \quad , \tag{2-31}$$

respectively. The variations in output due to the nonzero rise and fall

times can be determined.

In the response of the system to the ideal input pulse is given by

$$C(s) = \frac{(1 - e^{-Ts/2})}{[s^2(s + a)]} \quad . \tag{2-32}$$

Taking the inverse Laplace of C(s) yields

$$\begin{aligned} c(t) = {} & (10^{-3}\, t - 10^{-6} + 10^{-6}\, \varepsilon^{-10^3 t})\, u(t) \\ & - [10^{-3}(t - T/2) - 10^{-6} \\ & \quad + 10^{-6}\, \varepsilon^{-10^3(t-T/2)}]\, u(t - T/2) \quad . \end{aligned} \tag{2-33}$$

Likewise, the system output for a nonideal pulse input is

$$\hat{C}(s) = \frac{(1 - e^{-Ts/2})}{s^2(s + 10^3)} - \frac{(1 - e^{-Ts/2})}{s(s + \beta)(s + 10^3)} \quad , \tag{2-34}$$

which in the time domain is

$$\begin{aligned} \hat{C}(t) = {} & \left[10^{-3}t - 10^{-6} + 10^{-6}\, \varepsilon^{-10^3 t} - \tau\, 10^{-3} \right. \\ & \left. + \frac{10^{-3}\tau\, \varepsilon^{-10^3 t}}{1 - \tau\, 10^{-3}} + \frac{\tau\, \varepsilon^{\frac{t}{\tau}}}{\tau 10^3 - 1} \right] u(t) \\ & + \left[10^{-6} - 10^{-3}\, (t - \tfrac{T}{2}) - 10^{-6}\, \varepsilon^{-10^3 (t - \frac{T}{2})} \right. \\ & + \tau 10^{-3}\, \frac{10^{-3}\tau\, \varepsilon^{-10^3 (t - \frac{T}{2})}}{1 - \tau 10^3} \\ & \left. - \frac{\tau\, \varepsilon^{-\frac{1}{\tau}(t - \frac{T}{2})}}{\tau 10^3 - 1} \right] u(t - \tfrac{T}{2}) \end{aligned} \tag{2-35}$$

The responses for a system when the nonideal pulse area very closely approximates the ideal pulse area are shown in Table 2-3 and Figures 2-11 and 2-12.

Also, the responses of the system are shown in Table 2-4 and Figures 2-13 and 2-14 for an input pulse of an area which is about the same as the ideal area, but the rise and fall times are far from zero.

Remarks

From the preceding analysis and examples, the system output can be seen to be insensitive to variations in pulse shape provided the pulse area is constant. Also, the effects of the individual area deviations seem small relative to the overall response, but the errors due to the area differences occur with each pulse causing a cumulative effect which can be seen to be quite large for small individual pulse area errors. For this reason, the pulse generator must be capable of creating pulses with highly constant areas under changing conditions. Since this error is cumulative, as is the bias error, it also must be corrected by updating the computer at regular intervals. This, however, presents no new problem since other errors also necessitate the correction.

CONCLUSIONS

The results of the analysis presented in this chapter are useful in three different ways: (1) they allow an estimation of system errors for specific circuit designs and configurations, (2) they provide a criterion of allowable dc bias and waveshape variation for the circuit designer, and (3) when the sensor error is found by recalibration, they provide a means of determining how the error can be compensated by the digital computer.

Additional investigation is needed in the areas of dynamic error compensation and reliability of the individual functional units in the sensor loop. The reliability is of prime importance due to the system complexity.

TABLE 2-3

SYSTEM RESPONSE UNDER IDEAL AND NEAR-IDEAL PULSING CONDITIONS

Ideal Input	Actual Input	Time	Ideal Output	Actual Output
1.0	0.0	0.0	$.3678 \times 10^{-6}$	$.3082 \times 10^{-6}$
1.0	0.99996	0.001	1.1353×10^{-6}	1.108×10^{-6}
1.0	0.99999	0.002	2.0497×10^{-6}	1.955×10^{-6}
1.0	1.0	0.003	3.018×10^{-6}	2.9203×10^{-6}
1.0	1.0	0.004	4.0067×10^{-6}	3.9074×10^{-6}
1.0	1.0	0.005	5.0024×10^{-6}	4.9026×10^{-6}
1.0	1.0	0.006	6.0000×10^{-6}	5.9000×10^{-6}
1.0	1.0	0.007	7.0000×10^{-6}	6.9000×10^{-6}
1.0	1.0	0.008	8.0000×10^{-6}	7.9000×10^{-6}
1.0	1.0	0.009	9.0000×10^{-6}	8.9000×10^{-6}
0.0	1.0	0.010	9.6321×10^{-6}	9.6264×10^{-6}
0.0	0.00004	0.011	9.86467×10^{-6}	9.8621×10^{-6}
0.0	0.00001	0.012	9.9502×10^{-6}	9.9500×10^{-6}
0.0	0.0	0.013	9.98168×10^{-6}	9.98160×10^{-6}

$\tau = 10^{-4}$ sec.

$\tau = 2 \times 10^{-2}$ sec.

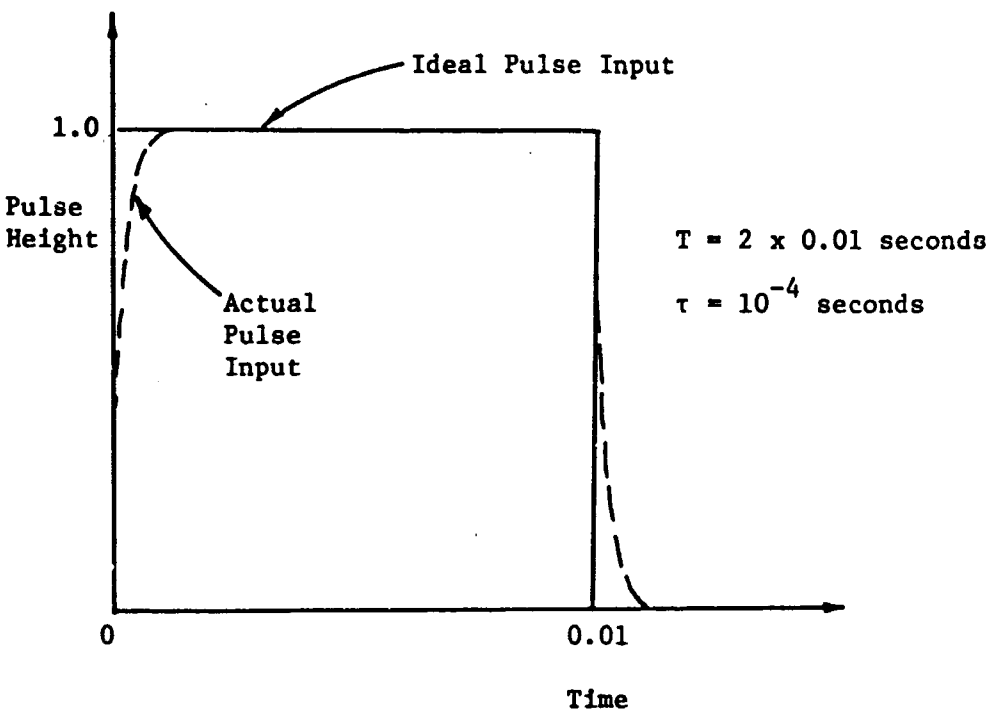

Figure 2-11. Ideal and Near-Ideal Area Conservation Input Pulses.

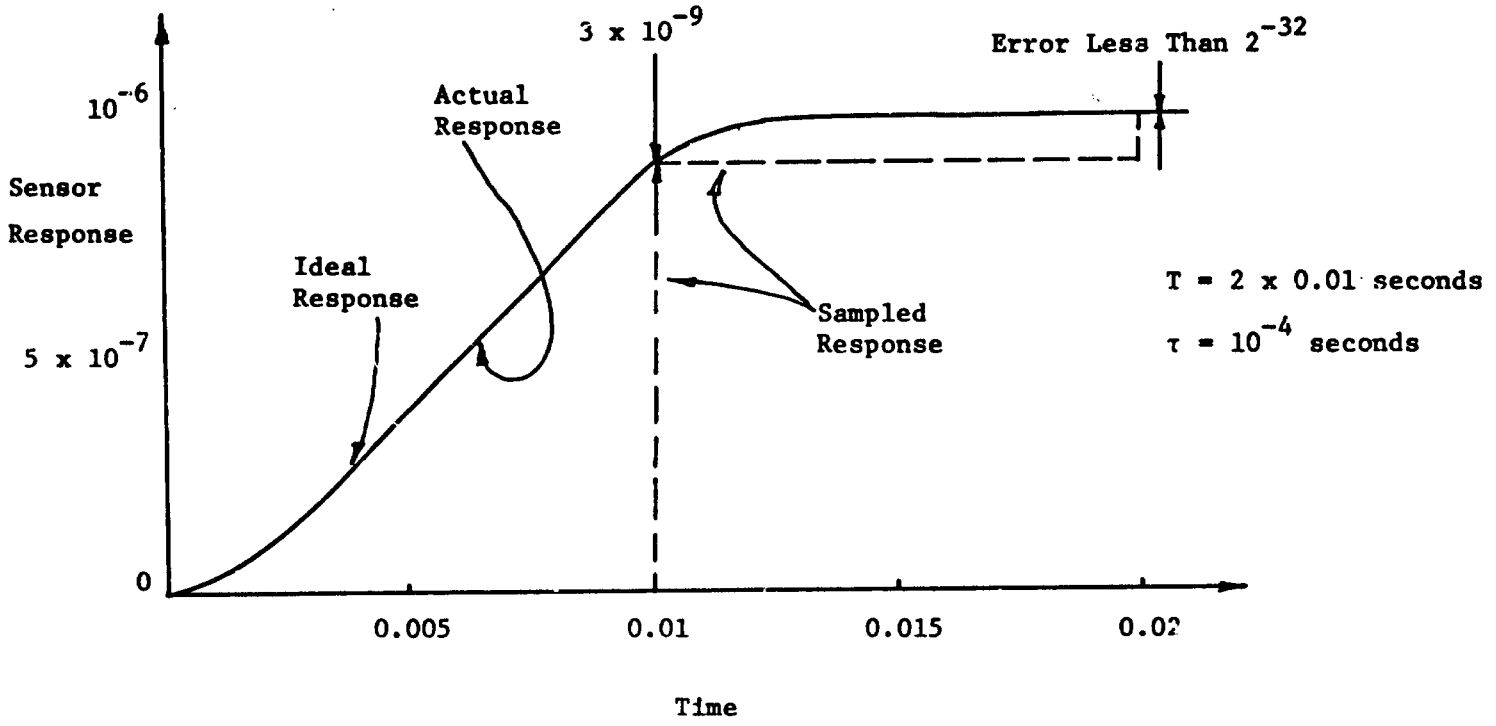

Figure 2-12. System Response Under Ideal and Near-Ideal Area Conservation Input Conditions.

TABLE 2-4

SYSTEM RESPONSE UNDER IDEAL AND POOR PULSING CONDITIONS

Ideal Input	Actual Input	Time	Ideal Output	Actual Output
1.0	0.0	0.0	0.0	0.0
1.0	0.63212	0.0001	0.048×10^{-6}	0.00132×10^{-6}
1.0	0.86467	0.0002	$0.187 \times .0^{-6}$	0.0603×10^{-6}
1.0	0.95022	0.0003	0.408×10^{-6}	0.1489×10^{-6}
1.0	0.98168	0.0004	0.703×10^{-6}	0.3735×10^{-6}
1.0	0.99326	0.0005	1.065×10^{-6}	0.6737×10^{-6}
1.0	0.99752	0.0006	1.488×10^{-6}	1.036×10^{-6}
1.0	0.99908	0.0007	1.966×10^{-6}	1.462×10^{-6}
1.0	0.99966	0.0008	2.994×10^{-6}	1.942×10^{-6}
1.0	0.99992	0.0009	3.065×10^{-6}	2.472×10^{-6}
0.0	0.99999	0.0010	3.678×10^{-6}	3.046×10^{-6}
0.0	0.36788	0.0011	4.280×10^{-6}	3.662×10^{-6}
0.0	0.13533	0.0012	4.825×10^{-6}	4.227×10^{-6}
0.0	0.04978	0.0013	5.457×10^{-6}	4.799×10^{-6}
0.0	0.018316	0.0014	5.763×10^{-6}	5.287×10^{-6}
0.0	0.006738	0.0015	6.166×10^{-6}	5.712×10^{-6}
0.0	0.000576	0.0016	6.531×10^{-6}	6.130×10^{-6}
0.0	0.0	0.0017	6.862×10^{-6}	6.520×10^{-6}
0.0	0.0	0.0018	7.158×10^{-6}	6.861×10^{-6}
0.0	0.0	0.0019	7.430×10^{-6}	7.172×10^{-6}
0.0	0.0	0.0020	7.675×10^{-6}	7.442×10^{-6}
0.0	0.0	0.0021	7.895×10^{-6}	7.805×10^{-6}

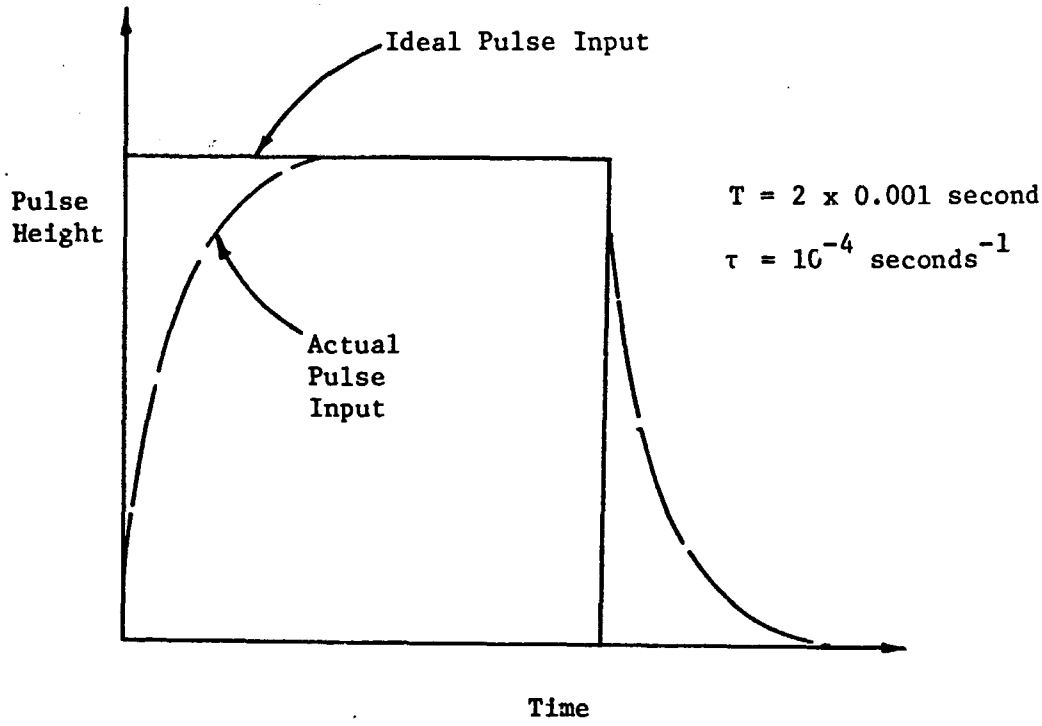

Figure 2-13. Ideal and Poor Area Conservation Input Pulses.

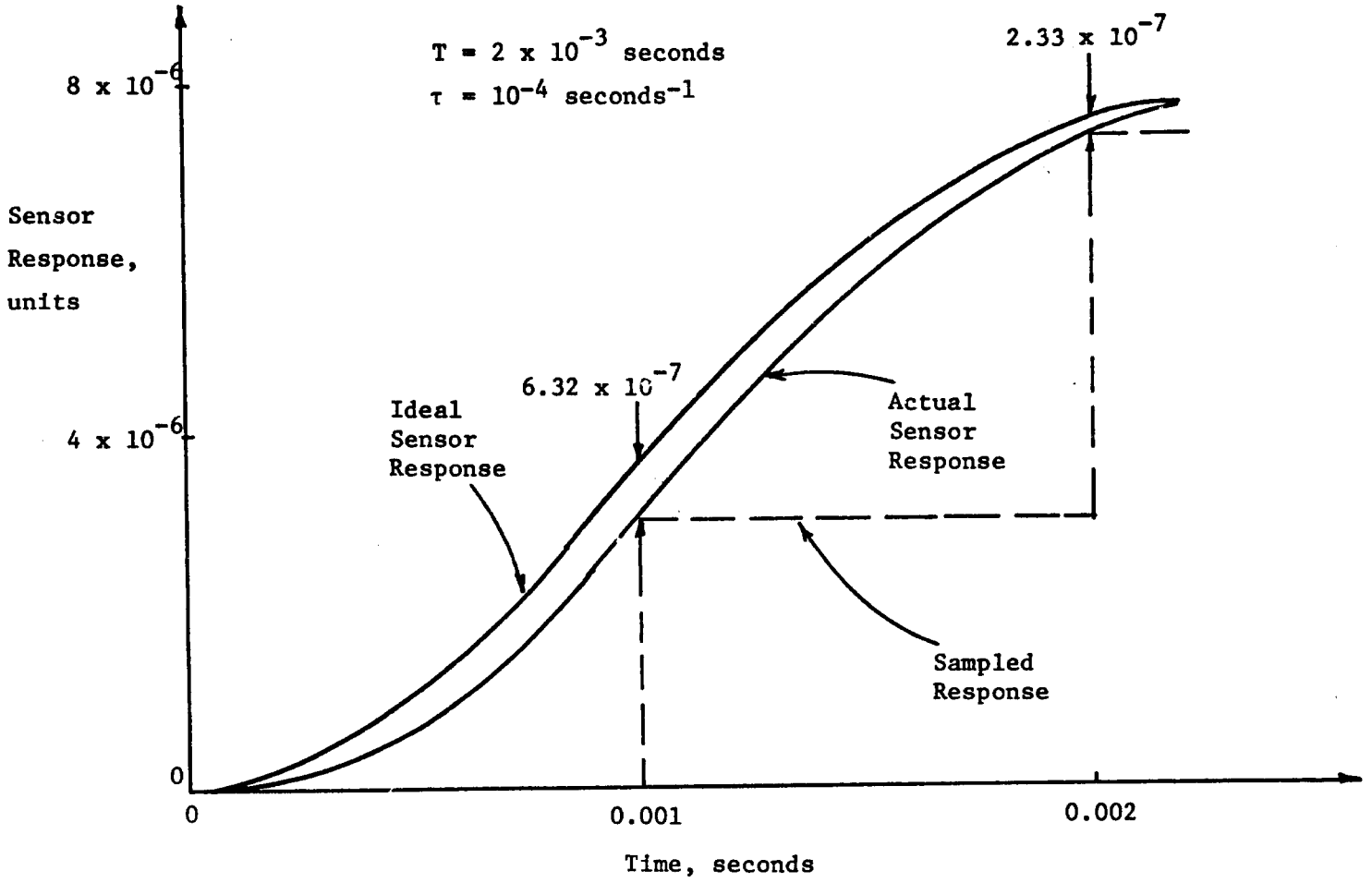

Figure 2-14. System Response Under Ideal and Poor Area Conservation Input Conditions.

CHAPTER 3

STRAPDOWN PLATFORMS USING REDUNDANT TWO-DEGREE-OF-FREEDOM GYROS

J.C. Hung and LeSi Han

ABSTRACT

This chapter presents a new concept of high reliability strapdown attitude sensing systems for space vehicles. Each system utilizes a set of redundant two-degree-of-freedom gyros. An optimum system configuration is obtained for maximum system reliability and the best measurement accuracy. Improved accuracy of the final data is obtained by using the least-square data reduction technique. Each system possesses a "sensor performance management" feature which is capable of failure detection, faulty gyro identification, system reconfiguration, and possibly, sensor recalibration. Improvement in reliability as compared to other types of strapdown systems is demonstrated. Details of the development are described in terms of a system containing four gyros. Results from systems containing three, five, and six gyros are included in the Appendix of this chapter.

INTRODUCTION

This chapter proposes a new redundancy scheme for high reliability strapdown navigation systems. The scheme involves the use of two-degree-of-freedom (TDF) gyros rather than SDF gyros for attitude sensing. The advantages of using TDF gyros as compared to SDF gyros are 1) higher reliability for the same number of gyros used, 2) less effect of sensor inaccuracy, 3) simpler computation for data reduction, and 4) provision of more redundant measurements for better data reduction. In this chapter, the system reliability of the proposed scheme will be presented; comparison will be made with respect to other known schemes; a discussion on the optimum configurations for TDF redundant sensors will be given; and the methods of failure detection, faulty sensor identification, and system reconfiguration will be described in detail.

SYSTEM RELIABILITY

Each TDF gyro senses attitude motion in two orthogonal directions. Therefore an attitude sensing system composed of n TDF gyros will operate satisfactorily if only 2 out of n gyros are in good condition as compared to 3 out of n for the system using SDF gyros. Thus, with the same number of gyros, the system using TDF gyros provides more redundancy and thus higher reliability than the one using SDF gyros.

Analytically, reliability is defined as the probability of success. Assume all individual gyros have equal reliability

$$r = e^{-\lambda t} \tag{3-1}$$

where λ is a positive real number and t represents time. Eq. (3-1) shows that reliability is a monotonically decreasing function of time. For an attitude sensing system formed by n TDF gyros the system reliability is given by

$$R_n = \binom{n}{n} r^n + \binom{n}{n-1} r^{n-1}(1 - r) + - - - - + \binom{n}{2} r^2 (1 - r)^{n-2} \tag{3-2}$$

a similar system formed by n SDF gyros has a system reliability of

$$R'_n = \binom{n}{n} r^n + \binom{n}{n-1} r^{n-1} (1 - r) + - - - - + \binom{n}{3} r^3 (1 - r)^{n-3}$$

$$= R_n - \binom{n}{2} r^2 (1 - r)^{n-2} \tag{3-3}$$

A plot of R_n and R'_n, for n = 2 to 6, versus the normalized time $T = \lambda t$ is shown in Fig. 3-1. It is evident that higher reliability is associated with TDF gyro strapdown systems. Note that in the above discussion it has been assumed that the reliability r of each individual SDF gyro is the same as that of each TDF gyro. This assumption is reasonable from a hardware construction point of view.

OPTIMUM SYSTEM CONFIGURATIONS

Three considerations are involved in arranging gyros for optimum system configurations. The first and the most important consideration is the maximum system reliability. For example, a group of four TDF gyros A, B, C, and D can be oriented with their sensitive axes directed in a way symbolically shown in

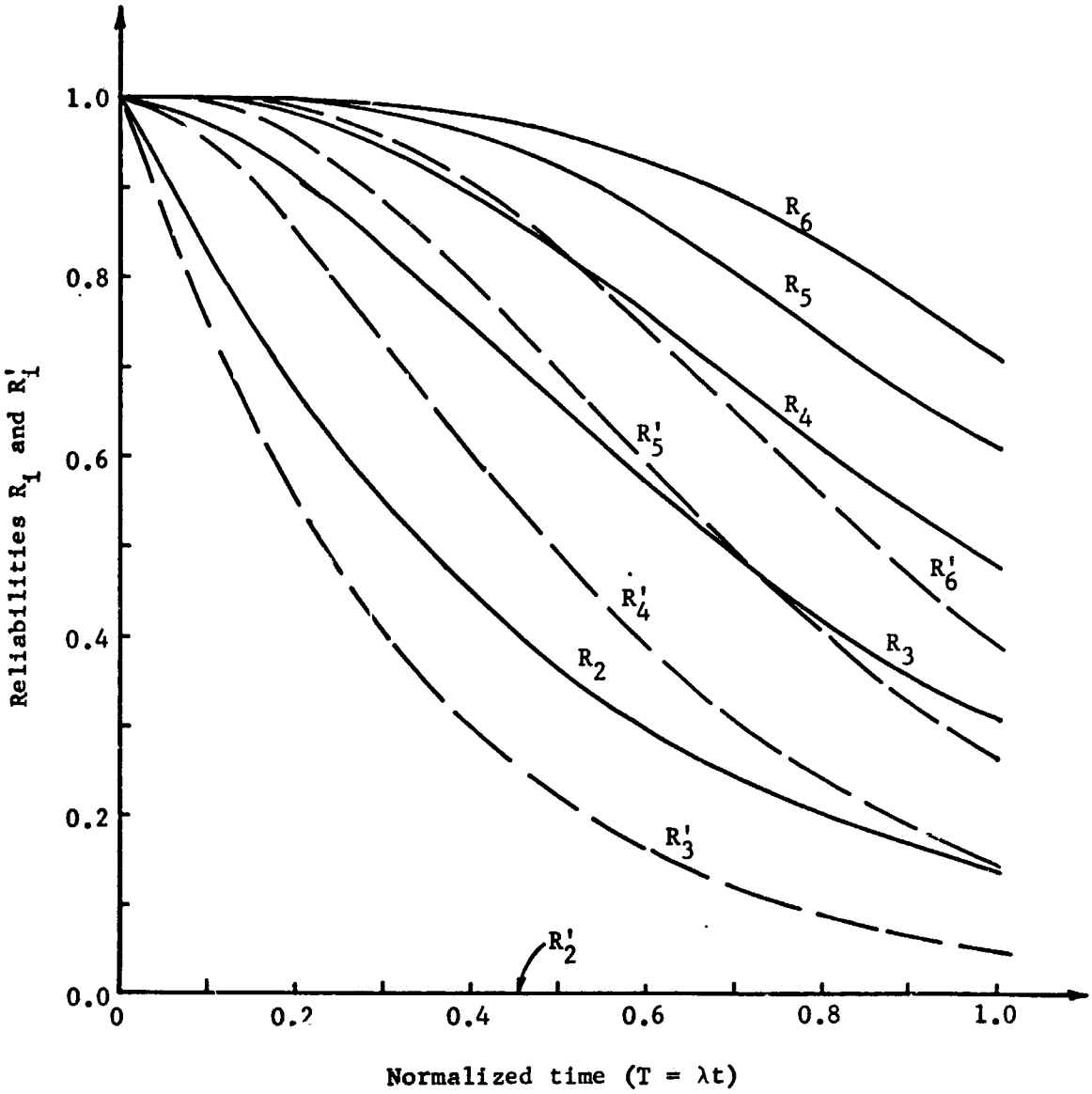

Figure 3-1. System Reliabilities.

Fig. 3-2. In this figure, the circles labeled A1 and A2 on x and y axes, respectively, represent the directions of two sensitive axes of gyro A. Similar representation is used for all other gyros. This arrangement is not optimum, since if gyros A and C fail the remaining gyros B and D cannot provide a full attitude sensing.

The second consideration is the effect of gyro orientation on measurement error introduced by sensor inaccuracy. Referring to Fig. 3-3, let ω be the desired vector quantity and S is the direction of sensor's sensitive axis which makes an angle α from vector ω. The measured quantity is

$$m = \omega \cos\alpha + e$$

where e represents the measurement error. The "normalized measurement error" is given by

$$e_N = \frac{e}{\omega \cos\alpha} \tag{3-4}$$

Eq. (3-4) shows that this error is the least when $\alpha = 0$. In other words, if we want to measure the vehicle attitude motion along three vehicle coordinates, the measurement error is the least if all sensitive axes of sensors are directed along vehicle coordinates.

The last consideration is the simplicity of computation. Simpler computation requirements result in less computation errors and shorter computation time. In a strapdown navigation system usually the attitude motion along vehicle axes is measured. Therefore a TDF gyro whose sensitive axes are along the vehicle axes senses directly the attitude motion along those two vehicle axes, no computation is needed.

It is assumed that if any one or both outputs of a gyro fail, the entire gyro is taken out of service.

Guided by the three considerations and the assumption above, optimum system configuration for high reliability strapdown systems using three, four, five and six TDF gyros are given below, where the desired quantities are vehicle rates ω_x, ω_y, and ω_z along three vehicle axes. The arrangements are also symbolically shown in Fig. 3-4.

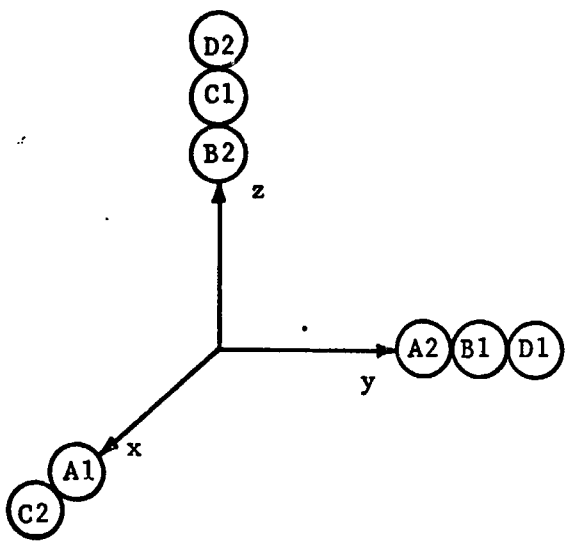

Gyro	Directions of sensitive axes
A	x and y axes
B	y and z axes
C	z and x axes
D	y and z axes

Figure 3-2. A Non-Optimum System Configuration.

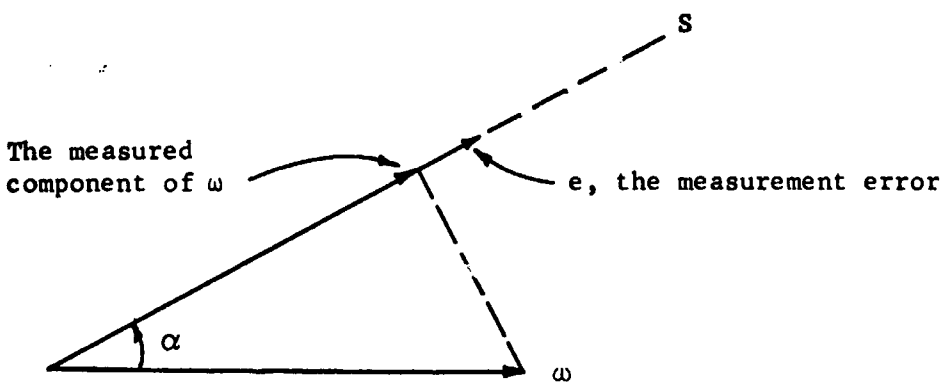

Desired signal: ω

Measured signal: $\omega \cos \alpha + e$

Normalized measurement error: $\frac{e}{\omega \cos \alpha}$

Figure 3-3. Normalized Measurement Error.

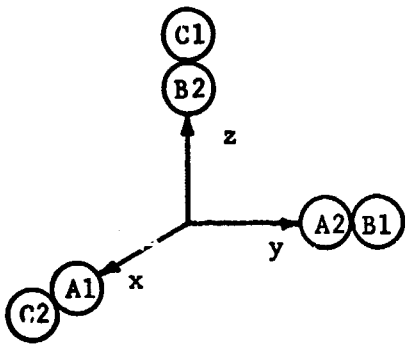

(a) 3-gyro system

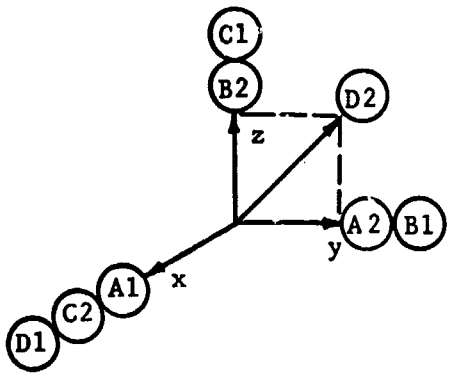

(b) 4-gyro system

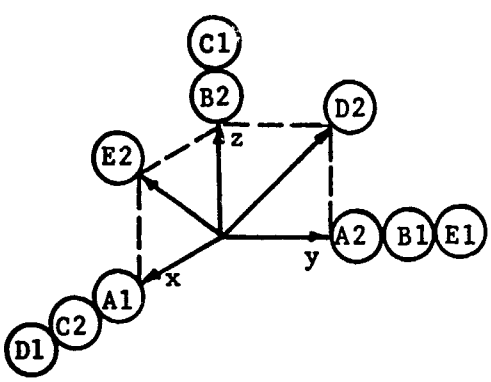

(c) 5-gyro system

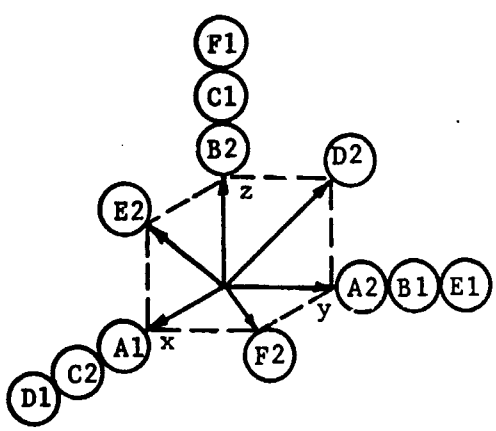

(d) 6-gyro system

Figure 3-4. Optimum System Configuration.

3 TDF Gyros

The arrangement and measurements for a 3 gyro system are shown in Table 3-1. The measurement equation is

$$\underline{m}(3) = R(3)\,\underline{\omega} \quad , \tag{3-5}$$

where

$$\underline{\omega} = \begin{bmatrix} \omega_x \\ \omega_y \\ \omega_z \end{bmatrix} \tag{3-6}$$

and

$$\left.\begin{aligned} \underline{m}(3) &= [m_1\ m_2\ m_3\ m_4\ m_5\ m_6]^T \\ R(3) &= \begin{bmatrix} 1 & 0 & 0 & 0 & 0 & 1 \\ 0 & 1 & 1 & 0 & 0 & 0 \\ 0 & 0 & 0 & 1 & 1 & 0 \end{bmatrix}^T \end{aligned}\right\} \tag{3-7}$$

The symbol $[\ ]^T$ denotes the transpose of a matrix.

4 TDF Gyros

The arrangement and measurements for a system composed of four gyros are shown in Table 3-2. The measurement equation is

$$\underline{m}(4) = R(4)\,\underline{\omega} \quad , \tag{3-8}$$

where

$$\left.\begin{aligned} \underline{m}(4) &= [m_1\ m_2\ m_3\ m_4\ m_5\ m_6\ m_7\ m_8]^T \\ R(4) &= \begin{bmatrix} 1 & 0 & 0 & 0 & 0 & 1 & 1 & 0 \\ 0 & 1 & 1 & 0 & 0 & 0 & 0 & c \\ 0 & 0 & 0 & 1 & 1 & 0 & 0 & c \end{bmatrix}^T \end{aligned}\right\} \tag{3-9}$$

Throughout this paper $c = \cos 45° = 0.707$.

Gyro	Direction of sensitive axis	Measurement
A	A1, x direction	$m_1 = \omega_x$
	A2, y direction	$m_2 = \omega_y$
B	B1, y direction	$m_3 = \omega_y$
	B2, z direction	$m_4 = \omega_z$
C	C1, z direction	$m_5 = \omega_z$
	C2, x direction	$m_6 = \omega_x$

Table 3-1. Arrangement for 3-TDF-gyro system.

Gyro	Direction of sensitive axis	Measurement
A	A1, x direction	$m_1 = \omega_x$
	A2, y direction	$m_2 = \omega_y$
B	B1, y direction	$m_3 = \omega_y$
	B2, z direction	$m_4 = \omega_z$
C	C1, z direction	$m_5 = \omega_z$
	C2, x direction	$m_6 = \omega_x$
D	D1, x direction	$m_7 = \omega_x$
	D2, y = z direction	$m_8 = 0.707\omega_y + 0.707\omega_z$

Table 3-2. Arrangement for 4-TDF-gyro system.

5 TDF Gyros

The arrangement and measurements for a 5 gyro system are shown in Table 3-3. The measurement equation is

$$\underline{m}(5) = R(5)\ \underline{\omega} \tag{3-10}$$

where

$$\left.\begin{aligned} \underline{m}(5) &= [m_1\ m_2\ m_3\ m_4\ m_5\ m_6\ m_7\ m_8\ m_9\ m_{10}]^T \\ R(5) &= \begin{bmatrix} 1 & 0 & 0 & 0 & 0 & 1 & 1 & 0 & 0 & c \\ 0 & 1 & 1 & 0 & 0 & 0 & 0 & c & 1 & 0 \\ 0 & 0 & 0 & 1 & 1 & 0 & 0 & c & 0 & c \end{bmatrix}^T \end{aligned}\right\} \tag{3-11}$$

6 TDF Gyros

The arrangement and measurements for a 6 gyro system are shown in Table 3-4. The measurement equation is

$$\underline{m}(6) = R(6)\ \underline{\omega} \tag{3-12}$$

where

$$\left.\begin{aligned} \underline{m}(6) &= [m_1\ m_2\ m_3\ -\ -\ -\ -\ -\ -\ m_{12}]^T \\ R(5) &= \begin{bmatrix} 1 & 0 & 0 & 0 & 0 & 1 & 1 & 0 & 0 & c & 0 & c \\ 0 & 1 & 1 & 0 & 0 & 0 & 0 & c & 1 & 0 & 0 & c \\ 0 & 0 & 0 & 1 & 1 & 0 & 0 & c & 0 & c & 1 & 0 \end{bmatrix}^T \end{aligned}\right\} \tag{3-13}$$

Notice that in any of these configurations, any two good gyros can provide a complete attitude sensing.

SENSOR PERFORMANCE MANAGEMENT

A high reliability navigation system employing a redundancy concept must be capable of "failure detection", "faulty sensor identification", "system reconfiguration", and possibly "sensor recalibration". All these functions can be handled by a centralized control called "sensor performance

Gyro	Direction of sensitive axis	Measurement
A	A1, x direction	$m_1 = \omega_x$
	A2, y direction	$m_2 = \omega_y$
B	B1, y direction	$m_3 = \omega_y$
	B2, z direction	$m_4 = \omega_z$
C	C1, z direction	$m_5 = \omega_z$
	C2, x direction	$m_6 = \omega_x$
D	D1, x direction	$m_7 = \omega_x$
	D2, y = z direction	$m_8 = 0.707\omega_y + 0.707\omega_z$
E	E1, y direction	$m_9 = \omega_y$
	E2, z = x direction	$m_{10} = 0.707\omega_z + 0.707\omega_x$

Table 3-3. Arrangement for 5-TDF-gyro system.

Gyro	Direction of sensitive axis	Measurement
A	A1, x direction	$m_1 = \omega_x$
	A2, y direction	$m_2 = \omega_y$
B	B1, y direction	$m_3 = \omega_y$
	B2, z direction	$m_4 = \omega_z$
C	C1, z direction	$m_5 = \omega_z$
	C2, x direction	$m_6 = \omega_x$
D	D1, x direction	$m_7 = \omega_x$
	D2, y = z direction	$m_8 = 0.707\omega_y + 0.707\omega_z$
E	E1, y direction	$m_9 = \omega_y$
	E2, z = x direction	$m_{10} = 0.707\omega_z + 0.707\omega_x$
F	F1, z direction	$m_{11} = \omega_z$
	F2, x = y direction	$m_{12} = 0.707\omega_x + 0.707\omega_y$

Table 3-4. Arrangement for 6-TDF-gyro system.

management" (SPM). This management task is performed by a computer software. Two SPM schemes are shown in Figures 3-5 and 3-6 in the form of operational flow diagrams. The first scheme involves failure detection, faulty sensor identification, and system reconfiguration. The second scheme involves the additional ability of determining whether the failure is a soft failure and the ability of sensor recalibration in case of a soft failure.

When the system consists of n gyros, the total number of states is 2^n, and $2^n - \binom{n}{0} - \binom{n}{1}$ of them allow faulty gyro identification.

In the following sections, details of the SPM concept are developed for a system containing four TDF gyros. Details for other systems are included in the Appendix of this chapter. The development is described in three separate parts, namely, failure detection and faulty gyro identification, system reconfiguration and data reduction, and sensor recalibration.

DETECTION AND IDENTIFICATION

The function of failure detection is to find out if a failure has occurred somewhere in the system while the function of faulty gyro identification is to identify the faulty gyro. When the system contains four TDF gyros, there is a total of sixteen possible states including the cases when all gyros are good, one is bad, two are bad, etc. It will be shown that although all states allow failure detection, not all of them allow faulty gyro identification.

Parity Check Equations

When all four TDF gyros are normal, the following conditions exist as can be seen from the measurement equation (3-8).

$$\left.\begin{aligned} &\text{i)} \quad m_6 - m_7 \simeq 0 \\ &\text{ii)} \quad m_8 - c\,m_3 - c\,m_4 \simeq 0 \\ &\text{iii)} \quad m_4 - m_5 \simeq 0 \\ &\text{iv)} \quad m_7 - m_1 \simeq 0 \\ &\text{v)} \quad m_6 - m_1 \simeq 0 \\ &\text{vi)} \quad m_2 - m_3 \simeq 0 \end{aligned}\right\} \qquad (3\text{-}14)$$

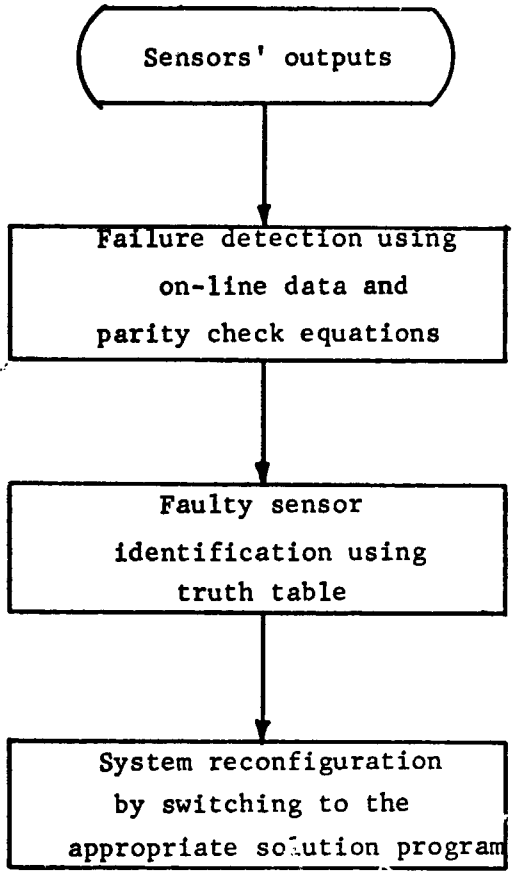

Figure 3-5. The First SPM Scheme.

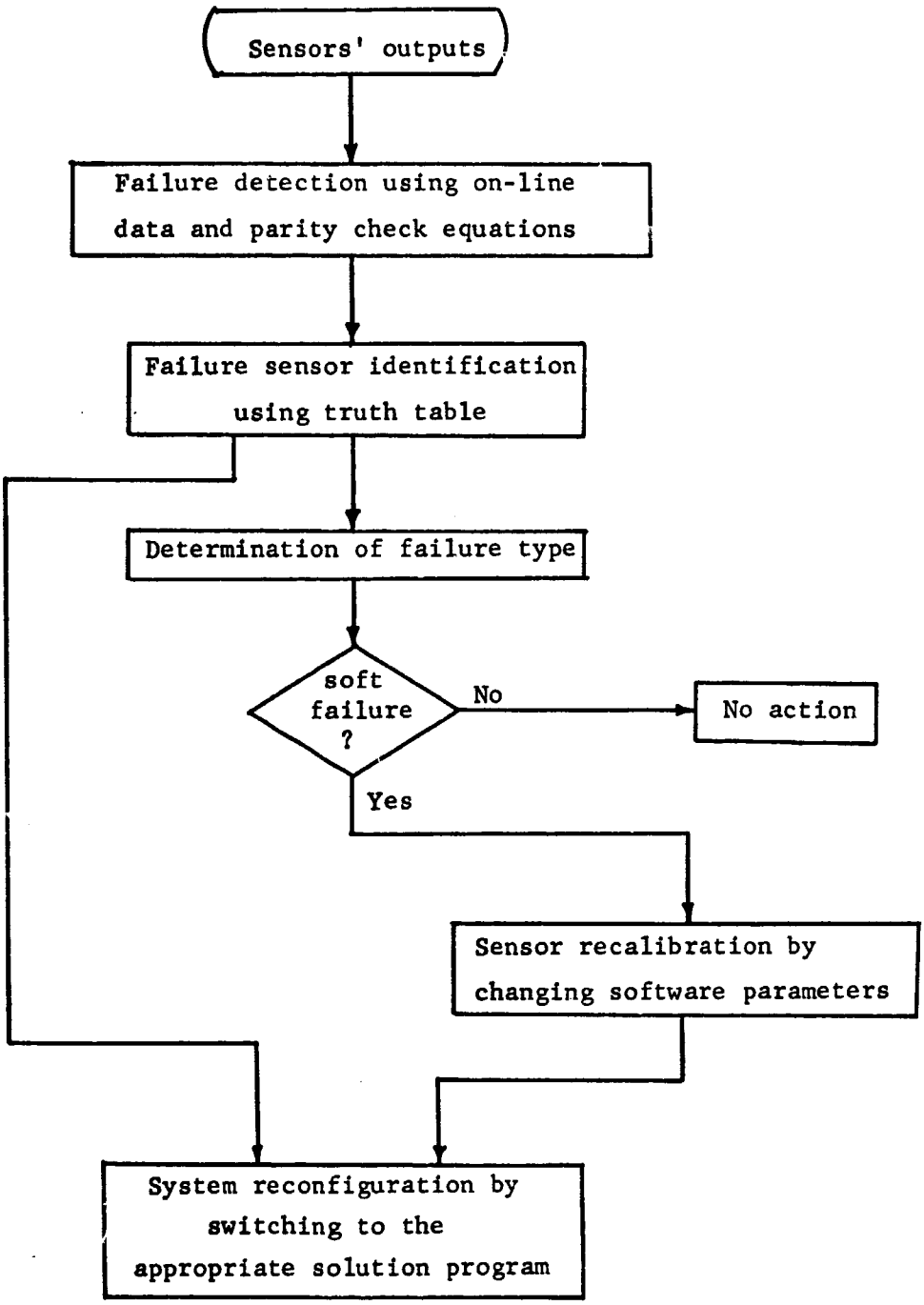

Figure 3-6. The Second SPM Scheme

The "approximately equal" sign "≈" accounts for the normal measurement error. Assume that no two faulty gyros have identical faults; or, if they do have identical faults, assume that both do not become bad at the same time. Then one or more of the six equations above will not be satisfied if any failure occurs. These six equations are called "parity check equations".

Truth Table for Faulty Gyro Identification

Let us associate with the ith parity check equation a binary valued quantity K_i. K_i equals "0" when the equation is satisfied and equals "1" when not satisfied.

Assume that when a TDF gyro fails, measurements from both axes are erroneous. The validity of this assumption is subject to discussion and further exploration. Now we are in a position to construct a truth table for faulty gyro identification. Suppose that gyros A and are bad, then measurements m_1, m_2, m_3 and m_4 are not consistent. Under this condition all parity check values K_i are equal to 1, except k_1 which is equal to 0. Reasoning in this manner we obtain a truth table which is shown in Table 3-5.

Examining the table shows that there are twelve distinguishable system states. Eleven of them, which include the events of not more than two failed gyros, allow both failure detection and faulty gyro identification. The last state, which includes the group of five events where more than two gyros are failed, allows failure detection only but not the identification of faulty gyros.

DATA REDUCTION AND SYSTEM RECONFIGURATION

Aside from increasing the system reliability the use of redundant gyros provides redundant measurements which can be used by means of a data reduction technique to reduce the effect of errors associated with individual gyros. The technique used will be the "least-square data reduction".[5] Since the system reconfiguration is accomplished by means of software control, it can readily be incorporated into the data reduction program.

Data Reduction

Rewrite Eq. (3-8) in its explicit form and omit the parentheses associated with $\underline{m}$ and R for simplicity.

Failed gyros	Parity check values						Reconfiguration solution program	SPM condition
	K1	K2	K3	K4	K5	K6		
None	0	0	0	0	0	0	P0	Failure detectable and faulty gyros identifiable
A	0	0	0	1	1	1	P1	
B	0	1	1	0	0	1	P2	
C	1	0	1	0	1	0	P3	
D	1	1	0	1	0	0	P4	
A, B	0	1	1	1	1	1	P5	
A, C	1	0	1	1	1	1	P6	
A, D	1	1	0	1	1	1	P7	
B, C	1	1	1	0	1	1	P8	
B, D	1	1	1	1	0	1	P9	
C, D	1	1	1	1	1	0	P10	
A, B, C	1	1	1	1	1	1	P11 Report total failure	Failure detectable only
A, B, D	1	1	1	1	1	1		
A, C, D	1	1	1	1	1	1		
B, C, D	1	1	1	1	1	1		
A, B, C, D	1	1	1	1	1	1		

Table 3-5. Truth table for failure detection and faulty gyro identification, with reconfiguration solution program indicated, for 4-gyro system.

$$\underbrace{\begin{bmatrix} m_1 \\ m_2 \\ m_3 \\ m_4 \\ m_5 \\ m_6 \\ m_7 \\ m_8 \end{bmatrix}}_{\underline{m}} = \underbrace{\begin{bmatrix} 1 & 0 & 0 \\ 0 & 1 & 0 \\ 0 & 1 & 0 \\ 0 & 0 & 1 \\ 0 & 0 & 1 \\ 1 & 0 & 0 \\ 1 & 0 & 0 \\ 0 & c & c \end{bmatrix}}_{R} \begin{bmatrix} \omega_x \\ \omega_y \\ \omega_z \end{bmatrix} \quad \underline{\omega} \tag{3-15}$$

In this equation the measurement $\underline{m}$ is available from sensor outputs while the attitude rate $\underline{\omega}$ is desired. Since R has more rows than columns, no simple $\underline{\omega}$ can be found to satisfy this equation. Instead, any selected $\underline{\omega}$ will result in a solution error

$$\underline{\varepsilon} = R\,\underline{\omega} - \underline{m} \tag{3-16}$$

The least-square error criterion is to choose a $\underline{\omega}$ such that the quality

$$I = \underline{\varepsilon}^T\underline{\varepsilon} = (R\underline{\omega} - \underline{m})^T\,(R\underline{\omega} - \underline{m}) \tag{3-17}$$

is minimized. Taking the gradient of (3-17) with respect to $\underline{\omega}$ and setting the result to zero gives

$$\nabla I = R^T(R\underline{\omega} - \underline{m}) = 0 \tag{3-18}$$

Solving for $\underline{\omega}$ yields

$$\underline{\omega} = (R^T R)^{-1} R^T \underline{m}$$

$$= \begin{bmatrix} \frac{1}{3} & 0 & 0 & 0 & 0 & \frac{1}{3} & \frac{1}{3} & 0 \\ 0 & \frac{5}{12} & \frac{5}{12} & \frac{-1}{12} & \frac{-1}{12} & 0 & 0 & \frac{1}{3}c \\ 0 & \frac{-1}{12} & \frac{-1}{12} & \frac{5}{12} & \frac{5}{12} & 0 & 0 & \frac{1}{3}c \end{bmatrix} \underline{m} \qquad \text{(PO)}$$

which is the desired data reduction equation readily be written into a computer program. Let us label this equation and its associated program PO.

It should be mentioned that if the statistics of the sensor inaccuracies are known, more sophisticated techniques can be used for better results.

System Reconfiguration

The system reconfiguration need not be done by hardware modification. Instead, it is conveniently and rapidly done by changing the software program, which can be executed by the computer. Consider the case that gyro A is found faulty. Under this condition measurements m_1 and m_2 will not be used in the data reduction. This is done simply by eliminating m_1 and m_2 rows from Eq. (3-14), giving

$$\underbrace{\begin{bmatrix} m_3 \\ m_4 \\ m_5 \\ m_6 \\ m_7 \\ m_8 \end{bmatrix}}_{\underline{m}_1} = \underbrace{\begin{bmatrix} 0 & 1 & 0 \\ 0 & 0 & 1 \\ 0 & 0 & 1 \\ 1 & 0 & 0 \\ 1 & 0 & 0 \\ 0 & c & c \end{bmatrix}}_{R_1} \begin{bmatrix} \omega_x \\ \omega_y \\ \omega_z \end{bmatrix} \qquad (3\text{-}19)$$

Denoting the reduced measurement vector $\underline{m}_1$ and measurement matrix R_1, the new least-square data reduction equation should be

$$\underline{\omega} = (R_1^T R_1)^{-1} R_1^T \underline{m}_1 \quad . \qquad \text{(P1)}$$

To generalize, the system reconfigurations for the first ten failure conditions can be accomplished by using the appropriate measurement vectors and measurement matrices in the data reduction equation

$$\underline{\omega} = (R_i^T R_i)^{-1} R_i^T m_i \quad , \qquad \text{(Pi)}$$

i = 1 to 10. For the last five failure conditions, no system reconfiguration is possible, and the computer should report a total-system failure. Table 3-6 lists all the measurement vectors $\underline{m}_i$ and measurement matrices R_i for various failure conditions.

It should be mentioned that there are other possible data reduction techniques. For example, if the statistics of sensor inaccuracies are known, more sophisticated techniques can be employed for better data reduction.

SENSOR RECALIBRATION

If a faulty gyro has a soft failure, such as a bias error, a change of scale factor, or showing erratic readings about a mean value, it can be recalibrated. The faulty gyro is taken out of service by system reconfiguration and put into a fault determination mode. During this mode, outputs of this faulty gyro are compared with the outputs of good gyros to determine the type of fault which has occurred and the amount of correction needed. The correction is made by changing parameters in the software. The system is then reconfigurated once.

While the functions of failure detection, faulty gyro identification, and system reconfiguration are indispensable in sensor performance management, the function of sensor recalibration is not. The inclusion of the latter maximizes the system reliability at the expense of an increased computer requirement, which may be a worthwhile investment.

For P1:

$$\underline{m}_1 = \begin{bmatrix} m_3 \\ m_4 \\ m_5 \\ m_6 \\ m_7 \\ m_8 \end{bmatrix} \qquad R_1 = \begin{bmatrix} 0 & 1 & 0 \\ 0 & 0 & 1 \\ 0 & 0 & 1 \\ 1 & 0 & 0 \\ 1 & 0 & 0 \\ 0 & c & c \end{bmatrix}$$

For P2:

$$\underline{m}_2 = \begin{bmatrix} m_1 \\ m_2 \\ m_5 \\ m_6 \\ m_7 \\ m_8 \end{bmatrix} \qquad R_2 = \begin{bmatrix} 1 & 0 & 0 \\ 0 & 1 & 0 \\ 0 & 0 & 1 \\ 1 & 0 & 0 \\ 1 & 0 & 0 \\ 0 & c & c \end{bmatrix}$$

For P3:

$$\underline{m}_3 = \begin{bmatrix} m_1 \\ m_2 \\ m_3 \\ m_4 \\ m_7 \\ m_8 \end{bmatrix} \qquad R_3 = \begin{bmatrix} 1 & 0 & 0 \\ 0 & 1 & 0 \\ 0 & 1 & 0 \\ 0 & 0 & 1 \\ 1 & 0 & 0 \\ 0 & c & c \end{bmatrix}$$

For P4:

$$\underline{m}_4 = \begin{bmatrix} m_1 \\ m_2 \\ m_3 \\ m_4 \\ m_5 \\ m_6 \end{bmatrix} \qquad R_4 = \begin{bmatrix} 1 & 0 & 0 \\ 0 & 1 & 0 \\ 0 & 1 & 0 \\ 0 & 0 & 1 \\ 0 & 0 & 1 \\ 1 & 0 & 0 \end{bmatrix}$$

For P5:

$$\underline{m}_5 = \begin{bmatrix} m_5 \\ m_6 \\ m_7 \\ m_8 \end{bmatrix} \qquad R_5 = \begin{bmatrix} 0 & 0 & 1 \\ 1 & 0 & 0 \\ 1 & 0 & 0 \\ 0 & c & c \end{bmatrix}$$

For P6:

$$\underline{m}_6 = \begin{bmatrix} m_3 \\ m_4 \\ m_7 \\ m_8 \end{bmatrix} \qquad R_6 = \begin{bmatrix} 0 & 1 & 0 \\ 0 & 0 & 1 \\ 1 & 0 & 0 \\ 0 & c & c \end{bmatrix}$$

For P7:

$$\underline{m}_7 = \begin{bmatrix} m_3 \\ m_4 \\ m_5 \\ m_6 \end{bmatrix} \qquad R_7 = \begin{bmatrix} 0 & 1 & 0 \\ 0 & 0 & 1 \\ 0 & 0 & 1 \\ 1 & 0 & 0 \end{bmatrix}$$

For P8:

$$\underline{m}_8 = \begin{bmatrix} m_1 \\ m_2 \\ m_7 \\ m_8 \end{bmatrix} \qquad R_8 = \begin{bmatrix} 1 & 0 & 0 \\ 0 & 1 & 0 \\ 1 & 0 & 0 \\ 0 & c & c \end{bmatrix}$$

For P9:

$$\underline{m}_9 = \begin{bmatrix} m_1 \\ m_2 \\ m_5 \\ m_6 \end{bmatrix} \qquad R_9 = \begin{bmatrix} 1 & 0 & 0 \\ 0 & 1 & 0 \\ 0 & 0 & 1 \\ 1 & 0 & 0 \end{bmatrix}$$

For P10:

$$\underline{m}_{10} = \begin{bmatrix} m_1 \\ m_2 \\ m_3 \\ m_4 \end{bmatrix} \qquad R_{10} = \begin{bmatrix} 1 & 0 & 0 \\ 0 & 1 & 0 \\ 0 & 1 & 0 \\ 0 & 0 & 1 \end{bmatrix}$$

Table 3-6. Vectors $\underline{m}_i$ and matrices R_i for reconfiguration solution program for 4-gyro system. (c=0.707)

REFERENCES

1. R.M. Bumstead and W.E. VanderVelde, "Navigation and Guidance Systems Employing a Gimballess IMU", Guidance and Control, Volume II, Edited by Langford and Mundo, Academic Press, 1963.

2. I. Rathan and R. Weiss, "An Ultra-Reliable Attitude Reference System for a Manned Orbiting Laboratory With Limited Sparing Capability", AIAA/JACC Guidance and Control Conference, August 15-17, 1966.

3. J.P. Gilmore, "A Non-Orthogonal Gyro Configuration", MIT/IL Report T-472, January, 1967.

4. M.L. Shooman, Probabilistic Reliability: An Engineering Approach, McGraw-Hill Book Co., New York, 1968.

5. J.E. Bennett and J.C. Hung, "Application of Statistical Techniques to Landmark Navigation", NAVIGATION, Journal of the Institute of Navigation, Vol. 17; No. 4, 1971, pp. 349-357.

APPENDIX

SPM DETAILS FOR SYSTEMS HAVING THREE, FIVE, AND SIX TDF GYROS

3-Gyro System

The set of three parity check equations for the 3-gyro system is given by

$$\left.\begin{aligned} m_4 - m_5 &\simeq 0 \\ m_6 - m_1 &\simeq 0 \\ m_2 - m_3 &\simeq 0 \end{aligned}\right\} \qquad (3\text{-}20)$$

The truth table for the identification of faulty gyros are shown in Table 3-7 with reconfiguration solution programs indicated. The data reduction equation for the normal condition, where all gyros are good, is given by

$$\underline{\omega} = (R^T R)^{-1} R^T \underline{m} \qquad (PO)$$

Failed Gyros	K1	K2	K3	Reconfiguration Solution Program	SPM Condition
None	0	0	0	P0	Failure detection and faulty gyro identification
A	0	1	1	P1	
B	1	0	1	P2	
C	1	1	0	P3	
A, B	1	1	1	P4 Report total failure	Failure detection only
A, C	1	1	1		
B, C	1	1	1		
A, B, C	1	1	1		

Table 3-7. Truth table for detection and faulty gyro identification, with reconfiguration solution program indicated, for the 3-gyro system.

where $\underline{m} = [m_1, m_2, m_3, m_4, m_5, m_6,]^T$ and

$$R = \begin{bmatrix} 1 & 0 & 0 \\ 0 & 1 & 0 \\ 0 & 1 & 0 \\ 0 & 0 & 1 \\ 0 & 0 & 1 \\ 1 & 0 & 0 \end{bmatrix}$$

There are seven abnormal conditions, of which only three are identifiable. Each reconfiguration solution program for data reduction has the form

$$\underline{\omega} = (R_i^T R_i)^{-1} R_i^T \underline{m}_1 \qquad i = 1, 2, 3, \qquad \text{(Pi)}$$

where the measurement vectors $\underline{m}_i$ and measurement matrices R_i are listed in Table 3-8.

5-Gyro System

The set of ten parity check equations for the 5-gyro system is given by

$$\left.\begin{aligned} m_8 + c\,m_7 - m_{10} - c\,m_9 &\simeq 0 \\ m_{10} - c\,m_5 - c\,m_6 &\simeq 0 \\ m_6 - m_7 &\simeq 0 \\ m_3 - m_9 &\simeq 0 \\ m_8 - c\,m_3 - c\,m_4 &\simeq 0 \\ m_4 - m_5 &\simeq 0 \\ m_2 - m_9 &\simeq 0 \\ m_1 - m_7 &\simeq 0 \\ m_1 - m_6 &\simeq 0 \\ m_2 - m_3 &\simeq 0 \end{aligned}\right\} \qquad (3\text{-}21)$$

For P1:

$$\underline{m}_1 = \begin{bmatrix} m_3 \\ m_4 \\ m_5 \\ m_6 \end{bmatrix} \qquad R_1 = \begin{bmatrix} 0 & 1 & 0 \\ 0 & 0 & 1 \\ 0 & 0 & 1 \\ 1 & 0 & 0 \end{bmatrix}$$

For P2:

$$\underline{m}_2 = \begin{bmatrix} m_1 \\ m_2 \\ m_5 \\ m_6 \end{bmatrix} \qquad R_2 = \begin{bmatrix} 1 & 0 & 0 \\ 0 & 1 & 0 \\ 0 & 0 & 1 \\ 1 & 0 & 0 \end{bmatrix}$$

For P3:

$$\underline{m}_3 = \begin{bmatrix} m_1 \\ m_2 \\ m_3 \\ m_4 \end{bmatrix} \qquad R_3 = \begin{bmatrix} 1 & 0 & 0 \\ 0 & 1 & 0 \\ 0 & 1 & 0 \\ 0 & 0 & 1 \end{bmatrix}$$

Table 3-8. Vectors $\underline{m}_i$ and matrices R_i for reconfiguration solution programs for 3-gyro system.

The truth table for the identification of faulty gyros are shown in Table 3-9, where the reconfiguration solution program for each abnormal condition is also shown. The data reduction equation for the normal condition where all gyros are good again has the form of Eq. (PO). But here

$$R = \begin{bmatrix} 1 & 0 & 0 \\ 0 & 1 & 0 \\ 0 & 1 & 0 \\ 0 & 0 & 1 \\ 0 & 0 & 1 \\ 1 & 0 & 0 \\ 1 & 0 & 0 \\ 0 & c & c \\ 0 & 1 & 0 \\ c & 0 & c \end{bmatrix} \quad \text{and} \quad \underline{m} = \begin{bmatrix} m_1 \\ m_2 \\ m_3 \\ m_4 \\ m_5 \\ m_6 \\ m_7 \\ m_8 \\ m_9 \\ m_{10} \end{bmatrix} \qquad (3\text{-}22)$$

There are thirty-one abnormal conditions, of which only twenty-five are identifiable. Each reconfiguration solution program for data reduction has the form

$$\underline{\omega} = (R_i^T R_i)^{-1} R_i^T \underline{m}_i \qquad i = 1 \text{ to } 25 \qquad (Pi)$$

where the measurement vectors $\underline{m}_i$ and measurement matrices R_i are listed in Table 3-10.

6-Gyro System

The set of fifteen parity check equations for the 6-gyro system is given by

Failed Gyros	Parity Check Equation										Reconfiguration Solution Program	SPM Condition
	K1	K2	K3	K4	K5	K6	K7	K8	K9	K10		
None	0	0	0	0	0	0	0	0	0	0	P0	Failure detectable and faulty gyro identifiable
A	0	0	0	0	0	0	1	1	1	1	P1	
B	0	0	0	1	1	1	0	0	0	1	P2	
C	0	1	1	0	0	1	0	0	1	0	P3	
D	1	0	1	0	1	0	0	1	0	0	P4	
E	1	1	0	1	0	0	1	0	0	0	P5	
A, B	0	0	0	1	1	1	1	1	1	1	P6	
A, C	0	1	1	0	0	1	1	1	1	1	P7	
A, D	1	0	1	0	1	0	1	1	1	1	P8	
A, E	1	1	0	1	0	0	1	1	1	1	P9	
B, C	0	1	1	1	1	1	0	0	1	1	P10	
B, D	1	0	1	1	1	1	0	1	0	1	P11	
B, E	1	1	0	1	1	1	1	0	0	1	P12	
C, D	1	1	1	0	1	1	0	1	1	0	P13	
C, E	1	1	1	1	0	1	1	0	1	0	P14	
D, E	1	1	1	1	1	0	1	1	0	0	P15	
A, B, C	0	1	1	1	1	1	1	1	1	1	P16	
A, B, D	1	0	1	1	1	1	1	1	1	1	P17	
A, B, E	1	1	0	1	1	1	1	1	1	1	P18	
A, C, D	1	1	1	0	1	1	1	1	1	1	P19	
A, C, E	1	1	1	1	0	1	1	1	1	1	P20	
A, D, E	1	1	1	1	1	0	1	1	1	1	P21	
B, C, D	1	1	1	1	1	1	0	1	1	1	P22	
B, C, E	1	1	1	1	1	1	1	0	1	1	P23	
B, D, E	1	1	1	1	1	1	1	1	0	1	P24	
C, D, E	1	1	1	1	1	1	1	1	1	0	P25	
A, B, C, D	1	1	1	1	1	1	1	1	1	1	P26 Report total failure	Failure detection only
A, B, C, E	1	1	1	1	1	1	1	1	1	1		
A, B, D, E	1	1	1	1	1	1	1	1	1	1		
A, C, D, E	1	1	1	1	1	1	1	1	1	1		
B, C, D, E	1	1	1	1	1	1	1	1	1	1		
A, B, C, D, E	1	1	1	1	1	1	1	1	1	1		

Table 3-9. Truth table for failure detection and faulty gyro identification, with reconfiguration solution programs indicated for 5-gyro system.

Reconfiguration Solution Program	$\underline{m}_i$ and R_i are obtained from $\underline{m}$ and R by removing the following rows from Eq. (3-22)
P1	1, 2
P2	3, 4
P3	5, 6
P4	7, 8
P5	9, 10
P6	1, 2, 3, 4
P7	1, 2, 5, 6
P8	1, 2, 7, 8
P9	1, 2, 1, 10
P10	3, 4, 5, 6
P11	3, 4, 7, 8
P12	3, 4, 9, 10
P13	5, 6, 7, 8
P14	5, 6, 9, 10
P15	7, 8, 9, 10
P16	1, 2, 3, 4, 5, 6
P17	1, 2, 3, 4, 7, 8
P18	1, 2, 3, 4, 9, 10
P19	1, 2, 5, 6, 7, 8
P20	1, 2, 5, 6, 9, 10
P21	1, 2, 7, 8, 9, 10
P22	3, 4, 5, 6, 7, 8
P23	3, 4, 5, 6, 9, 10
P24	3, 4, 7, 8, 9, 10
P25	5, 6, 7, 8, 9, 10

Table 3-10. Vector $\underline{m}_i$ and matrices R_i for reconfiguration programs for the 5-gyro system.

$$
\left.
\begin{aligned}
& m_{10} + c\, m_9 - m_{12} - c\, m_{11} \simeq 0 \\
& m_8 + c\, m_7 - m_{12} - c\, m_{11} \simeq 0 \\
& m_8 + c\, m_7 - m_{10} - c\, m_9 \simeq 0 \\
& m_5 - m_{11} \quad 0 \\
& m_{10} - c\, m_5 - c\, m_6 \simeq 0 \\
& m_6 - m_7 \simeq 0 \\
& m_4 - m_{11} \simeq 0 \\
& m_3 - m_9 \simeq 0 \\
& m_8 - c\, m_3 - c\, m_4 \simeq 0 \\
& m_4 - m_5 \simeq 0 \\
& m_{12} - c\, m_1 - c\, m_2 \simeq 0 \\
& m_2 - m_9 \simeq 0 \\
& m_1 - m_7 \simeq 0 \\
& m_1 - m_6 \simeq 0 \\
& m_2 - m_3 \simeq 0
\end{aligned}
\right\} \qquad (3\text{-}23)
$$

The truth table for the identification of faulty gyros are shown in Table 3-11 where the reconfiguration solution program for each abnormal condition is also shown. The data reduction equation for the normal condition where all gyros are good is again given by Eq. (PO). But here

Failed Gyros	Parity Check Equations															Reconfiguration Solution Program	SPM Condition
	K1	K2	K3	K4	K5	K6	K7	K8	K9	K10	K11	K12	K13	K14	K15		
None	0	0	0	0	0	0	0	0	0	0	0	0	0	0	0	P0	Failure detectable and faulty gyros identifiable
A	0	0	0	0	0	0	0	0	0	0	1	1	1	1	1	P1	
B	0	0	0	0	0	0	1	1	1	1	0	0	0	0	1	P2	
C	0	0	0	1	1	1	0	0	0	1	0	0	0	1	0	P3	
D	0	1	1	0	0	1	0	0	1	0	0	0	1	0	0	P4	
E	1	0	1	0	1	0	0	1	0	0	0	1	0	0	0	P5	
F	1	1	0	1	0	0	1	0	0	0	1	0	0	0	0	P6	
A, B	0	0	0	0	0	0	1	1	1	1	1	1	1	1	1	P7	
A, C	0	0	0	1	1	1	0	0	0	1	1	1	1	1	1	P8	
A, D	0	1	1	0	0	1	0	0	1	0	1	1	1	1	1	P9	
A, E	1	0	1	0	1	0	0	1	0	0	1	1	1	1	1	P10	
A, F	1	1	0	1	0	0	1	0	0	0	1	1	1	1	1	P11	
B, C	0	0	0	1	1	1	1	1	1	1	0	0	0	1	1	P12	
B, D	0	1	1	0	0	1	1	1	1	1	0	0	1	0	1	P13	
B, E	1	0	1	0	1	0	1	1	1	1	0	1	0	0	1	P14	
B, F	1	1	0	1	0	0	1	1	1	1	0	0	0	0	1	P15	
C, D	0	1	1	1	1	1	0	0	1	1	0	0	1	1	0	P16	
C, E	1	0	1	1	1	1	0	1	0	1	1	1	0	1	0	P17	
C, F	1	1	0	1	1	1	1	0	0	1	1	0	0	1	0	P18	
D, E	1	1	1	0	1	1	0	1	1	0	0	1	1	0	0	P19	
D, F	1	1	1	1	0	1	1	0	1	0	1	0	1	0	0	P20	
E, F	1	1	1	1	1	0	1	1	0	0	1	1	0	0	0	P21	
A, B, C	0	0	0	1	1	1	1	1	1	1	1	1	1	1	1	P22	
A, B, D	0	1	1	0	0	1	1	1	1	1	1	1	1	1	1	P23	
A, B, E	1	0	1	0	1	0	1	1	1	1	1	1	1	1	1	P24	
A, B, F	1	1	0	1	0	0	1	1	1	1	1	1	1	1	1	P25	
A, C, D	0	1	1	1	1	1	0	0	1	1	1	1	1	1	1	P26	
A, C, E	1	0	1	1	1	1	0	1	0	1	1	1	1	1	1	P27	
A, C, F	1	1	0	1	1	1	1	0	0	1	1	1	1	1	1	P28	
A, D, E	1	1	1	0	1	1	0	1	1	0	1	1	1	1	1	P29	
A, D, F	1	1	1	1	0	1	1	0	1	0	1	1	1	1	1	P30	
A, E, F	1	1	1	1	1	0	1	1	0	0	1	1	1	1	1	P31	
B, C, D	0	1	1	1	1	1	1	1	1	1	0	0	1	1	1	P32	
B, C, E	1	0	1	1	1	1	1	1	1	1	0	1	0	1	1	P33	
B, C, F	1	1	0	1	1	1	1	1	1	1	1	0	0	1	1	P34	
B, D, E	1	1	1	0	1	1	1	1	1	1	0	1	1	0	1	P35	
B, D, F	1	1	1	1	0	1	1	1	1	1	1	0	1	0	1	P36	
B, E, F	1	1	1	1	1	0	1	1	1	1	1	1	0	0	1	P37	
C, D, E	1	1	1	1	1	1	0	1	1	1	0	1	1	1	0	P38	
C, D, F	1	1	1	1	1	1	1	0	1	1	1	0	1	1	0	P39	
C, E, F	1	1	1	1	1	1	1	1	0	1	1	1	0	1	0	P40	
D, E, F	1	1	1	1	1	1	1	1	1	0	1	1	1	0	0	P41	
A, B, C, D	0	1	1	1	1	1	1	1	1	1	1	1	1	1	1	P42	
A, B, D, E	1	0	1	1	1	1	1	1	1	1	1	1	1	1	1	P43	
A, B, C, F	1	1	0	1	1	1	1	1	1	1	1	1	1	1	1	P44	
A, B, D, E	1	1	1	0	1	1	1	1	1	1	1	1	1	1	1	P45	
A, B, D, F	1	1	1	1	0	1	1	1	1	1	1	1	1	1	1	P46	
A, B, E, F	1	1	1	1	1	0	1	1	1	1	1	1	1	1	1	P47	
A, C, D, E	1	1	1	1	1	1	0	1	1	1	1	1	1	1	1	P48	
A, C, D, F	1	1	1	1	1	1	1	0	1	1	1	1	1	1	1	P49	
A, C, E, F	1	1	1	1	1	1	1	1	0	1	1	1	1	1	1	P50	
A, D, E, F	1	1	1	1	1	1	1	1	1	0	1	1	1	1	1	P51	
B, C, D, E	1	1	1	1	1	1	1	1	1	1	0	1	1	1	1	P52	
B, C, D, F	1	1	1	1	1	1	1	1	1	1	1	0	1	1	1	P53	
B, C, E, F	1	1	1	1	1	1	1	1	1	1	1	1	0	1	1	P54	
B, D, E, F	1	1	1	1	1	1	1	1	1	1	1	1	1	0	1	P55	
C, D, E, F	1	1	1	1	1	1	1	1	1	1	1	1	1	1	0	P56	
A, B, C, D, E	1	1	1	1	1	1	1	1	1	1	1	1	1	1	1	P57 Report total failure	Failure detectable only
A, B, C, D, F	1	1	1	1	1	1	1	1	1	1	1	1	1	1	1		
A, B, C, E, F	1	1	1	1	1	1	1	1	1	1	1	1	1	1	1		
A, B, D, E, F	1	1	1	1	1	1	1	1	1	1	1	1	1	1	1		
A, C, D, E, F	1	1	1	1	1	1	1	1	1	1	1	1	1	1	1		
B, C, D, E, F	1	1	1	1	1	1	1	1	1	1	1	1	1	1	1		
A, B, C, D, E, F	1	1	1	1	1	1	1	1	1	1	1	1	1	1	1		

Table 3-11. Truth table for failure detection and faulty gyro identification, with reconfiguration solution program indicated, for the 6-gyro system.

$$R = \begin{bmatrix} 1 & 0 & 0 \\ 0 & 1 & 0 \\ 0 & 1 & 0 \\ 0 & 0 & 1 \\ 0 & 0 & 1 \\ 1 & 0 & 0 \\ 1 & 0 & 0 \\ 0 & c & c \\ 0 & 1 & 0 \\ c & 0 & c \\ 0 & 0 & 1 \\ c & c & 0 \end{bmatrix} \quad \text{and } \underline{m} = \begin{bmatrix} m_1 \\ m_2 \\ m_3 \\ m_4 \\ m_5 \\ m_6 \\ m_7 \\ m_8 \\ m_9 \\ m_{10} \\ m_{11} \\ m_{12} \end{bmatrix} \qquad (3\text{-}24)$$

There are sixty-three abnormal conditions, of which only fifty-six are identifiable. Each reconfiguration solution program for data reduction has the form

$$\underline{\omega} = (R_i^T R_i)^{-1} R_i^T \underline{m}_i \quad i = 1 \sim 56 \qquad (Pi)$$

where the measurement vectors $\underline{m}_i$ and measurement matrices R_i are listed in Table 3-12.

Reconfiguration Solution Program	$\underline{m}_i$ and R_i are obtained from $\underline{m}$ and R by removing the following rows from Eq. (3-24).
P1	1, 2
P2	3, 4
P3	5, 6
P4	7, 8
P5	9, 10
P6	11, 12
P7	1, 2, 3, 4
P8	1, 2, 5, 6
P9	1, 2, 7, 8
P10	1, 2, 9, 10
P11	1, 2, 11, 12
P12	3, 4, 5, 6
P13	3, 4, 7, 8
P14	3, 4, 9, 10
P15	3, 4, 11, 12
P16	5, 6, 7, 8
P17	5, 6, 9, 10
P18	5, 6, 11, 12
P19	7, 8, 9, 10
P20	7, 8, 11, 12
P21	9, 10, 11, 12
P22	1, 2, 3, 4, 5, 6
P23	1, 2, 3, 4, 7, 8
P24	1, 2, 3, 4, 9, 10
P25	1, 2, 3, 4, 11, 12
P26	1, 2, 5, 6, 7, 8
P27	1, 2, 5, 6, 9, 10
P28	1, 2, 5, 6, 11, 12
P29	1, 2, 7, 8, 9, 10
P30	1, 2, 7, 8, 11, 12
P31	1, 2, 9, 10, 11, 12
P32	3, 4, 5, 6, 7, 8
P33	3, 4, 5, 6, 9, 10
P34	3, 4, 5, 6, 11, 12
P35	3, 4, 7, 8, 9, 10
P36	3, 4, 7, 8, 11, 12
P37	3, 4, 9, 10, 11, 12
P38	5, 6, 7, 8, 9, 10
P39	5, 6, 7, 8, 11, 12
P40	5, 6, 9, 10, 11, 12
P41	7, 8, 9, 10, 11, 12
P42	1, 2, 3, 4, 5, 6, 7, 8
P43	1, 2, 3, 4, 5, 6, 9, 10
P44	1, 2, 3, 4, 5, 6, 11, 12
P45	1, 2, 3, 4, 7, 8, 9, 10
P46	1, 2, 3, 4, 7, 8, 11, 12
P47	1, 2, 3, 4, 9, 10, 11, 12
P48	1, 2, 5, 6, 7, 8, 9, 10
P49	1, 2, 5, 6, 7, 8, 11, 12
P50	1, 2, 5, 6, 9, 10, 11, 12
P51	1, 2, 7, 8, 9, 10, 11, 12
P52	3, 4, 5, 6, 7, 8, 9, 10
P53	3, 4, 5, 6, 7, 8, 11, 12
P54	3, 4, 5, 6, 9, 10, 11, 12
P55	3, 4, 7, 8, 9, 10, 11, 12
P56	5, 6, 7, 8, 9, 10, 11, 12

Table 3-12. Vectors $\underline{m}_i$ and matrices R_i for reconfiguration programs for the 6-gyro system.

CHAPTER 4

DDA REALIZATIONS OF ATTITUDE ALGORITHMS

J.C. Hung and Y. Yeh

ABSTRACT

This chapter presents 1) a review of six attitude transformation algorithms, and 2) the realizations of these algorithms by digital differential analyzers (DDA's). The number of DDA's for each algorithm is either smaller than, or equal to that obtained by others.

INTRODUCTION

The use of strapdown platforms for the guidance and control of space vehicles has received a good deal of attention in recent years. In using a strapdown platform, the attitude of a space vehicle is measured along a coordinate frame fixed to the vehicle body. However, it is commonly desired to determine the attitude of the space vehicle with respect to a different coordinate frame, such as an inertial coordinate frame or an earth fixed coordinate frame. Therefore, a transformation of attitude information from the vehicle body frame to a desired coordinate frame is needed. Several different attitude transformation algorithms are available. The most common ones are (1) direction cosine algorithm, (2) Euler angle algorithm, (3) Euler's four parameter algorithms, (4) quaternion algorithm, (5) Cayley-Klein algorithm, and (6) Vector representation algorithm.

An analog computer, a digital computer, or a group of digital differential analyzers (DDA's) can be used to implement the attitude algorithms. The advantages of using DDA's include high accuracy and compact size.

This chapter begins with a review of the analytics for the six attitude algorithms. Then, each algorithm is realized by a group of digital differential analyzers (DDA's). It will be shown that the number of DDA's required for the realization of each algorithm is either smaller than, or equal to that obtained by others.[1,2] The different numbers of required DDA's

for various algorithms, also serve as an indirect comparison of computation requirements if the algorithms are to be realized by digital computer.

THE DDA

DDA is a device which has two incremental inputs Δx_k and Δy_k, one memory memorizing the quantity y_{k-1} and one output Δz_k. The device performs the following mathematical operation

$$\Delta z_k = (y_{k-1} + \Delta y_k)\ \Delta x_k \qquad (4\text{-}1)$$

The following symbol is used to represent a DDA. By connecting a number of

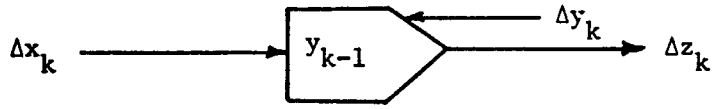

Figure 4-1. The DDA

DDA's together in conjunction with summing devices, various computation algorithms can be realized.

DIRECTION COSINE ALGORITHMS

Direction Cosine Matrix

Consider two orthogonal coordinate systems S_1 and S_2 in a three dimensional space:

$$S_1 \begin{cases} \text{Coordinates} & v_1,\ v_2,\ v_3 \\ \text{Unit Vectors} & \hat{i},\ \hat{j},\ \hat{k} \end{cases}$$

$$S_2 \begin{cases} \text{Coordinates} & v_1',\ v_2',\ v_3' \\ \text{Unit Vectors} & \hat{i}',\ \hat{k}',\ \hat{k}' \end{cases}$$

For any vector V in the space, it can be expressed in terms of coordinate components in "vector-analysis" form[3]

$$V = \hat{i}\, v_1 + \hat{j}\, v_2 + \hat{k}\, v_3 = \hat{i}'v_1' + \hat{j}'v_2' + \hat{k}'v_3' \tag{4-2}$$

By the property of dot product v_i' can be expressed in terms of v_j as

$$\left.\begin{aligned} v_1' &= \hat{i}' \cdot V = \hat{i}' \cdot \hat{i}\, v_1 + \hat{i}' \cdot \hat{j}\, v_2 + \hat{i}' \cdot \hat{k}\, v_3 \\ v_2' &= \hat{j}' \cdot V = \hat{j}' \cdot \hat{i}\, v_1 + \hat{j}' \cdot \hat{j}\, v_2 + \hat{j}' \cdot \hat{k}\, v_3 \\ v_3' &= \hat{k}' \cdot V = \hat{k}' \cdot i\, v_1 + \hat{k}' \cdot \hat{j}\, v_2 + \hat{k}' \cdot \hat{k}\, v_3 \end{aligned}\right\} \tag{4-3}$$

In "vector-matrix" form[4], we have

$$\underbrace{\begin{bmatrix} v_1' \\ v_2' \\ v_3' \end{bmatrix}}_{\underline{v}'} = \underbrace{\begin{bmatrix} \hat{i}' \cdot \hat{i} & \hat{i}' \cdot \hat{j} & \hat{i}' \cdot \hat{k} \\ \hat{j}' \cdot \hat{k} & \hat{j}' \cdot \hat{j} & \hat{j}' \cdot \hat{k} \\ \hat{k}' \cdot \hat{i} & \hat{k}' \cdot \hat{j} & \hat{k}' \cdot \hat{k} \end{bmatrix}}_{C} \underbrace{\begin{bmatrix} v_1 \\ v_2 \\ v_3 \end{bmatrix}}_{\underline{v}} \tag{4-4}$$

where $\underline{v}$ is a column vector whose three elements are components of V along coordinate system S_1 and $\underline{v}'$ is a column vector whose three elements are components of V along coordinate system S_2 The matrix C is called the "direction cosine matrix", whose elements are cosines of angles between two sets of unit vectors of S_1 and S_2. Thus (4-4) can be written as

$$\underline{v}' = C\, \underline{v} \tag{4-5}$$

A similar derivation by expressing v_j in terms of v_i' gives

$$\underline{v} = C^T\, \underline{v}' \tag{4-6}$$

Using both (4-5) and (4-6),

$$\underline{v} = C^T C \, \underline{v}$$

that is

$$C^T C = I \tag{4-7}$$

Hence, C is an orthogonal matrix. Denote the elements in C by C_{ij}, Eq. (4-7) says that

$$\sum_{k=1}^{3} C_{mk} C_{kn} = \begin{cases} 1 \text{ if } m = n \\ 0 \text{ if } m \neq n \end{cases} \tag{4-8}$$

which is a set of six constraint equations. Therefore, among the nine elements of C, only three are independent.

An Example: A two dimensional case.

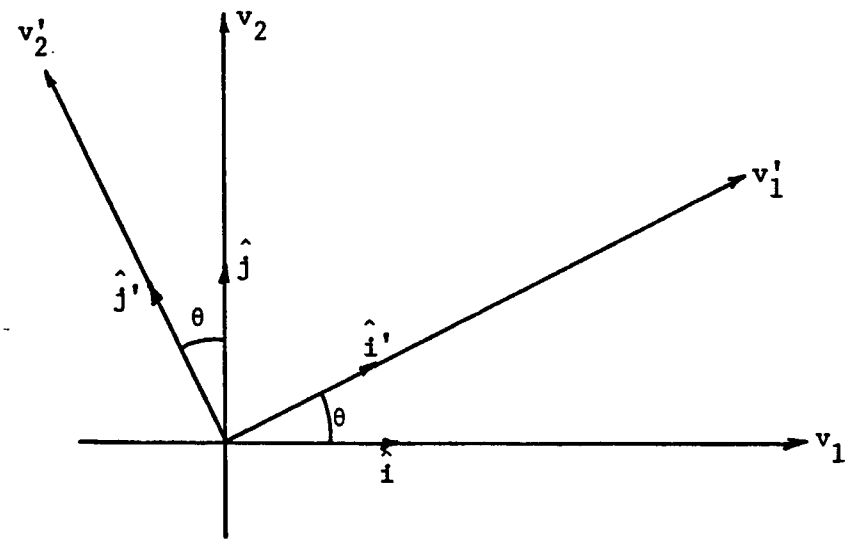

Figure 4-2. The Two Dimensional Case.

$$\begin{bmatrix} v_1' \\ v_2' \end{bmatrix} = \begin{bmatrix} \hat{i}' \cdot \hat{i} & \hat{i}' \cdot \hat{j} \\ \hat{j}' \cdot \hat{i} & \hat{j}' \cdot \hat{j} \end{bmatrix} \begin{bmatrix} v_1 \\ v_2 \end{bmatrix}$$

$$= \begin{bmatrix} \cos\theta & \cos(90+\theta) \\ \cos(90+\theta) & \cos\theta \end{bmatrix} \begin{bmatrix} v_1 \\ v_2 \end{bmatrix}$$

$$= \begin{bmatrix} \cos\theta & \sin\theta \\ -\sin\theta & \cos\theta \end{bmatrix} \begin{bmatrix} v_1 \\ v_2 \end{bmatrix}$$

Relationship Between Two Sets of Unit Vectors

Consider a vector V making angles α, β, and γ with the set of unit vectors $\hat{i}$, $\hat{j}$, and $\hat{k}$, respectively, as represented by

$$V = \hat{i}\cos\alpha + \hat{j}\cos\beta + \hat{k}\cos\gamma \qquad (4\text{-}9)$$

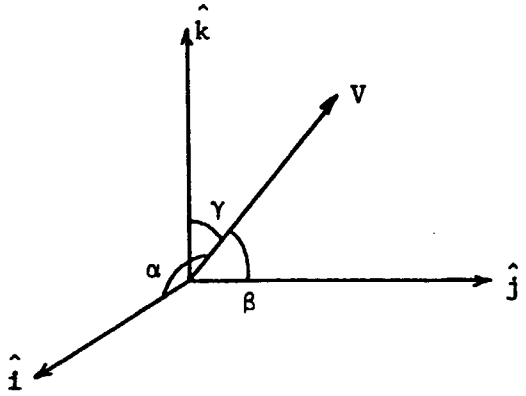

Figure 4-3. Angles α, β, and γ.

Since $\cos^2\alpha + \cos^2\beta + \cos^2\gamma = 1$, V is also a unit vector. If we let $V = \hat{i}'$, $\hat{j}'$, and then $\hat{k}'$, we have the relationship between the two sets of unit vectors.

$$\left.\begin{aligned}
\hat{i}' &= (\hat{i}' \cdot \hat{i})\,\hat{i} + (\hat{i}' \cdot \hat{j})\,\hat{j} + (\hat{i}' \cdot \hat{k})\,\hat{k} \\
\hat{j}' &= (\hat{j}' \cdot \hat{i})\,\hat{i} + (\hat{j}' \cdot \hat{j})\,\hat{j} + (\hat{j}' \cdot \hat{k})\,\hat{k} \\
\hat{k}' &= (\hat{k}' \cdot \hat{i})\,\hat{i} + (\hat{k}' \cdot \hat{j})\,\hat{j} + (\hat{k}' \cdot \hat{k})\,\hat{k}
\end{aligned}\right\} \qquad (4\text{-}10)$$

Representing the two sets of unit vectors by

$$U = \begin{bmatrix} \hat{i} \\ \hat{j} \\ \hat{k} \end{bmatrix} \quad \text{and} \quad U' = \begin{bmatrix} \hat{i}' \\ \hat{j}' \\ \hat{k}' \end{bmatrix} \qquad (4\text{-}11)$$

(4-10) can be expressed as

$$U' = CU \qquad (4\text{-}12)$$

where C is defined in (4-4). Notice that U and U' are not vectors; their elements are unit vectors!

Now consider any vector V. From (4-2)

$$V = \underbrace{[v_1\ v_2\ v_3]}_{\underline{v}^T} \underbrace{\begin{bmatrix} \hat{i} \\ \hat{j} \\ \hat{k} \end{bmatrix}}_{U} = \underbrace{[v_1'\ v_2'\ v_2']}_{\underline{v}'^T} \underbrace{\begin{bmatrix} \hat{i}' \\ \hat{j}' \\ \hat{k}' \end{bmatrix}}_{U'} \qquad (4\text{-}13)$$

or simply

$$V = \underline{v}^T U = \underline{v}'^T U' \quad .$$

Using (4-12)

$$\underline{v}'^T U' = \underline{v}^T U = v^T C^T U'$$

indicating

$$\underline{v}'^T = \underline{v}^T C^T$$

therefore

$$\underline{v}' = C\,\underline{v} \qquad (4\text{-}14)$$

which is the same as (4-5).

Differential Equation of Direction Cosine Matrix

Let S_1 frame with unit vectors $\hat{i}$, $\hat{j}$, and $\hat{k}$ be stationary, and S_2 frame with unit vectors $\hat{i}'$, $\hat{j}'$, and $\hat{k}'$ be rotating. Let

$$\underline{\omega} = \begin{bmatrix} \omega_x \\ \omega_y \\ \omega_z \end{bmatrix}$$

be the angular velocity of S_2 with respect to S_1 expressed along S_2 axes, and C be the "direct cosine matrix" transforming S_2 coordinates to S_1 coordinates, i.e.,

$$C = \begin{bmatrix} C_{11} & C_{12} & C_{13} \\ C_{21} & C_{22} & C_{23} \\ C_{31} & C_{32} & C_{33} \end{bmatrix} = \begin{bmatrix} \hat{i} \cdot \hat{i}' & \hat{i} \cdot \hat{j}' & \hat{i} \cdot \hat{k}' \\ \hat{j} \cdot \hat{i}' & \hat{j} \cdot \hat{j}' & \hat{j} \cdot \hat{k}' \\ \hat{k} \cdot \hat{i}' & \hat{k} \cdot \hat{j}' & \hat{k} \cdot \hat{k}' \end{bmatrix} \qquad (4\text{-}15)$$

Note that this C is different from that in (4-4)! One is the transpose of the other.

$$\dot{C} = \begin{bmatrix} \dot{C}_{11} = \hat{i} \cdot \frac{d\hat{i}'}{dt} & \dot{C}_{12} = \hat{i} \cdot \frac{d\hat{j}'}{dt} & \dot{C}_{13} = \hat{i} \cdot \frac{d\hat{k}'}{dt} \\ = \hat{i} \cdot (\hat{j}'\omega_z - \hat{k}'\omega_y) & = \hat{i} \cdot (\hat{k}'\omega_x - \hat{i}'\omega_z) & = \hat{i} \cdot (\hat{i}'\omega_y - \hat{j}'\omega_x) \\ = C_{12}\omega_z - C_{13}\omega_y & = C_{13}\omega_x - C_{11}\omega_z & = C_{11}\omega_y - C_{12}\omega_x \\ \dot{C}_{21} = \hat{j} \cdot \frac{d\hat{i}'}{dt} & \dot{C}_{22} = \hat{j} \cdot \frac{d\hat{j}'}{dt} & \dot{C}_{23} = \hat{j} \cdot \frac{d\hat{k}'}{dt} \\ = \hat{j} \cdot (\hat{j}'\omega_z - \hat{k}'\omega_y) & = \hat{j} \cdot (\hat{k}'\omega_x - \hat{i}'\omega_z) & = \hat{j} \cdot (\hat{i}'\omega_y - \hat{j}'\omega_x) \\ = C_{22}\omega_z - C_{23}\omega_y & = C_{23}\omega_x - C_{21}\omega_z & = C_{21}\omega_y - C_{22}\omega_x \\ \dot{C}_{31} = \hat{k} \cdot \frac{d\hat{i}'}{dt} & \dot{C}_{32} = \hat{k} \cdot \frac{d\hat{j}'}{dt} & \dot{C}_{33} = \hat{k} \cdot \frac{d\hat{k}'}{dt} \\ = \hat{k} \cdot (\hat{j}'\omega_z - \hat{k}'\omega_y) & = \hat{k} \cdot (\hat{k}'\omega_x - \hat{i}'\omega_z) & = \hat{k} \cdot (\hat{i}'\omega_y - \hat{j}'\omega_x) \\ = C_{32}\omega_z - C_{33}\omega_y & = C_{33}\omega_x - C_{31}\omega_z & = C_{31}\omega_y - C_{32}\omega_x \end{bmatrix}$$

$$= \begin{bmatrix} C_{11} & C_{12} & C_{13} \\ C_{21} & C_{22} & C_{23} \\ C_{31} & C_{32} & C_{33} \end{bmatrix} \underbrace{\begin{bmatrix} 0 & -\omega_z & \omega_y \\ \omega_z & 0 & -\omega_x \\ -\omega_y & \omega_x & 0 \end{bmatrix}}_{\Omega}$$

Let

$$\Omega = \begin{bmatrix} 0 & -\omega_z & \omega_y \\ \omega_z & 0 & -\omega_x \\ -\omega_y & \omega_x & 0 \end{bmatrix} \tag{4-16}$$

be the matrix characterizing the angular velocity of the S_2 frame with respect to the S_1 frame. Then we have

$$\dot{C} = C\,\Omega \tag{4-17}$$

Any vector in S_2 coordinates can then be transformed to S_1 coordinates via

$$\underline{v}_{s1} = C\,\underline{v}_{s2} \tag{4-18}$$

In a strapdown navigation system, ω_x, ω_y, and ω_z are measured by a set of strapdown rate gyros. The transformation from $\underline{v}_{s2}$ to $\underline{v}_{s1}$ is represented by the diagram shown in Fig. 4-4.

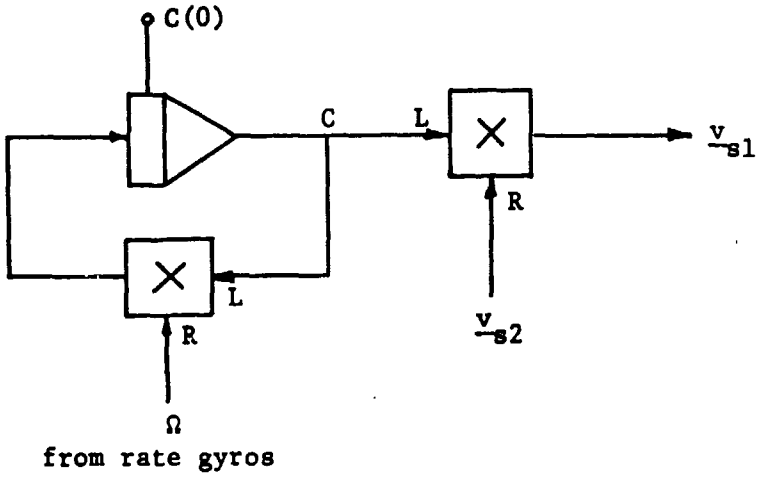

Figure 4-4. Direction Cosine Transformation.

The symbol

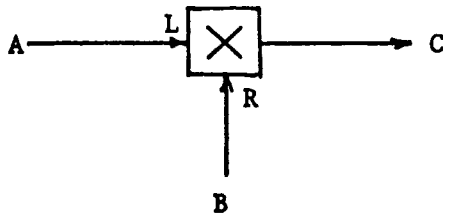

indicates the matrix multiplication C = AB.

EULER ANGLE TRANSFORMATION ALGORITHM

Euler Angle Transformation Matrix[5]

Two coordinate systems (X, Y, Z) and (x, y, z) can be related by three rotations of coordinates as shown in Fig. 4-5.

First, rotate along Z axis by an angle ϕ.

Next, rotate along x_1 axis by an angle θ .

Finally, rotate along z_2 axis by an angle ψ.

The angle ϕ, θ, and ψ are called "Euler angles", and the three successive transformations are represented by the following equations

$$\begin{bmatrix} x_1 \\ y_1 \\ z_1 \end{bmatrix} = \underbrace{\begin{bmatrix} \cos\phi & \sin\phi & 0 \\ -\sin\phi & \cos\phi & 0 \\ 0 & 0 & 1 \end{bmatrix}}_{\Gamma_\phi} \begin{bmatrix} X \\ Y \\ Z \end{bmatrix} \tag{4-19}$$

$$\begin{bmatrix} x_2 \\ y_2 \\ z_2 \end{bmatrix} = \underbrace{\begin{bmatrix} 1 & 0 & 0 \\ 0 & \cos\theta & \sin\theta \\ 0 & -\sin\theta & \cos\theta \end{bmatrix}}_{\Gamma_\theta} \begin{bmatrix} x_1 \\ y_1 \\ z_1 \end{bmatrix} \tag{4-20}$$

$$\begin{bmatrix} x \\ y \\ z \end{bmatrix} = \underbrace{\begin{bmatrix} \cos\psi & \sin\psi & 0 \\ -\sin\psi & \cos\psi & 0 \\ 0 & 0 & 1 \end{bmatrix}}_{\Gamma_\psi} \begin{bmatrix} x_2 \\ y_2 \\ z_2 \end{bmatrix} \tag{4-21}$$

Thus, the overall transformation is given by

$$\begin{bmatrix} x \\ y \\ z \end{bmatrix} = \Gamma \begin{bmatrix} X \\ Y \\ Z \end{bmatrix} \tag{4-22}$$

where the transformation matrix is

$$\Gamma = \Gamma_\psi \Gamma_\theta \Gamma_\phi$$

$$= \begin{bmatrix} \cos\psi \cos\phi - \cos\theta \sin\phi \sin\psi & & \\ -\sin\psi \cos\phi - \cos\theta \sin\phi \cos\psi & & \\ \sin\theta \sin\phi & & \end{bmatrix}$$

$$\begin{bmatrix} \cos\psi \sin\phi + \cos\theta \cos\phi \sin\psi & \sin\psi \sin\theta \\ -\sin\psi \sin\phi + \cos\theta \cos\phi \cos\psi & \cos\psi \sin\theta \\ -\sin\theta \cos\phi & \cos\theta \end{bmatrix} \tag{4-23}$$

Euler Angle Differential Equations

If the xyz-frame is rotating with respect to the XYZ-frame, then the Euler angles ϕ, θ, and ψ change with time. The rotation can be described as a function of their time rates, namely, $\dot{\phi}$, $\dot{\theta}$, and $\dot{\psi}$.

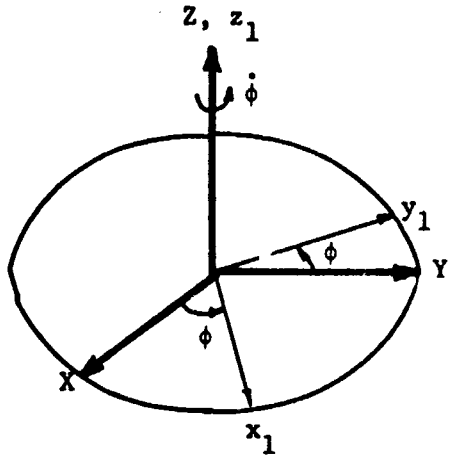

$$\begin{bmatrix} x_1 \\ y_1 \\ z_1 \end{bmatrix} = \underbrace{\begin{bmatrix} \cos\phi & \sin\phi & 0 \\ -\sin\phi & \cos\phi & 0 \\ 0 & 0 & 1 \end{bmatrix}}_{\Gamma_\phi} \begin{bmatrix} X \\ Y \\ Z \end{bmatrix}$$

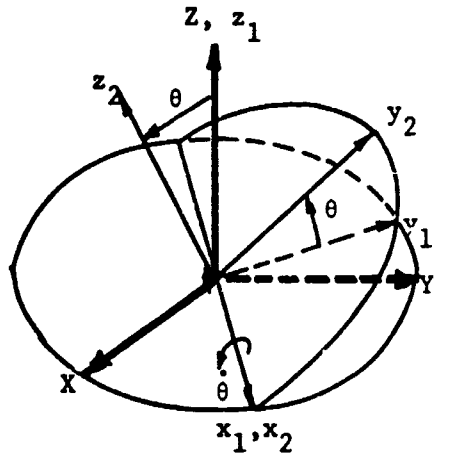

$$\begin{bmatrix} x_2 \\ y_2 \\ z_2 \end{bmatrix} = \underbrace{\begin{bmatrix} 1 & 0 & 0 \\ 0 & \cos\theta & \sin\theta \\ 0 & -\sin\theta & \cos\theta \end{bmatrix}}_{\Gamma_\theta} \begin{bmatrix} x_1 \\ y_1 \\ z_1 \end{bmatrix}$$

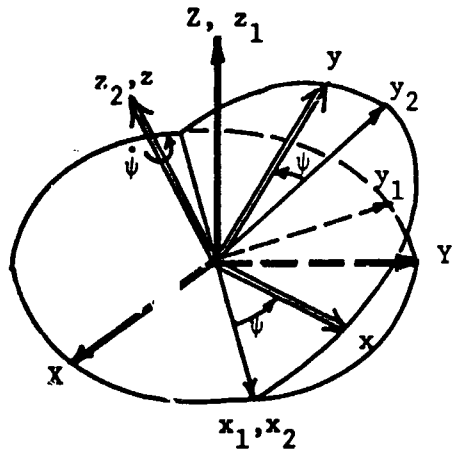

$$\begin{bmatrix} x \\ y \\ z \end{bmatrix} \quad \underbrace{\begin{bmatrix} \cos\psi & \sin\psi & 0 \\ -\sin\psi & \cos\psi & 0 \\ 0 & 0 & 1 \end{bmatrix}}_{\Gamma_\psi} \begin{bmatrix} x_2 \\ y_2 \\ z_2 \end{bmatrix}$$

Figure 4-5. Euler Angles ϕ, θ, and ψ.

Let $\underline{\omega}$ be a vector representing the angular velocity of the xyz-frame with respect to the XYZ-frame. Then

$$\underline{\omega} = \begin{bmatrix} \omega_x \\ \omega_y \\ \omega_z \end{bmatrix}$$

$$= \Gamma_\psi \Gamma_\theta \begin{bmatrix} 0 \\ 0 \\ \dot{\phi} \end{bmatrix} + \Gamma_\psi \begin{bmatrix} \dot{\theta} \\ 0 \\ 0 \end{bmatrix} + \begin{bmatrix} 0 \\ 0 \\ \dot{\psi} \end{bmatrix}$$

$$= \begin{bmatrix} \sin\psi \sin\theta & \cos\psi & 0 \\ \cos\psi \sin\theta & -\sin\psi & 0 \\ \cos\theta & 0 & 1 \end{bmatrix} \begin{bmatrix} \dot{\phi} \\ \dot{\theta} \\ \dot{\psi} \end{bmatrix} \qquad (4\text{-}24)$$

The time rates of Euler angles can be obtained by inverting (4-24)

$$\underbrace{\begin{bmatrix} \dot{\phi} \\ \dot{\theta} \\ \dot{\psi} \end{bmatrix}}_{\dot{\underline{\varepsilon}}} = \frac{1}{\sin\theta} \underbrace{\begin{bmatrix} \sin\psi & \cos\psi & 0 \\ \cos\psi \sin\theta & -\sin\psi \sin\theta & 0 \\ -\sin\psi \cos\theta & -\cos\theta \cos\psi & \sin\theta \end{bmatrix}}_{T(\underline{\varepsilon})} \underbrace{\begin{bmatrix} \omega_x \\ \omega_y \\ \omega_z \end{bmatrix}}_{\underline{\omega}} \qquad (4\text{-}25)$$

Denoting the Euler angle vector by $\underline{\varepsilon}$ and the transformation matrix by $T(\underline{\varepsilon})$ which is a function of $\underline{\varepsilon}$, we get

$$\dot{\underline{\varepsilon}} = T(\varepsilon)\, \underline{\omega} \qquad (4\text{-}26)$$

Note that, in (4-25), the transformation equation has singular points at $\theta = n\pi$, n = integer. At these values of θ, $\sin\theta = 0$ and $\frac{1}{\sin\theta}$ does not exist.

For a strapdown navigation system, the body fixed sensors measure the rates ω_x, ω_y and ω_z. The (4-26) is used to generate the Euler angle rates

and (4-22) is used to make the coordinate transformation. The computation requirement is represented by the diagram shown in Fig. 4-6.

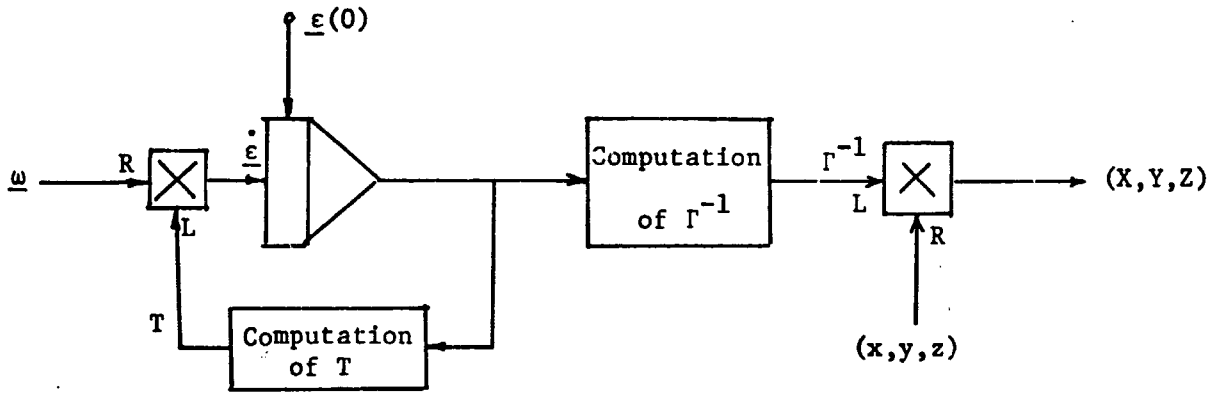

Figure 4-6. Euler Angle Transformation.

EULER FOUR PARAMETER ALGORITHM

Euler Four Parameter Transformation Matrix

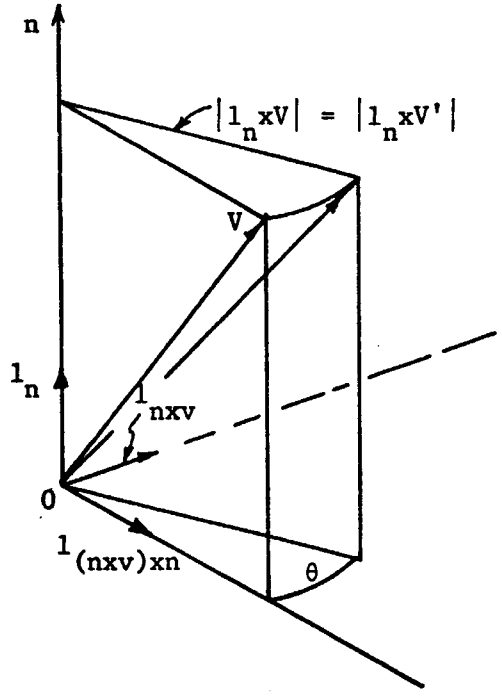

Figure 4-7. Rotation of a Vector.

Consider a vector V in space. Another vector V' is obtained by rotating V about an axis in n direction through an angle θ as shown in Fig. 4-7. Let 1_n be the unit vector in n direction, which is related to a cartesian coordinate system by

$$1_n = \eta_1 \hat{i} + \eta_2 \hat{j} + \eta_3 \hat{k} \tag{4-27}$$

where $\hat{i}$, $\hat{j}$, $\hat{k}$ are the three unit vectors of the cartesian coordinates, and η_1, η_2, η_3 are the three direction cosines of 1_n with respect to $\hat{i}$, $\hat{j}$, $\hat{k}$ as shown in Fig. 4-8.

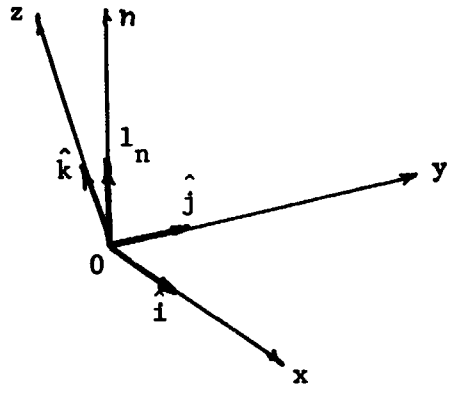

Figure 4-8. Relationship Between $\hat{i}$, $\hat{j}$, $\hat{k}$ and 1_n.

From Fig. 4-7,

$$V = (1_n \cdot V)\, 1_n + |1_n \times V|\, 1_{(nxv)xn} \tag{4-28}$$

and

$$V' = (1_n \cdot V')\, 1_n + |1_n \times V'| \cos\theta\, 1_{(nxv)xn} + |1_n \times V'| \sin\theta\, 1_{nxv} \tag{4-29}$$

Adding and subtracting $(1_n \cdot V) \cos\theta\, 1_n$ to (4-29),

$$V' = (1_n \cdot V')(1 - \cos\theta)\, 1_n + |1_n \times V'| \sin\theta\, 1_{nxv} + \underbrace{[(1_n \cdot V)\, 1_n + |1_n \times V'|\, 1_{(nxv)xn}]}_{V} \cos\theta \tag{4-30}$$

But

$$|1_n \times V'|\ 1_{nxv} = |1_n \times V|\ 1_{nxv} = 1_n \times V$$

$$1_n \cdot V' = 1_n \cdot V$$

Equation (4-30) becomes

$$V' = (1_n \cdot V)(1 - \cos\theta)\ 1_n + V\cos\theta + (1_n \times V)\sin\theta$$

Adding and subtracting V,

$$V' = V + (1_n \times V)\sin\theta + (1_n \cdot V)(1 - \cos\theta)\ 1_n - (1 - \cos\theta)\ V$$

$$= V + (1_n \times V)\sin\theta + [(1_n \cdot V)\ 1_n - V]\ (1 - \cos\theta).$$

Using the relationship

$$1_n \times (1_n \times V) = (1_n \cdot V)\ 1_n - (1_n \cdot 1_n)\ V = (1_n \cdot V)\ 1_n - V$$

we get

$$V' = V + (1_n \times V)\sin\theta + 1_n \times (1_n \times V)(1 - \cos\theta) \qquad (4\text{-}31)$$

Now let us relate the quantities in (4-31) to the cartesian coordinates and express them in the vector-matrix form.

$$\underline{v} = \begin{bmatrix} v_1 \\ v_2 \\ v_3 \end{bmatrix} \qquad \underline{v}' = \begin{bmatrix} v_1' \\ v_2' \\ v_3' \end{bmatrix} \qquad 1_n = \begin{bmatrix} \eta_1 \\ \eta_2 \\ \eta_3 \end{bmatrix}$$

We then see that

$$1_n \times V = \begin{bmatrix} \eta_2 v_3 - \eta_3 v_2 \\ \eta_3 v_1 - \eta_1 v_3 \\ \eta_1 v_2 - \eta_2 v_1 \end{bmatrix} = \begin{bmatrix} 0 & -\eta_3 & \eta_2 \\ \eta_3 & 0 & -\eta_1 \\ -\eta_2 & \eta_1 & 0 \end{bmatrix} \begin{bmatrix} v_1 \\ v_2 \\ v_3 \end{bmatrix} = N\underline{v} \qquad (4\text{-}32)$$

where

$$N = \begin{bmatrix} 0 & -\eta_3 & \eta_2 \\ \eta_3 & 0 & -\eta_1 \\ -\eta_2 & \eta_1 & 0 \end{bmatrix} \qquad (4\text{-}33)$$

is a "direction cosine matrix". Also

$$1_n \times (1_n \times V) = N^2 V \qquad (4\text{-}34)$$

Hence, (4-31) can be expressed in the form

$$V' = E\,V \qquad (4\text{-}35)$$

where

$$E = I + (\sin\theta)N + (1 - \cos\theta)N^2 \qquad (4\text{-}36)$$

is the desired "transformation matrix", which is determined by the angle of rotation θ and the direction cosine matrix N. Since N consists of three elements, three are a total of four parameters, namely, θ, η_1, η_2, and η_3. They are called "Euler four parameters". Among these four parameters, only three are independent, the fourth one can be eliminated by the relationship

$$\eta_1^2 + \eta_2^2 + \eta_3^2 = 1 \qquad (4\text{-}37)$$

Differential Equations for Euler's Four Parameters

In the next section, we shall see that the differential equations for the quaternion method of coordinate transformation is given by

$$\begin{bmatrix} \dot{s} \\ \dot{v}_x \\ \dot{v}_y \\ \dot{v}_z \end{bmatrix} = \begin{bmatrix} 0 & \frac{-\omega_x}{2} & \frac{-\omega_y}{2} & \frac{-\omega_z}{2} \\ \frac{\omega_x}{2} & 0 & -\omega_z & \omega_y \\ \frac{\omega_y}{2} & \omega_z & 0 & -\omega_x \\ \frac{\omega_z}{2} & -\omega_y & \omega_x & 0 \end{bmatrix} \begin{bmatrix} s \\ v_x \\ v_y \\ v_z \end{bmatrix} \qquad (4\text{-}38)$$

where s, v_x, v_y, and v_z are the four parameters of quaternion operator. Eq. (4-38) can also be expressed as

$$\begin{bmatrix} \dot{s} \\ \dot{v}_x \\ \dot{v}_y \\ \dot{v}_z \end{bmatrix} = \frac{1}{2} \begin{bmatrix} -v_x & -v_y & -v_z \\ s & v_z & -v_y \\ -v_z & s & v_x \\ v_y & -v_x & s \end{bmatrix} \begin{bmatrix} \omega_x \\ \omega_y \\ \omega_z \end{bmatrix} . \qquad (4\text{-}39)$$

It will also be shown in the next section that the Euler's four parameters are related to the quaternion parameters by

$$\left.\begin{aligned} \cos\frac{\theta}{2} &= s \\ \eta_1 \sin\frac{\theta}{2} &= v_x \\ \eta_2 \sin\frac{\theta}{2} &= v_y \\ \eta_3 \sin\frac{\theta}{2} &= v_z \end{aligned}\right\} \qquad (4\text{-}40)$$

Differentiating (4-40), gives

$$\begin{bmatrix} \dot{s} \\ \dot{v}_x \\ \dot{v}_y \\ \dot{v}_z \end{bmatrix} = \underbrace{\begin{bmatrix} -\frac{1}{2}\sin\frac{\theta}{2} & 0 & 0 & 0 \\ \frac{1}{2}\eta_1 \sin\frac{\theta}{2} & \sin\frac{\theta}{2} & 0 & 0 \\ \frac{1}{2}\eta_2 \sin\frac{\theta}{2} & 0 & \sin\frac{\theta}{2} & 0 \\ \frac{1}{2}\eta_3 \sin\frac{\theta}{2} & 0 & 0 & \sin\frac{\theta}{2} \end{bmatrix}}_{W} \begin{bmatrix} \dot{\theta} \\ \dot{\eta}_1 \\ \dot{\eta}_2 \\ \dot{\eta}_3 \end{bmatrix} \tag{4-41}$$

Substituting (4-41) and (4-40) to the left and right sides of (4-39), respectively, and then premultiplying both sides of the equation by W^{-1}, yields the desired differential equation

$$\begin{bmatrix} \dot{\theta} \\ \dot{\eta}_1 \\ \dot{\eta}_2 \\ \dot{\eta}_3 \end{bmatrix} = \frac{1}{2} \underbrace{\begin{bmatrix} -2\eta_1 & -2\eta_2 & -2\eta_3 \\ (1-\eta_1^2)\cot\frac{\theta}{2} & -\eta_1\eta_2\cot\frac{\theta}{2} + \eta_3 & -\eta_3\eta_1\cot\frac{\theta}{2} - \eta_2 \\ -\eta_1\eta_2\cot\frac{\theta}{2} - \eta_3 & (1-\eta_2^2)\cot\frac{\theta}{2} & -\eta_2\eta_3\cot\frac{\theta}{2} - \eta_1 \\ -\eta_3\eta_1\cot\frac{\theta}{2} + \eta_2 & -\eta_2\eta_3\cot\frac{\theta}{2} - \eta_1 & (1-\eta_3^2)\cot\frac{\theta}{2} \end{bmatrix}}_{S} \begin{bmatrix} \omega_x \\ \omega_y \\ \omega_z \end{bmatrix} \tag{4-42}$$

Equations (4-35) and (4-42) form the algorithm for the Euler four parameter transformation. The computation requirement for this algorithm is shown in Fig. 4-9.

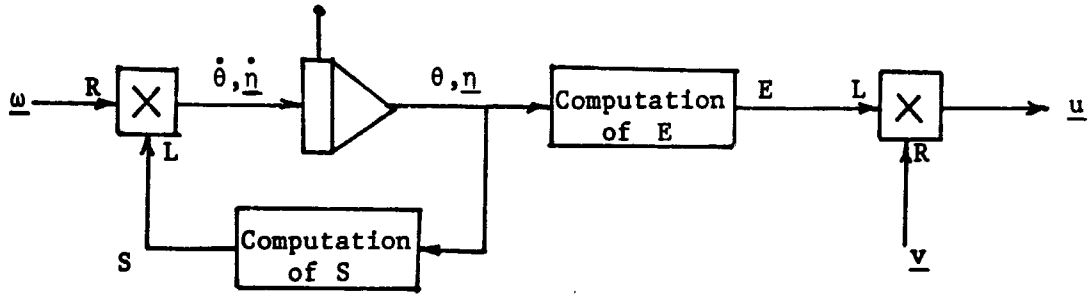

Figure 4-9. Euler's 4 Parameter Transformation.

QUATERNION ALGORITHM

Quaternion Algebra

A "quaternion" Q is defined as

$$Q = s + \hat{i}\, v_x + \hat{j}\, v_y + \hat{k}\, v_z = s + V \tag{4-43}$$

where s is a scalar and $V = \hat{i}\, v_x + \hat{j}\, v_y + \hat{k}\, v_z$ is a vector.

"Addition" for quaternions is defined as

$$\begin{aligned} Q_1 + Q_2 &= (s_1 + s_2) + (V_1 + V_2) \\ &= (s_1 + s_2) + \hat{i}\,(v_{1x} + v_{2x}) + \hat{j}\,(v_{1y} + v_{2y}) + \hat{k}\,(v_{1x} + v_{2z}) \end{aligned} \tag{4-44}$$

It is obvious that addition is associative and commutative.

"Equality" is defined as

$$Q_1 = Q_2 \quad \text{if only if} \quad s_1 = s_2 \quad \& \quad V_1 = V_2 \tag{4-45}$$

"Multiplication" is defined by using the distributive law on the elements as in ordinary algebra, but with the order preserved, and by defining the products of unit vectors $\hat{i}$, $\hat{j}$, $\hat{k}$ as

$$\begin{gathered} \hat{i}^2 = \hat{j}^2 = \hat{k}^2 = -1 \\ \hat{i}\hat{j} = -\hat{j}\hat{i} = \hat{k} \quad \hat{j}\hat{k} = -\hat{k}\hat{j} = \hat{i} \quad \hat{k}\hat{i} = -\hat{i}\hat{k} = \hat{j} \end{gathered} \tag{4-46}$$

We can then write

$$\begin{aligned} Q_1 Q_2 &= (s_1 + V_1)(s_2 + V_2) \\ &= s_1 s_2 + s_1 V_2 + s_2 V_1 + V_1 V_2 \end{aligned}$$

But

$$V_1 V_2 = (\hat{i}\, v_{1x} + \hat{j}\, v_{1y} + \hat{k}\, v_{1z})(\hat{i}\, v_{2x} + \hat{j}\, v_{2y} + \hat{k}\, v_{2z})$$

$$= - v_{1x}v_{2x} - v_{1y}v_{2y} - v_{1z}v_{2z}$$

$$+ \hat{i}\, v_{1y}v_{2z} - \hat{i}\, v_{1z}v_{2y}$$

$$+ \hat{j}\, v_{2x}v_{1z} - \hat{j}\, v_{1x}v_{2z}$$

$$+ \hat{k}\, v_{1x}v_{2y} = \hat{k}\, v_{1y}v_{2x}$$

$$= - (V_1 \cdot V_2) + (V_1 \times V_2) \quad ,$$

therefore

$$Q_1Q_2 = [s_1s_2 - V_1 \cdot V_2] + [s_1V_2 + s_2V_1 + V_1 \times V_2] \qquad (4\text{-}47)$$

Note (i) the product of quaternions is defined differently from both of the dot and the cross products associated with pure vectors, (ii) the product of quaternions is not commutative due to the term $V_1 \times V_2$ in (4-47), and (iii) the multiplication is distributive and associative, i.e.

$$Q_1(Q_2 + Q_3) = Q_1Q_2 + Q_1Q_3$$

$$Q_1(Q_2\, Q_3) = (Q_1\, Q_2)\, Q_3$$

"Conjugate" Q^* of Q is defined as

$$Q^* = s - V \qquad (4\text{-}48)$$

The conjugate of product is the product of conjugate in reverse order, i.e.

$$[Q_1Q_2]^* = [(s_1s_2 - V \cdot V) + (s_1V_2 + s_2V_1 + V_1 \times V_2)]^*$$

$$= (s_1s_2 - V_1 \cdot V_2) - (s_1V_2 + s_2V_1 + V_1 \times V_2)$$

$$= Q_2^*\, Q_1^*$$

"Norm" of a quaternion, $N(Q)$, is a scalar defined as

$$N(Q) = s^2 + v_x^2 + v_y^2 + v_z^2 = QQ^* \tag{4-49}$$

A unit norm is defined as $N(Q) = 1$. The norm of the product is the product of the norms, i.e.,

$$N(Q_1Q_2) = (Q_1Q_2)(Q_1Q_2)^* = Q_1Q_2Q_2^*Q_1^*$$

$$= Q_1\, N(Q_2)Q_1^* = N(Q_2)Q_1Q_1^* = N(Q_2)\, N(Q_1)$$

"Inverse" Q^{-1} of Q is defined as

$$Q^{-1}Q = QQ^{-1} = 1 \tag{4-50}$$

Since $N(Q) = QQ^* = Q^*Q$, so

$$Q^{-1} = \frac{Q^*}{N(Q)} \tag{4-51}$$

For a unit quaternion, $N(Q) = 1$, so $Q^{-1} = Q^*$

Quaternion as Transformation Operator

Let

$$Q = s + V \quad \text{and} \quad N(Q) = 1 \ . \tag{4-52}$$

Consider two vectors A and B related by quaternion operator Q via

$$A = QBQ^* \tag{4-53}$$

Now

$$QBQ^* = (s + V)\, B\, (s - V)$$

$$= (s + V)\, [B \cdot V + (sB - B \times V)]$$

$$= s\,(B \cdot V) - V \cdot (sB - B \times V) + V \times (sB - B \times V)$$

$$+ s\,(sB - B \times V) + V\,(B \cdot V)$$

$$= s^2B + 2sV \times B + (B \cdot V)\, V - V \times (B \times V)$$

Adding and subtracting v^2B, where

$$v^2 = V \cdot V = v_x^2 + v_y^2 + v_z^2$$

then

$$QBQ^* = (s^2 + v^2)B + 2sV \times B + V \times (V \times B)$$

$$+ \underbrace{(B \cdot V)V - (V \cdot V)B]}_{V \times (V \times B)}$$

$$= (s^2 + v^2)B + 2sV \times B + 2V \times (V \times B)$$

from (4-52), $s^2 + v^2 = 1$, therefore (4-53) becomes

$$A = B + 2sV \times B + 2V \times (V \times B) \qquad (4\text{-}54)$$

Expressing (4-54) in the vector-matrix notation in terms of cartesian coordinates x, y, z, using the following correspondences

$$A \longleftrightarrow \underline{a} = \begin{bmatrix} a_x \\ a_y \\ a_z \end{bmatrix}$$

$$B \longleftrightarrow \underline{b} = \begin{bmatrix} b_x \\ b_y \\ b_z \end{bmatrix}$$

$$V \longleftrightarrow \underline{v} = \begin{bmatrix} v_x \\ v_y \\ v_z \end{bmatrix}.$$

$$V \times B \longleftrightarrow \begin{bmatrix} 0 & -v_z & v_y \\ v_z & 0 & -v_x \\ -v_y & v_x & 0 \end{bmatrix} \begin{bmatrix} b_x \\ b_y \\ b_z \end{bmatrix} \tag{4-55}$$

Let

$$P = \begin{bmatrix} 0 & -v_z & v_y \\ v_z & 0 & -v_x \\ -v_y & v_x & 0 \end{bmatrix} \tag{4-56}$$

$$V \times (V \times B) \longleftrightarrow P^2 \underline{b} \tag{4-57}$$

Then (4-54) becomes

$$\underline{a} = \underbrace{[I + 2\,s\,P + 2\,P^2]}_{W}\,\underline{b} \tag{4-58}$$

Let

$$W = I + 2\,s\,P + 2\,P^2 \tag{4-59}$$

Then (4-58) becomes

$$\underline{a} = K\,\underline{b} \tag{4-60}$$

Eq. (4-58) or (4-60) relates vectors $\underline{a}$ and $\underline{b}$ through the matrix transformation W which is composed of four paramaters s, v_x, v_y and v_z.

Isomorphism Between Quaternion and Direction Cosine Transformation

Quaternion	Direction Cosine
$U' = Q_1 \, U \, Q_1^*$	$\underline{u}' = C_1 \, \underline{u}$
$U'' = Q_2 \, U' \, Q_2^*$	$\underline{u}'' = C_2 \, \underline{u}'$
$U'' = Q_2 Q_1 \, U \, Q_1^* Q_2^*$	$\underline{u}'' = C_2 C_1 \underline{u}$
$= (Q_2 Q_1) \, U \, (Q_2 Q_1)^*$	$= C \, \underline{u}$
$= Q \, U \, Q^*$	
$Q = Q_2 Q_1$	$C = C_2 C_1$

Hence, there exists a one-to-one correspondence between direction cosine matrices and quaternion transformation elements.

Equivalence of Quaternion and Euler's 4-Parameter Method

Recall (4-58) the quaternion transformation equation,

$$\underline{a} = [I + 2sP + 2P^2] \, \underline{b} \tag{4-61}$$

where

$$\cdot = \begin{bmatrix} 0 & -v_z & v_y \\ v_z & 0 & -v_x \\ -v_y & v_x & 0 \end{bmatrix} \tag{4-62}$$

Also, recall (4-35), the Euler 4-parameter transformation equation,

$$\underline{a} = [I + (\sin\theta) \, N + (1 - \cos\theta) \, N^2] \, \underline{b} \tag{4-63}$$

where

$$N = \begin{bmatrix} 0 & -\eta_3 & \eta_2 \\ \eta_3 & 0 & -\eta_1 \\ -\eta_2 & \eta_1 & 0 \end{bmatrix} \tag{4-64}$$

Substituting (4-62) into (4-61), we get, for the quaternion method,

$$\underline{a} = \left\{ \begin{bmatrix} 1 & 0 & 0 \\ 0 & 1 & 0 \\ 0 & 0 & 1 \end{bmatrix} + 2s \begin{bmatrix} 0 & -v_z & v_y \\ v_z & 0 & -v_x \\ -v_y & v_x & 0 \end{bmatrix} + 2 \begin{bmatrix} -v_z^2-v_y^2 & v_x v_y & v_x v_z \\ v_x v_y & -v_x^2-v_z^2 & v_y v_z \\ v_x v_z & v_z v_y & -v_y^2-v_x^2 \end{bmatrix} \right\} \underline{b}$$

$$\begin{bmatrix} 1 - 2(v_z^2+ v_y^2) & 2(-s\, v_z+ v_x v_y) & 2(s\, v_y+ v_x v_z) \\ 2(s\, v_z+ v_x v_y) & 1 - 2(v_z^2+ v_x^2) & 2(-s\, v_x+ v_z v_y) \\ 2(-s\, v_y+ v_x v_z) & 2(s\, v_x+ v_z v_y) & 1 - 2(v_y^2+ v_x^2) \end{bmatrix} \underline{b} \tag{4-65}$$

Substituting (4-64) into (4-65) gives for the Euler 4-parameter method,

$$\underline{a} = \left\{ \begin{bmatrix} 1 & 0 & 0 \\ 0 & 1 & 0 \\ 0 & 0 & 1 \end{bmatrix} + \sin\theta \begin{bmatrix} 0 & -\eta_3 & \eta_2 \\ \eta_3 & 0 & -\eta_1 \\ -\eta_2 & \eta_1 & 0 \end{bmatrix} \right.$$

$$\left. + (1 - \cos\theta) \begin{bmatrix} -\eta_3^2 - \eta_2^2 & \eta_1\eta_2 & \eta_1\eta_3 \\ \eta_1\eta_2 & -\eta_1^2 - \eta_3^2 & \eta_2\eta_3 \\ \eta_1\eta_3 & \eta_3\eta_2 & -\eta_2^2 - \eta_1^2 \end{bmatrix} \right\} \underline{b}$$

Since $\sin\theta = 2\sin\frac{\theta}{2}\cos\frac{\theta}{2}$ and $1 - \cos\theta = 2\sin^2\frac{\theta}{2}$ this equation can be expressed as

$$\underline{a} = \left\{ \begin{bmatrix} 1 & 0 & 0 \\ 0 & 1 & 0 \\ 0 & 0 & 1 \end{bmatrix} + 2\cos\frac{\theta}{2} \begin{bmatrix} 0 & -\eta_3\sin\frac{\theta}{2} & \eta_2\sin\frac{\theta}{2} \\ \eta_3\sin\frac{\theta}{2} & 0 & -\eta_1\sin\frac{\theta}{2} \\ -\eta_2\sin\frac{\theta}{2} & \eta_1\sin\frac{\theta}{2} & 0 \end{bmatrix} + 2 \begin{bmatrix} -\sin^2\frac{\theta}{2}(\eta_3^2+\eta_2^2) & \sin^2\frac{\theta}{2}\eta_1\eta_2 & \sin^2\frac{\theta}{2}\eta_1\eta_3 \\ \sin^2\frac{\theta}{2}\eta_1\eta_2 & -\sin^2\frac{\theta}{2}(\eta_1^2+\eta_3^2) & \sin^2\frac{\theta}{2}\eta_2\eta_3 \\ \sin^2\frac{\theta}{2}\eta_1\eta_3 & \sin^2\frac{\theta}{2}\eta_2\eta_3 & -\sin^2\frac{\theta}{2}(\eta_1^2+\eta_2^2) \end{bmatrix} \right\} \quad (4\text{-}66)$$

Also recall that for the quaternion method,

$$A = B + 2sV \times B + 2V \times (V \times B) \quad (4\text{-}67)$$

and for Euler's 4-parameter method,

$$A = B + (1_n \times B)\sin\theta + 1_n \times (1_n \times B)(1 - \cos\theta) \quad (4\text{-}68)$$

Let us make the following identification:

If V is taken as a vector along the 1_n direction, then

$$2sv = \sin\theta \quad (4\text{-}69)$$

$$2v^2 = (1 - \cos\theta)$$

Solving for v and s from (4-69),

$$\left.\begin{aligned} v &= \pm\sin\frac{\theta}{2} \\ s &= \pm\cos\frac{\theta}{2} \end{aligned}\right\} \quad (4\text{-}70)$$

Since (4-70) satisfies N(Q) = 1 irrespective of signs chosen and since

$$A = QBQ^* = (-Q)\ B\ (-Q)^* \tag{4-71}$$

the rotation quaternion is arbitrarily chosen using positive signs in (4-70)

$$Q = s + V = \cos\frac{\theta}{2} + 1_n \sin\frac{\theta}{2} = s + 1_n\, v \tag{4-72}$$

where

$$\left.\begin{aligned} s &= \cos\frac{\theta}{2} \\ v &= \sin\frac{\theta}{2} \end{aligned}\right\} \tag{4-73}$$

Comparing (4-64) and (4-66) and using (4-73), we have the following equivalance between the quaternion and Euler's 4-parameter methods:

$$\left.\begin{aligned} s &= \cos\frac{\theta}{2} \\ v_x &= \cos\alpha \sin\frac{\theta}{2} = \eta_1 \sin\frac{\theta}{2} \\ v_y &= \cos\beta \sin\frac{\theta}{2} = \eta_2 \sin\frac{\theta}{2} \\ \underbrace{v_z}\ &= \underbrace{\cos\gamma \sin\frac{\theta}{2} = \eta_3 \sin\frac{\theta}{2}} \end{aligned}\right\} \tag{4-74}$$

Quaternion Method	Euler's 4-Parameter Method
Parameters:	Parameters:
s, v_x, v_y, v_z	$\theta, \eta_1, \eta_2, \eta_3$

The relationship among various variables is shown in Fig. 4-10.

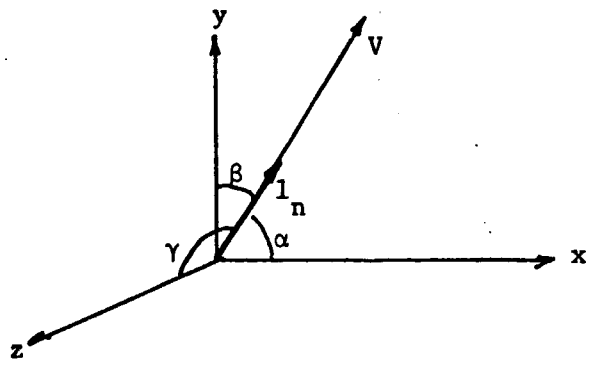

Figure 4-10. Relationship Between α, β, γ and 1_n.

Among 4 quaternion parameters, only 3 are independent; the 4th one can be eliminated by using the constraint N(Q) = 1.

Quaternion Differential Equations

Let Q(t) be a quaternion representing the transformation from a rotating body frame to the inertial frame. Let Q_1 be the value of Q(t) at time t, i.e.,

$$A^i(t) = Q_1 A^b(t)\ Q_1^* \tag{4-75}$$

and Q_2 be the value of Q(t) at time t+Δt, i.e.,

$$A^i(t+\Delta t) = Q_2\ A^b(t+\Delta t)\ Q_2^* \tag{4-76}$$

The quaternion representing the rotation of the body frame during the time Δt is therefore,

$$Q_1^{-1} Q_2 = Q_1^* Q_2$$

This relationship is shown in Fig. 4-11.

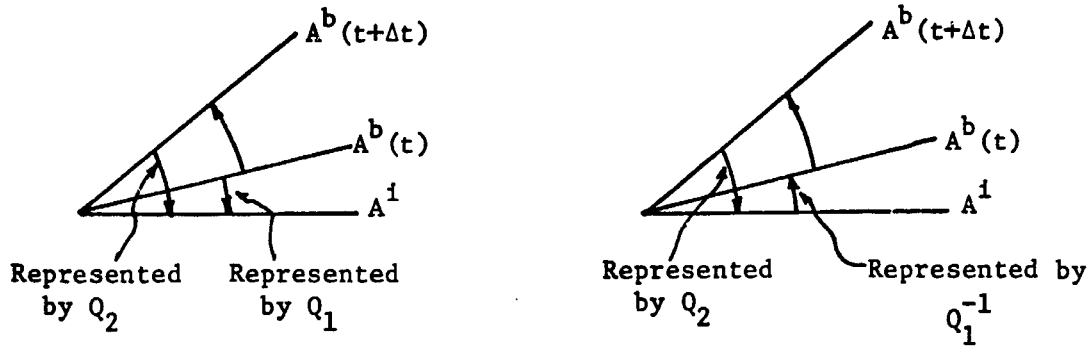

Figure 4-11. Quaternion and Vector Rotation.

Since the angular velocity Ω of the rotating body frame can be considered constant for small Δt the angular displacement of the body frame is

$$\Delta\theta = \omega\Delta t,$$

where

$$1_n = \frac{\Omega}{\omega} \quad \text{and} \quad |\Omega| = \omega \quad .$$

Therefore

$$Q_1^* Q_2 = \cos\frac{\omega\Delta t}{2} + \frac{\Omega}{\omega}\sin\frac{\omega\Delta t}{2} \tag{4-77}$$

and

$$Q_2 = Q_1 \left[\cos\frac{\omega\Delta t}{2} + \frac{\Omega}{\omega}\sin\frac{\omega\Delta t}{2} \right] \tag{4-78}$$

The time derivation of the quaternion Q is obtained from

$$\dot{Q}(t) = \lim_{\Delta t\to o}\frac{Q_2 - Q_1}{\Delta t} = \lim_{\Delta t\to o}\frac{Q}{\Delta t}\left[\cos\frac{\omega\Delta t}{2} - 1 + \frac{\Omega}{\omega}\sin\frac{\omega\Delta t}{2}\right]$$

$$= \lim_{\Delta t\to o}\frac{Q}{\Delta t}\left[1 - \left(\frac{\omega\Delta t}{2}\right)^2 + \cdots - 1 + \frac{\Omega}{\omega}\left(\frac{\omega\Delta t}{2}\right) - \cdots\right]$$

$$= \frac{1}{2} Q\,\Omega$$

$$= \frac{1}{2}(s + V)\,\Omega = \frac{1}{2}\left[(-V\cdot\Omega) + (s\,\Omega + V\times\Omega)\right] \tag{4-79}$$

Hence, we get the desired differential equations

$$\dot{s} = -\frac{1}{2}\,[V\cdot\Omega] \tag{4-80}$$

$$\dot{V} = \frac{1}{2}\,[s\,\Omega + V\times\Omega] \tag{4-81}$$

To express in vector-matrix rotation, let

$$Q = (s,V) = \begin{bmatrix} s \\ v_x \\ v_y \\ v_z \end{bmatrix} \tag{4-82}$$

Then (4-80) and (4-81) can be expressed as

$$\begin{bmatrix} \dot{s} \\ \dot{v}_x \\ \dot{v}_y \\ \dot{v}_z \end{bmatrix} = \underbrace{\begin{bmatrix} 0 & -\frac{\omega_x}{2} & -\frac{\omega_y}{2} & -\frac{\omega_z}{2} \\ \frac{\omega_x}{2} & 0 & -\frac{\omega_z}{2} & \frac{\omega_y}{2} \\ \frac{\omega_y}{2} & \frac{\omega_z}{2} & 0 & -\frac{\omega_x}{2} \\ \frac{\omega_z}{2} & -\frac{\omega_y}{2} & \frac{\omega_x}{2} & 0 \end{bmatrix}}_{M} \begin{bmatrix} s \\ v_x \\ v_y \\ v_z \end{bmatrix} \tag{4-83}$$

$$A^i(t+\Delta t) = Q_2 Q_b^* A^b(t) Q_b Q_2^*$$

$$= Q_2 Q_b^* Q_1^* A^i(t) Q_1 Q_b Q_2^*$$

Since $V^i(t+\Delta t) = V^i(t)$, the stationary inertial frame,

$$Q_2 Q_b^* Q_1 = 1$$

$$Q_b = Q_1^* Q_2 \tag{4-84}$$

The computation procedure from body axis measurements to inertial axis measurements is shown in Fig. 4-12.

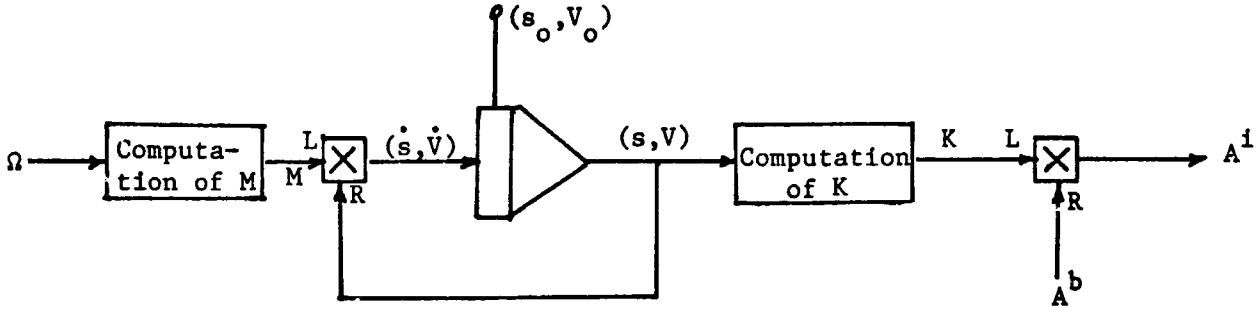

Figure 4-12. Quaternion Transformation.

Remarks

1. Transformation of coordinates can more generally be expressed as quaternion operated on quaternion. Let $\underline{v}$ and $\underline{u}$ be the same 3-dimensional vector represented WRT two different coordinate systems. Let

$$Q = s + V = \text{operator quaternion}$$

$$Q_1 = s_1 + V = \text{quaternion representing vector } \underline{v}$$

$$Q_2 = s_2 + V_2 = \text{quaternion representing vector } \underline{u}$$

Then (4-53) can be expressed as

$$\begin{aligned} Q_2 &= QQ_1Q^* \\ &= (s + V)(s_1 + V_1)(s - V) \\ &= \underbrace{(s + V)\, s_1\, (s - V)}_{s_1} + \underbrace{(s + V)\, V_1\, (s - V)}_{\text{let it be } V_2} \\ &= s_1 + V_2 \end{aligned} \tag{4-85}$$

Thus, the operation does not change the value of the scalar term.

2. Let Q_b represent the rotation of the body frame from time t to t+Δt

$$A^b(t+\Delta t) = Q_b^*\, A^b(t)\, Q_b \tag{4-86}$$

Then at time t

$$A^i(t) = Q_1\, A^b(t)\, Q_1^* \tag{4-87}$$

and at time t+Δt

$$A^i(t+\Delta t) = Q_2\, A^b(t+\Delta t)\, Q_2^* \tag{4-88}$$

$$A^i(t+\Delta t) = Q_2Q_b^*\, A^b(t)\, Q_bQ_2^* = Q_2Q_b^*Q_1\, A^i(t)\, Q_1Q_bQ_2$$

Since $A^i(t+\Delta t) = A^i(t)$, the stationary frame vector, so $Q_2Q_b^*Q_1 = 1$. Hence

$$Q_b = Q_1^*Q_2 \quad .$$

CAYLEY-KLEIN PARAMETER ALGORITHM

Transformation in Two Dimensional Complex Space

Consider the transformation of two complex axes (u,v) to (u',v') through the linear relationship

$$\begin{bmatrix} u' \\ v' \end{bmatrix} = \underbrace{\begin{bmatrix} \alpha & \beta \\ \gamma & \delta \end{bmatrix}}_{K} \begin{bmatrix} u \\ v \end{bmatrix} \tag{4-89}$$

Where α, β, γ and δ, called Cayley-Klein Parameters, are all complex numbers. Eq. (4-89) denotes a transformation in a two-dimensional complex space, or, equivalently, in a four-dimensional real space.

Eg. Transformation in 1-dimensional complex space

$$(a'+jb') = (\alpha+j\beta)(a+jb)$$

can also be expressed as transformation in 2-dimensional real space as

$$\begin{bmatrix} a' \\ b' \end{bmatrix} = \begin{bmatrix} \alpha & -\beta \\ \beta & \alpha \end{bmatrix} \begin{bmatrix} a \\ b \end{bmatrix}$$

Since α, β, γ and δ are complex, there are eight parameters to be specified. However, if one tries to apply the K matrix to a transformation in a 3-dimensional real space, only three of the eight parameters are independent. To eliminate the remaining five parameters, some constraints are needed. The constraints are:

1. K be a unitary matrix, i.e., $K^{-1} = K^*$, or just

$$K^*K = 1 \tag{4-90}$$

2. The determinant of K be 1, i.e.,

$$|K| = 1 \tag{4-91}$$

Using (4-89)

$$K^*K = \begin{bmatrix} \alpha & \beta \\ \gamma & \delta \end{bmatrix} \begin{bmatrix} \alpha^* & \gamma^* \\ \beta^* & \delta^* \end{bmatrix}$$

$$\begin{bmatrix} \alpha^*\alpha + \beta^*\beta & \alpha\gamma^* + \beta\delta^* \\ \alpha^*\gamma + \beta^*\delta & \gamma\gamma^* + \delta\delta^* \end{bmatrix} = \begin{bmatrix} 1 & 0 \\ 0 & 1 \end{bmatrix}$$

requiring

$$\alpha\alpha^* + \beta\,\beta^* = 1 \qquad (4\text{-}92)$$

$$\gamma\gamma^* + \delta\,\delta^* = 1 \qquad (4\text{-}93)$$

$$\alpha^*\gamma + \beta^*\delta = 0 \quad . \qquad (4\text{-}94)$$

From (4-91)

$$\alpha\delta - \beta\,\gamma = 1 \quad . \qquad (4\text{-}95)$$

Eqs. (4-92) and (4-93) are real, while (4-94) is complex, so that together they provide four conditions. Eq. (4-95) provides the fifth condition. From (4-94)

$$\frac{\delta}{\gamma} = -\frac{\alpha^*}{\beta^*} \qquad (4\text{-}96)$$

Substituting into (4-95)

$$\alpha\alpha^* \left(-\frac{\gamma}{\beta^*}\right) - \beta\beta^* \left(\frac{\gamma}{\beta^*}\right) = 1$$

$$(\alpha\alpha^* + \beta\beta^*) \frac{\gamma}{\beta^*} = -1$$

By the relationship of (4-92), we have

$$\gamma = -\beta^* \qquad (4\text{-}97)$$

Using (4-97) in (4-96)

$$\delta = -\alpha^* \qquad (4\text{-}98)$$

Therefore, the matrix K can be written as

$$K = \begin{bmatrix} \alpha & \beta \\ -\beta^* & \alpha^* \end{bmatrix} \tag{4-99}$$

Constrained by

$$\alpha\alpha^* + \beta\beta^* = 1 \tag{4-100}$$

Notice that the derivation of (4-99) used (4-92), (4-94), (4-95) but not (4-93). (4-93) is used as the constraint to (4-99). On account of (4-97) and (4-98), (4-93) = (4-92), so we have (4-100).

Now let D be a Hermitian matrix in this 2-dimensional complex space having the specific form

$$D = \begin{bmatrix} x & z-jy \\ z+jy & -x \end{bmatrix} \qquad j = \sqrt{-1} \tag{4-101}$$

The quantities x, y, z are reals, and they can be considered as representing three coordinates defining a vector $\underline{r}$ in a three dimensional real space. Notice that the determinant of D is

$$|D| = -(x^2 + y^2 + z^2) = -\underline{r}^T\underline{r} = -r^2 \tag{4-102}$$

and

$$\text{Trace } D = 0 \tag{4-103}$$

Applying a similarity transformation to V using the unitary matrix K, gives

$$D' = K D K^* \tag{4-104}$$

Under similarity transformation the Hermitian property of a matrix is preserved, so are the determinant and trace, i.e.,

$$|D'| = -(x'^2 + y'^2 + z'^2) = |D|$$

$$\text{Trace } D' = 0$$

Isomorphism Between Cayley-Klein Parameters and Quaternion Parameters

Matrix D can be written as

$$D = \begin{bmatrix} x & j-jy \\ z+jy & -x \end{bmatrix}$$

$$= x \begin{bmatrix} 1 & 0 \\ 0 & -1 \end{bmatrix} + y \begin{bmatrix} 0 & -j \\ j & 0 \end{bmatrix} + z \begin{bmatrix} 0 & 1 \\ 1 & 0 \end{bmatrix}$$

$$= x \Sigma_x + y \Sigma_y + z \Sigma_z \qquad (4\text{-}107)$$

where

$$\left.\begin{aligned} \Sigma_x &= \begin{bmatrix} 1 & 0 \\ 0 & -1 \end{bmatrix} \\ \Sigma_y &= \begin{bmatrix} 0 & -j \\ j & 0 \end{bmatrix} \\ \Sigma_z &= \begin{bmatrix} 0 & 1 \\ 1 & 0 \end{bmatrix} \end{aligned}\right\} \qquad (4\text{-}108)$$

In addition

$$\left.\Sigma_I = \begin{bmatrix} 1 & 0 \\ 0 & 1 \end{bmatrix}\right\}$$

Since these 4 matrices are linearly independent, any 2 x 2 matrix involving only 4 independent quantities can be formed by linear combination of them. Let

$$\left.\begin{aligned} \alpha &= a + jb \\ \beta &= c + jd \end{aligned}\right\} \qquad (4\text{-}109)$$

Then using (4-108) we have

$$K = \begin{bmatrix} \alpha & \beta \\ -\beta^* & \alpha^* \end{bmatrix} = \begin{bmatrix} a+jb & c+jd \\ -c+jb & a-jb \end{bmatrix}$$

$$= a\left\{ \begin{bmatrix} 1 & 0 \\ 0 & 1 \end{bmatrix} + j \quad b \begin{bmatrix} 1 & 0 \\ 0 & -1 \end{bmatrix} + c \begin{bmatrix} 0 & -j \\ j & 0 \end{bmatrix} + d \begin{bmatrix} 0 & 1 \\ 1 & 0 \end{bmatrix} \right\}$$

$$\therefore \quad K = a\,\Sigma_I + j\left[b\Sigma_x + c\Sigma_y + d\Sigma_z \right] \tag{4-110}$$

Recalling the quaternion Q,

$$Q = s + V = s + \hat{i}v_x + \hat{j}v_y + \hat{k}v_z \tag{4-111}$$

There is an isomorphism relationship between K and Q where:

$$K \longleftrightarrow Q$$

$$a \longleftrightarrow s$$

$$b \longleftrightarrow v_x$$

$$c \longleftrightarrow v_y$$

$$d \longleftrightarrow v_z$$

$$j\Sigma_x \longleftrightarrow \hat{i}$$

$$j\Sigma_x \longleftrightarrow \hat{j}$$

$$j\Sigma_x \longleftrightarrow \hat{k}$$

Addition: $K_1 + K_2 \longleftrightarrow Q_1 + Q_2$

Equality: $K_1 = K_2 \longleftrightarrow Q_1 = Q_2$

Multiplication:

$$(j\Sigma_x)^2 = (j\Sigma_y)^2 = (j\Sigma_z)^2 = -\Sigma_I \longleftrightarrow \hat{i}^2 = \hat{j}^2 = \hat{k}^2 = -1$$

$$(j\Sigma_x)(j\Sigma_y) = -(j\Sigma_y)(j\Sigma_x) = j\Sigma_z \longleftrightarrow \hat{i}\hat{j} = -\hat{j}\hat{i} = \hat{k}$$

$$(j\Sigma_y)(j\Sigma_z) = -(j\Sigma_z)(j\Sigma_y) = j\Sigma_x \longleftrightarrow \hat{j}\hat{k} = -\hat{k}\hat{j} = \hat{i}$$

$$(j\Sigma_z)(j\Sigma_x) = -(j\Sigma_x)(j\Sigma_z) = j\Sigma_y \longleftrightarrow \hat{k}\hat{i} = -\hat{i}\hat{k} = \hat{j}$$

$$K_1K_2 = [a_1\Sigma_I + b_1(j\Sigma_x) + c_1(j\Sigma_y) + d_1(j\Sigma_z)]$$

$$[a_2\Sigma_I + b_2(j\Sigma_x) + c_2(j\Sigma_y) + d_2(j\Sigma_z)]$$

$$= [a_1a_2 - (b_1b_2 + c_1c_2 + d_1d_2)]\,\Sigma_I$$

$$+ a_1\,[b_2(j\Sigma_x) + c_2(j\Sigma_y) + d_2(j\Sigma_z)]$$

$$+ a_2\,[b_1(j\Sigma_x) + c_1(j\Sigma_y) + d_1(j\Sigma_z)]$$

$$+ \begin{vmatrix} j\Sigma_x & j\Sigma_y & j\Sigma_z \\ b_1 & c_1 & d_1 \\ b_2 & c_2 & d_2 \end{vmatrix}$$

$$Q_1Q_2 = (s_1 + V_1)\,(s_2 + V_2)$$

$$= (s_1 + \hat{i}v_{1x} + \hat{j}v_{1y} + \hat{k}v_{1z})(s_2 + \hat{i}v_{2x} + \hat{j}v_{2y} + \hat{k}v_{2z})$$

$$= (s_1s_2 - V_1V_2) + (s_1V_2 + s_2V_1 + V_1 \times V_2)$$

Thus

$$a_1a_2 \longleftrightarrow s_1s_2$$

$$b_1b_2 + c_1c_2 + d_1d_2 \longleftrightarrow V_1 \cdot V_2$$

$$a_1[b_2(j\Sigma_x) + c_2(j\Sigma_z) + d_2(j\Sigma_z)] \longleftrightarrow s_1V_2$$

$$a_2[b_1(j\Sigma_x) + c_1(j\Sigma_y) + d_1(j\Sigma_z)] \longleftrightarrow s_2V_1$$

$$\begin{vmatrix} j\Sigma_x & j\Sigma_y & j\Sigma_z \\ b_1 & c_1 & d_1 \\ b_2 & c_2 & d_2 \end{vmatrix} \longleftrightarrow V_1 \times V_2$$

Norm: $|K| = a^2 + b^2 + c^2 + d^2 \longleftrightarrow N(Q) = s^2 + v_x^2 + v_y^2 + v_z^2$

That is, in Cayley-Klein parameters, the norm is taken to the determinant of K matrix.

Conjugation: K* = transpose conjugate of K $\longleftrightarrow$ Q* = s - V

Transformation of Coordinates

In view of the isomorphism between the Cayley-Klein algebra and the quaternion algebra, and in view of the fact that vector transformation in quaternion algebra is represented by

$$Q_2 = QQ_1Q^* \tag{4-112}$$

therefore, the vector transformation in Cayley-Klein algebra can be expressed as

$$D_2 = KD_1K^* \tag{4-113}$$

where the two sets of parameters, in the operators K and Q, are made identical to each other in the corresponding terms. That is,

Cayley-Klein		Quaternion
a	=	s
b	=	v_x
c	=	v_y
d	=	v_z

(4-114)

Therefore, basing on the result of quaternion transformation method, we can express the Cayley-Klein transformation method as

$$\underline{u} = \underbrace{[I + 2aP + 2P^2]}_{G}\,\underline{v} \tag{4-115}$$

where

$$P = \begin{bmatrix} 0 & -d & c \\ d & 0 & -b \\ -c & b & 0 \end{bmatrix} \tag{4-116}$$

Cayley-Klein Parameter Differential Equations

Due to the relationship (4-114) we have, based on the differential equations for quaternions,

$$\begin{bmatrix} \dot{a} \\ \dot{b} \\ \dot{c} \\ \dot{d} \end{bmatrix} = \underbrace{\begin{bmatrix} 0 & -\frac{\omega_x}{2} & -\frac{\omega_y}{2} & -\frac{\omega_z}{2} \\ \frac{\omega_x}{2} & 0 & -\omega_z & \omega_y \\ \frac{\omega_y}{2} & \omega_z & 0 & -\omega_x \\ \frac{\omega_z}{2} & -\omega_y & \omega_x & 0 \end{bmatrix}}_{M} \begin{bmatrix} a \\ b \\ c \\ d \end{bmatrix} \tag{4-117}$$

The computation procedure from body axis information to inertial axis quantities is shown in Fig. 4-13.

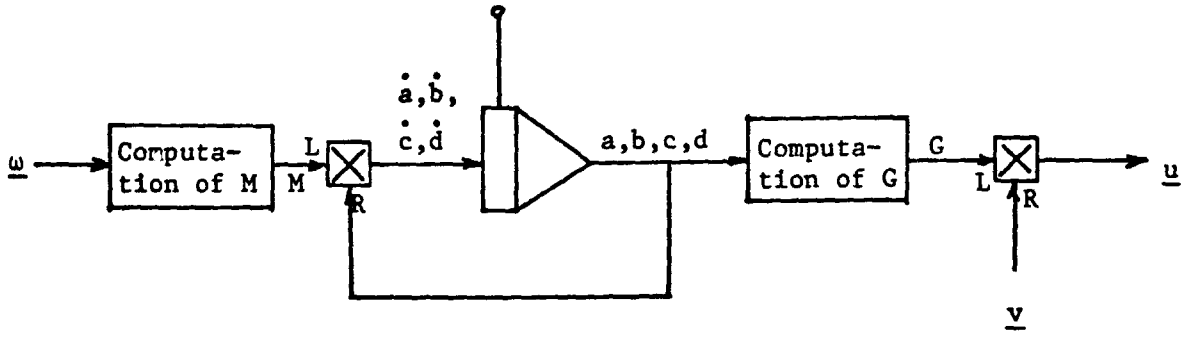

Figure 4-13. Cayley-Klein Parameter Transformation.

VECTOR REPRESENTATION ALGORITHM

Vector Representation

Let 1_n be the unit vector along the axis of rotation, and θ be the angular displacement as shown in Fig. 4-14.

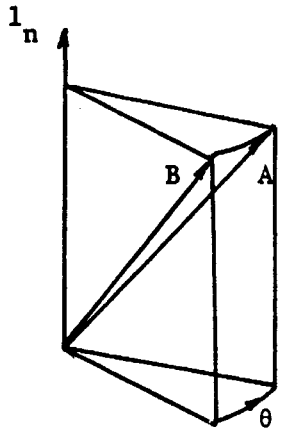

Figure 4-14. Vector Representation.

Define a vector Σ

$$\Sigma = 1_n \tan\frac{\theta}{4} = 1_n \frac{\sin\frac{\theta}{4}}{\cos\frac{\theta}{4}} = 1_n \frac{\sin\frac{\theta}{4}\cos\frac{\theta}{4}}{\cos^2\frac{\theta}{4}}$$

$$= 1_n \frac{\sin\frac{\theta}{2}}{2\cos\frac{\theta}{4}} = 1_n \frac{\sin\frac{\theta}{2}}{1+\cos\frac{\theta}{2}}$$

Recall that in the quaternion method where $Q = s + V$, we have

$$s = \cos\frac{\theta}{2} \qquad \text{and } V = 1_n \sin\frac{\theta}{2}$$

Therefore

$$\Sigma = \frac{V}{1+s} \quad , \tag{4-119}$$

so

$$V = (1 + s)\,\Sigma \tag{4-120}$$

Solve for s and V in terms of Σ. Note

$$1 + s = 1 + \cos\frac{\theta}{2} = 2\cos^2\frac{\theta}{4} = \frac{2}{\csc^2\frac{\theta}{4}} = \frac{2}{1+\tan^2\frac{\theta}{4}} = \frac{2}{1+\sigma^2}$$

where $\sigma^2 = |\Sigma|^2 = \tan^2\frac{\theta}{4}$

$$\therefore \quad s = \frac{1-\sigma^2}{1+\sigma^2} \tag{4-121}$$

Substituting (4-120) into (4-119)

$$V = \frac{2}{1+\sigma^2}\,\Sigma \tag{4-122}$$

Recalling the quaternion transformation equation,

$$A = B + 2s(V \times B) + 2\,V \times (V \times B)$$

then by using (4-121) and (4-122), we have the transformation in using the vector representation method.

$$A = B + 4\frac{(1-\sigma^2)}{(1+\sigma^2)^2}(\Sigma \times B) + \frac{8}{(1+\sigma^2)^2}\,\Sigma \times (\Sigma \times B) \tag{4-123}$$

Expressing in vector-matrix rotation

$$\Sigma \times B = \underbrace{\begin{bmatrix} 0 & -\sigma_z & \sigma_y \\ \sigma_z & 0 & -\sigma_x \\ -\sigma_y & \sigma_x & 0 \end{bmatrix}}_{S} \underbrace{\begin{bmatrix} b_x \\ b_y \\ b_z \end{bmatrix}}_{\underline{b}} \tag{4-124}$$

and

$$\Sigma \times (\Sigma \times B) = S^2\underline{b} \tag{4-125}$$

where

$$B = \hat{i}\,b_x + \hat{j}\,b_y + \hat{k}\,b_z$$

Using (4-124) and (4-125) in (4-123)

$$\underline{a} = \underbrace{\left[I + 4 \frac{(1-\sigma^2)}{(1+\sigma^2)^2} S + \frac{8}{(1+\sigma^2)^2} S^2 \right]}_{T} \underline{b} \qquad (4\text{-}126)$$

Let

$$T = I + 4 \frac{(1-\sigma^2)}{(1+\sigma^2)^2} S + \frac{8}{(1+\sigma^2)^2} S^2 \qquad (4\text{-}127)$$

(4-126) becomes

$$\underline{a} = T \underline{b} \qquad (4\text{-}128)$$

Differentiation Equation for Vector Representation

Differentiating (4-120)

$$\dot{V} = (1 + s) \dot{\Sigma} + \dot{s} \Sigma \qquad (4\text{-}129)$$

Since

$$\dot{s} = - \frac{1}{2} V \cdot \Omega$$

$$\dot{V} = \frac{1}{2} (s \Omega + V \times \Omega)$$

(4-129) gives

$$(1 + s) \dot{\Sigma} = \frac{1}{2} (s \Omega + V \times \Omega) + \frac{1}{2} (V \cdot \Omega) \Sigma \qquad (4\text{-}130)$$

Using (4-120) in (4-130)

$$(1 + s)\dot{\Sigma} = \frac{1}{2} [s \Omega + (1 + s)(\Sigma \times \Omega) + (1 + s)(\Sigma \cdot \Omega) \Sigma]$$

$$\dot{\Sigma} = \frac{1}{2} \left[\frac{s}{1+s} \Omega + (\Sigma \times \Omega) + (\Sigma \cdot \Omega) \Sigma \right] \qquad (4\text{-}131)$$

From (4-121)

$$\frac{s}{1+s} = \frac{1-\sigma^2}{2}$$

Using this in (4-131)

$$\dot{\Sigma} = \frac{1}{2}\left[\underbrace{\frac{1-\sigma^2}{2}\,\Omega}_{\text{Nonlinear terms}} + (\Sigma \times \Omega) + \underbrace{(\Sigma \cdot \Omega)\Sigma}_{\text{Nonlinear terms}}\right] \qquad (4\text{-}132)$$

By using the identity

$$A \times (B \times C) = (A \cdot C)B - (A \cdot B)C$$

we have

$$\Sigma \times (\Sigma \times \Omega) = (\Sigma \cdot \Omega)\Sigma - (\Sigma \cdot \Sigma)\Omega$$

$$\therefore \quad (\Sigma \cdot \Omega)\Sigma = \sigma^2\Omega + \Sigma \times (\Sigma \times \Omega)$$

Therefore (4-132) can also be written as

$$\dot{\Sigma} = \frac{1}{2}\left[\underbrace{\frac{1+\sigma^2}{2}\,\Omega}_{\text{Nonlinear terms}} + (\Sigma \times \Omega) + \underbrace{\Sigma \times (\Sigma \times \Omega)}_{\text{Nonlinear terms}}\right] \qquad (4\text{-}133)$$

DDA REALIZATIONS OF ATTITUDE ALGORITHMS

Direction Cosine Algorithm

The transformation equations are

$$\dot{C} = C\,\Omega \qquad (4\text{-}17)$$

$$V^I = C\,V^B \qquad (4\text{-}18)$$

Taking the differentials and let $\Omega\Delta t = \Delta A$, the angular increments,

$$\left.\begin{aligned} \Delta C_{i1} &= C_{i2}\,\Delta A_3 - C_{i3}\,\Delta A_2 \\ \Delta C_{i2} &= C_{i3}\,\Delta A_1 - C_{i1}\,\Delta A_3 \\ \Delta C_{i3} &= C_{i1}\,\Delta A_2 - C_{i2}\,\Delta A_1 \end{aligned}\right\} i = 1,2,3 \qquad (4\text{-}134)$$

$$\begin{bmatrix} \Delta V_1^I \\ \Delta V_2^I \\ \Delta V_3^I \end{bmatrix} = \begin{bmatrix} C_{11} & C_{12} & C_{13} \\ C_{21} & C_{22} & C_{23} \\ C_{31} & C_{32} & C_{33} \end{bmatrix} \begin{bmatrix} \Delta V_1^B \\ \Delta V_2^B \\ \Delta V_3^B \end{bmatrix} \tag{4-135}$$

The DDA realization for (4-134) is shown in Fig. 4-15a. The realization for all i = 1,2,3 requires 6 x 3 = 18 DDA's. The DDA realization for (4-135) is shown in Fig. 4-15b. The realization for all i = 1,2,3 requires 3 x 3 = 9 DDA's. Therefore, the complete realization of both (4-134) and (4-135) for all coordinate variables requires a total of 18 + 9 = 27 DDA's.

Euler Angle Algorithm

The Euler angle differential equations are given by

$$\begin{bmatrix} \dot{\phi} \\ \dot{\theta} \\ \dot{\psi} \end{bmatrix} = \begin{bmatrix} \frac{\sin\psi}{\sin\theta} & \frac{\cos\psi}{\sin\theta} & 0 \\ \cos\psi & -\sin\psi & 0 \\ -\frac{\sin\psi\cos\theta}{\sin\theta} & -\frac{\cos\theta\cos\psi}{\sin\theta} & 1 \end{bmatrix} \begin{bmatrix} \omega_x \\ \omega_y \\ \omega_z \end{bmatrix} \tag{4-25}$$

In incremental form,

$$\begin{bmatrix} \Delta\phi \\ \Delta\theta \\ \Delta\psi \end{bmatrix} = \begin{bmatrix} \frac{\sin\psi}{\sin\theta} & \frac{\cos\psi}{\sin\theta} & 0 \\ \cos\psi & -\sin\psi & 0 \\ -\frac{\sin\psi\cos\theta}{\sin\theta} & -\frac{\cos\psi\cos\theta}{\sin\theta} & 1 \end{bmatrix} \begin{bmatrix} \omega_x\Delta t \\ \omega_y\Delta t \\ \omega_z\Delta t \end{bmatrix}$$

Let

$$\left.\begin{aligned} \Delta A_1 &= \omega_x\Delta t \\ \Delta A_2 &= \omega_y\Delta t \\ \Delta A_3 &= \omega_z\Delta t \end{aligned}\right\} , \tag{4-136}$$

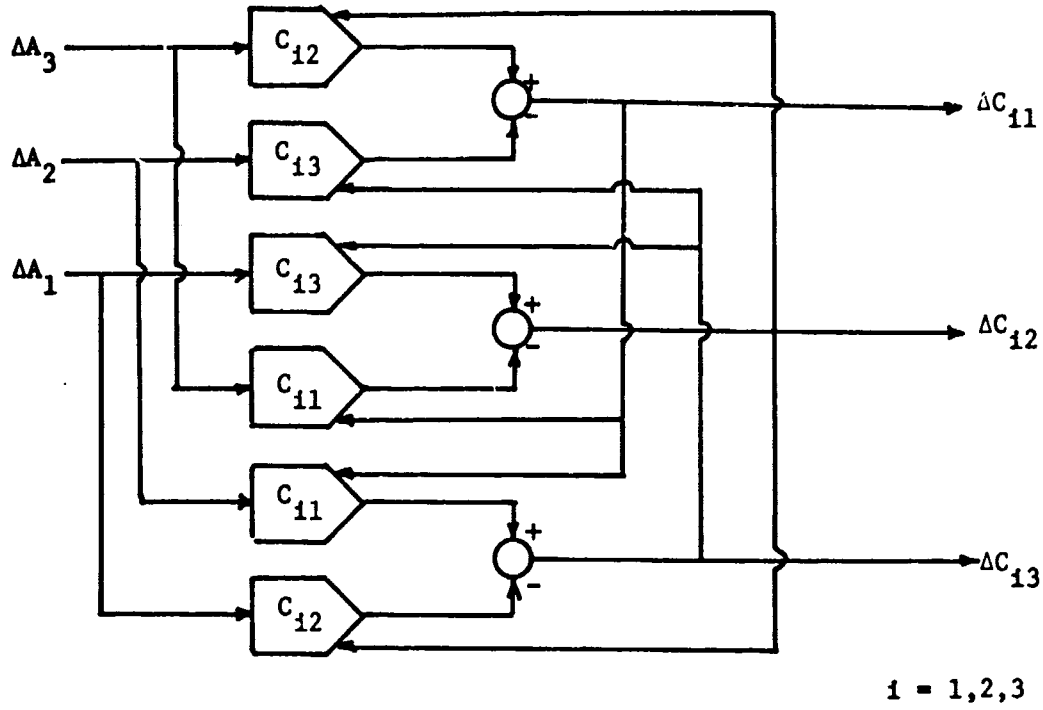

(a)

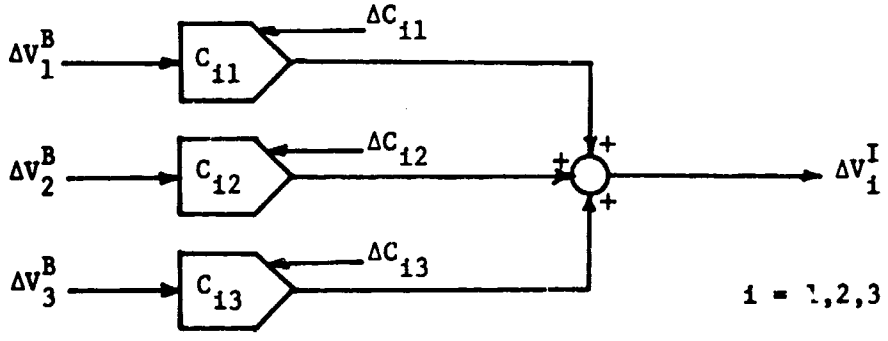

(b)

Figure 4-15. Realization of Direction Cosine Algorithm.

We get

$$\left.\begin{aligned} \Delta\phi &= (\Delta A_1 \sin\psi + \Delta A_2 \cos)\psi \frac{1}{\sin\theta} \\ \Delta\theta &= \Delta A_1 \cos\psi - \Delta A_2 \sin\psi \\ \Delta\psi &= (\Delta A_1 \sin\psi + \Delta A_2 \cos\psi) \frac{1}{\sin\theta} \cos\theta + \Delta A_3 \end{aligned}\right\} \quad (4\text{-}137)$$

The transformation equations are given by

$$\begin{bmatrix} \Delta V_1^I \\ \Delta V_2^I \\ \Delta V_3^I \end{bmatrix} = \begin{bmatrix} \cos\psi\cos\phi - \cos\theta\sin\phi\sin\psi & \cos\psi\sin\phi + \cos\theta\cos\phi\sin\psi & \sin\psi\sin\theta \\ -\sin\psi\cos\phi - \cos\theta\sin\phi\cos\psi & -\sin\psi\sin\phi + \cos\theta\cos\phi\cos\psi & \cos\psi\sin\theta \\ \sin\theta\sin\phi & -\sin\theta\cos\phi & \cos\theta \end{bmatrix} \begin{bmatrix} \Delta V_1^B \\ \Delta V_2^B \\ \Delta V_3^B \end{bmatrix} \quad (4\text{-}138)$$

Furthermore, the following relationships exist.

$$\left.\begin{aligned} \Delta\sin\phi &= \Delta\phi\ \cos\phi & \Delta\cos\phi &= -\Delta\phi\sin\phi \\ \Delta\sin\theta &= \Delta\theta\ \cos\phi & \Delta\cos\theta &= -\Delta\theta\sin\theta \\ \Delta\sin\psi &= \Delta\psi\ \cos\psi & \Delta\cos\psi &= -\Delta\psi\sin\psi \\ \Delta\frac{1}{\sin\theta} &= -\frac{1}{\sin^2\theta}\ \Delta\sin\theta \end{aligned}\right\} \quad (4\text{-}139)$$

The DDA realization of (4-137) is shown in Fig. 4-16a, using 6 DDA's and the realization of (4-139) is shown in Fig. 4-16b, using 8 DDA's. The DDA realization of (4-138) is shown in Fig. 4-16c, using 13 DDA's. Therefore,

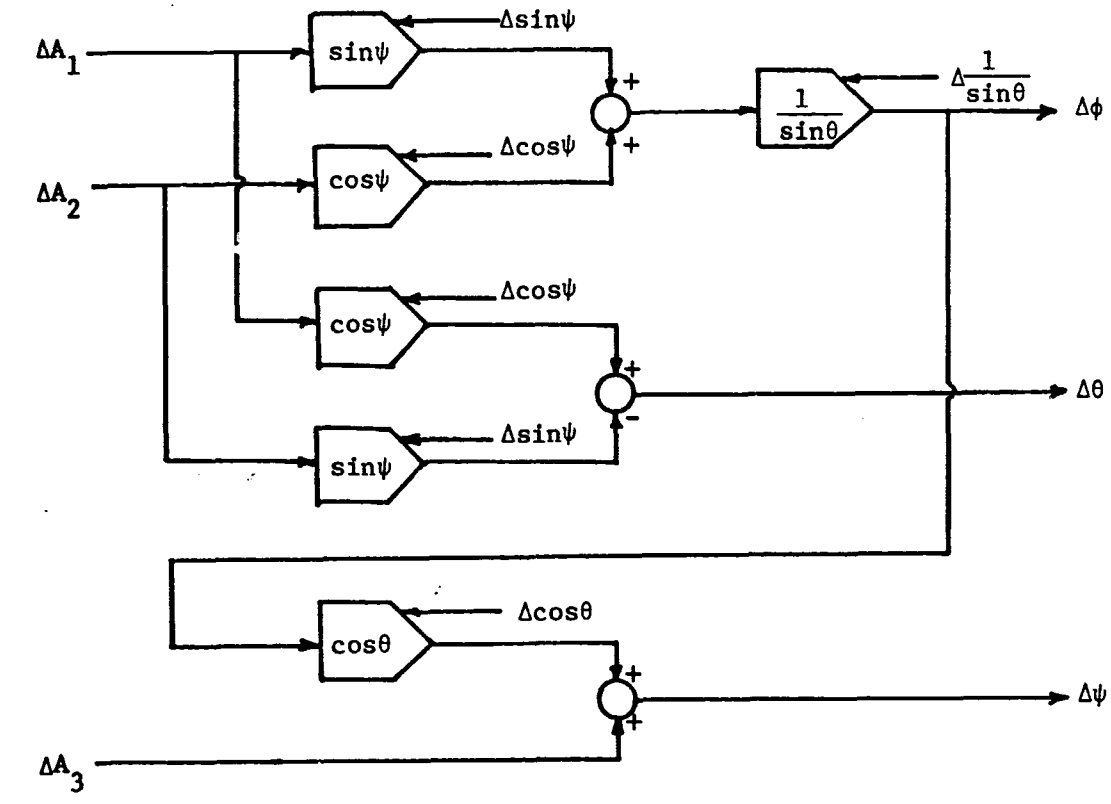

(a)

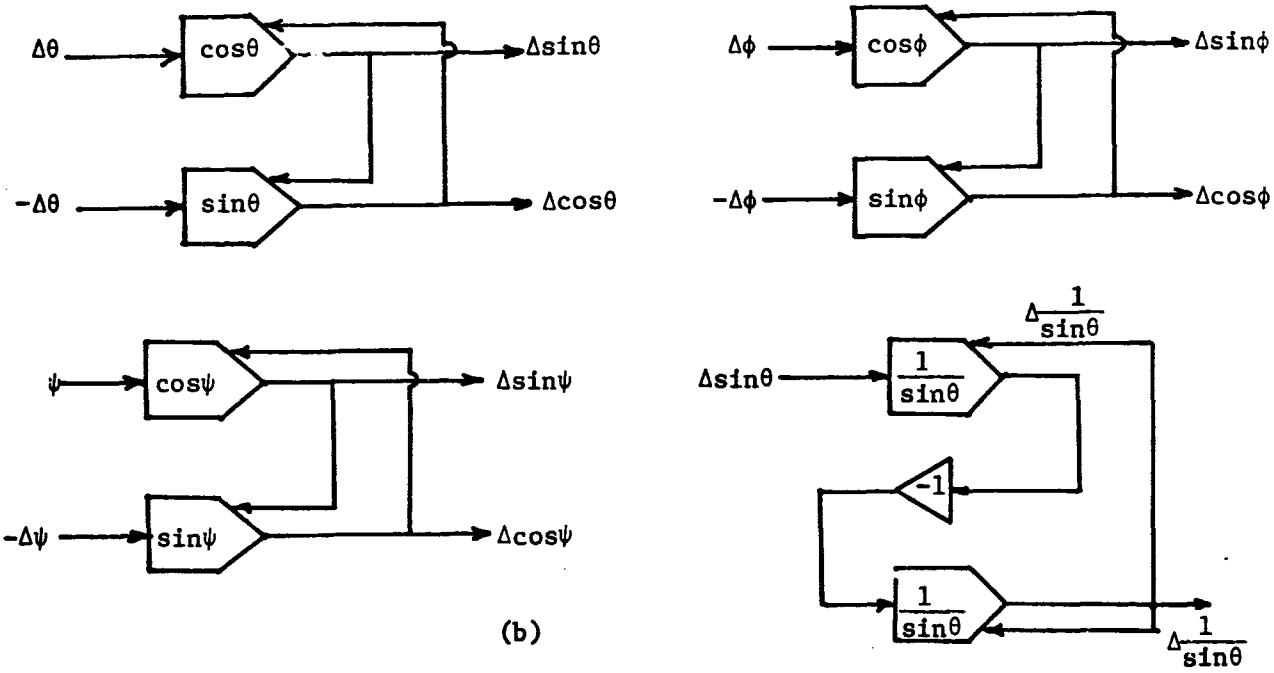

(b)

Figure 4-16. Realization of Euler Angle Algorithm.

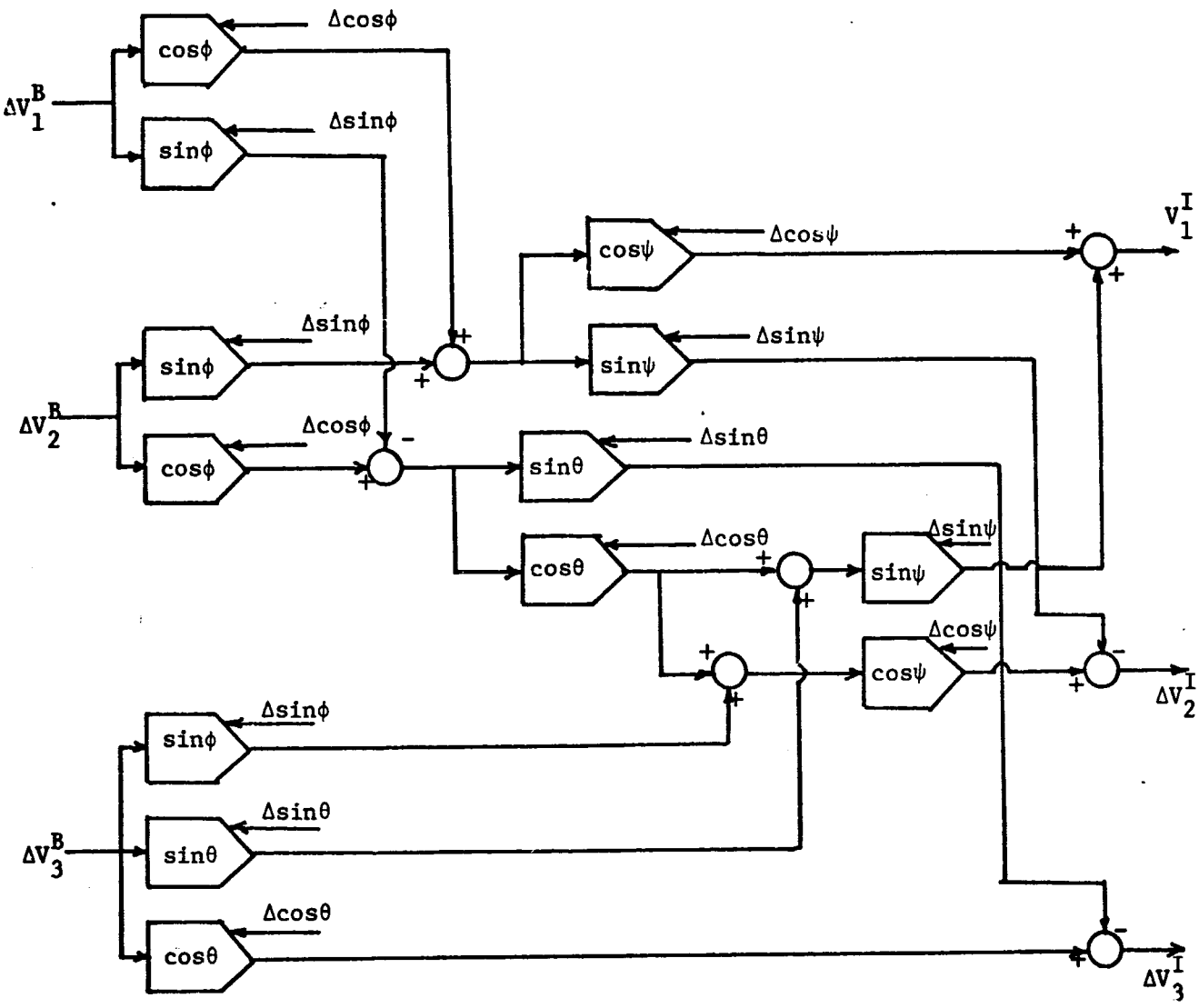

(c)

Figure 4-16. (Continued)

the complete realization of all (4-137), (4-138) and (4-139) for all coordinate variables requires a total of 6 + 8 + 13 = 27 DDA's.

Euler's 4 Parameter Algorithm

The Differential equation is

$$\begin{bmatrix} \dot{\theta} \\ \dot{\eta}_x \\ \dot{\eta}_y \\ \dot{\eta}_z \end{bmatrix} = \frac{1}{2} \begin{bmatrix} -2\eta_x & -2\eta_y & -2\eta_z \\ \cot\frac{\theta}{2}\,(1-\eta_x^2) & -\eta_x\eta_y \cot\frac{\theta}{2} - \eta_z & -\eta_x\eta_z \cot\frac{\theta}{2} + \eta_y \\ -\eta_x\eta_y \cot\frac{\theta}{2} + \eta_z & \cot\frac{\theta}{2}\,(1-\eta_y^2) & -\eta_z\eta_y \cot\frac{\theta}{2} - \eta_x \\ -\eta_x\eta_z \cot\frac{\theta}{2} - \eta_y & -\eta_y\eta_z \cot\frac{\theta}{2} + \eta_x & \cot\frac{\theta}{2}\,(1-\eta_z^2) \end{bmatrix} \begin{bmatrix} \omega_x \\ \omega_y \\ \omega_z \end{bmatrix}$$

or, in the incremental form,

$$\begin{bmatrix} \Delta\theta \\ \Delta\eta_x \\ \Delta\eta_y \\ \Delta\eta_z \end{bmatrix} = \frac{1}{2} \begin{bmatrix} -2\eta_x & -2\eta_y & -2\eta_z \\ \cot\frac{\theta}{2}\,(1-\eta_x^2) & -\eta_x\eta_y \cot\frac{\theta}{2} - \eta_z & -\eta_x\eta_y \cot\frac{\theta}{2} + \eta_y \\ -\eta_x\eta_y \cot\frac{\theta}{2} + \eta_y & \cot\frac{\theta}{2}\,(1-\eta_y^2) & -\eta_z\eta_y \cot\frac{\theta}{2} - \eta_x \\ -\eta_x\eta_z \cot\frac{\theta}{2} - \eta_y & -\eta_y\eta_z \cot\frac{\theta}{2} + \eta_x & \cot\frac{\theta}{2}\,(1-\eta_z^2) \end{bmatrix} \begin{bmatrix} \Delta A_1 \\ \Delta A_2 \\ \Delta A_3 \end{bmatrix} \qquad (4\text{-}140)$$

The transformation equation is

$$\Delta V^I = [I + N \sin\theta + N^2(1 - \cos\theta)]\ \Delta V^B$$

where

$$N = \begin{bmatrix} 0 & -\eta_z & \eta_x \\ \eta_z & 0 & -\eta_y \\ \eta_x & \eta_y & 0 \end{bmatrix} .$$

Or, we can write it in the form of

$$\Delta V^I = \Delta V^B + \sin\theta\ 1_n \times \Delta V^B + (1 - \cos\theta)\ 1_n \times (1_n \times \Delta V^B) \qquad (4\text{-}141)$$

$$1_n = \hat{i}\,\eta_x + \hat{j}\,\eta_y + \hat{k}\,\eta_z$$

Eq. (4-141) can be written in the following more explicit form

$$\left.\begin{aligned} \Delta v_1^I &= \Delta v_1^B + \sin\theta \cdot u_3 + (1 - \cos\theta)(u_2\eta_x - u_1\eta_z) \\ \Delta v_2^I &= \Delta v_2^B + \sin\theta \cdot u_1 + (1 - \cos\theta)(u_3\eta_z - u_2\eta_x) \\ \Delta v_3^I &= \Delta v_3^B + \sin\theta \cdot u_2 + (1 - \cos\theta)(u_1\eta_x - u_3\eta_y) \end{aligned}\right\} \qquad (4\text{-}142)$$

where

$$\left.\begin{aligned} u_1 &= \eta_z\,\Delta v_1^B - \eta_x\,\Delta v_3^B \\ u_2 &= \eta_x\,\Delta v_2^B - \eta_y\,\Delta v_1^B \\ u_3 &= \eta_y\,\Delta v_3^B - \eta_z\,\Delta v_2^B \end{aligned}\right\} \qquad (4\text{-}143)$$

It takes 2 DDA's to take care of the factor $\cot\frac{\theta}{2}$ using the relationship

$$\Delta\cot\frac{\theta}{2} = -\csc^2\frac{\theta}{2} \cdot \Delta\theta = -\left(1 + \cot^2\frac{\theta}{2}\right)\Delta\theta \qquad (4\text{-}144)$$

The realization of (4-144) is shown in Fig. 4-17a. Six DDA's are needed to realize (4-143) as shown in Fig. 4-17b, and fifteen are needed to realize (4-140) as shown in Fig. 4-17c. It takes 2 DDA's to get the factor $\sin\theta$ and $\cos\theta$ using the relationships

$$\left.\begin{aligned} \Delta\sin\theta &= \cos\theta \cdot \Delta\theta \\ -\Delta\cos\theta &= \sin\theta \cdot \Delta\theta \end{aligned}\right\} \qquad (4\text{-}145)$$

The realization is shown in Fig. 4-17d. Twelve DDA's are needed to realize (4-142) as shown in Fig. 4-17e. Therefore, it takes a total of 2 + 15 + 6 + 12 + 2 = 37 DDA's.

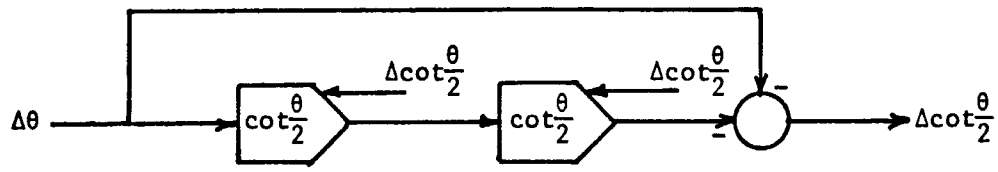

(a)

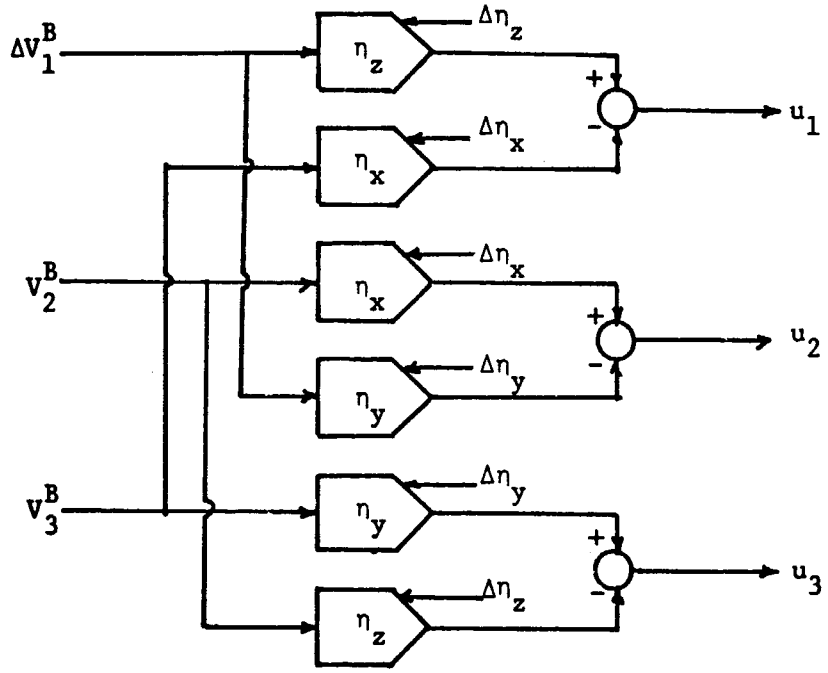

(b)

Figure 4-17. Realization of Euler 4 Parameter Algorithm.

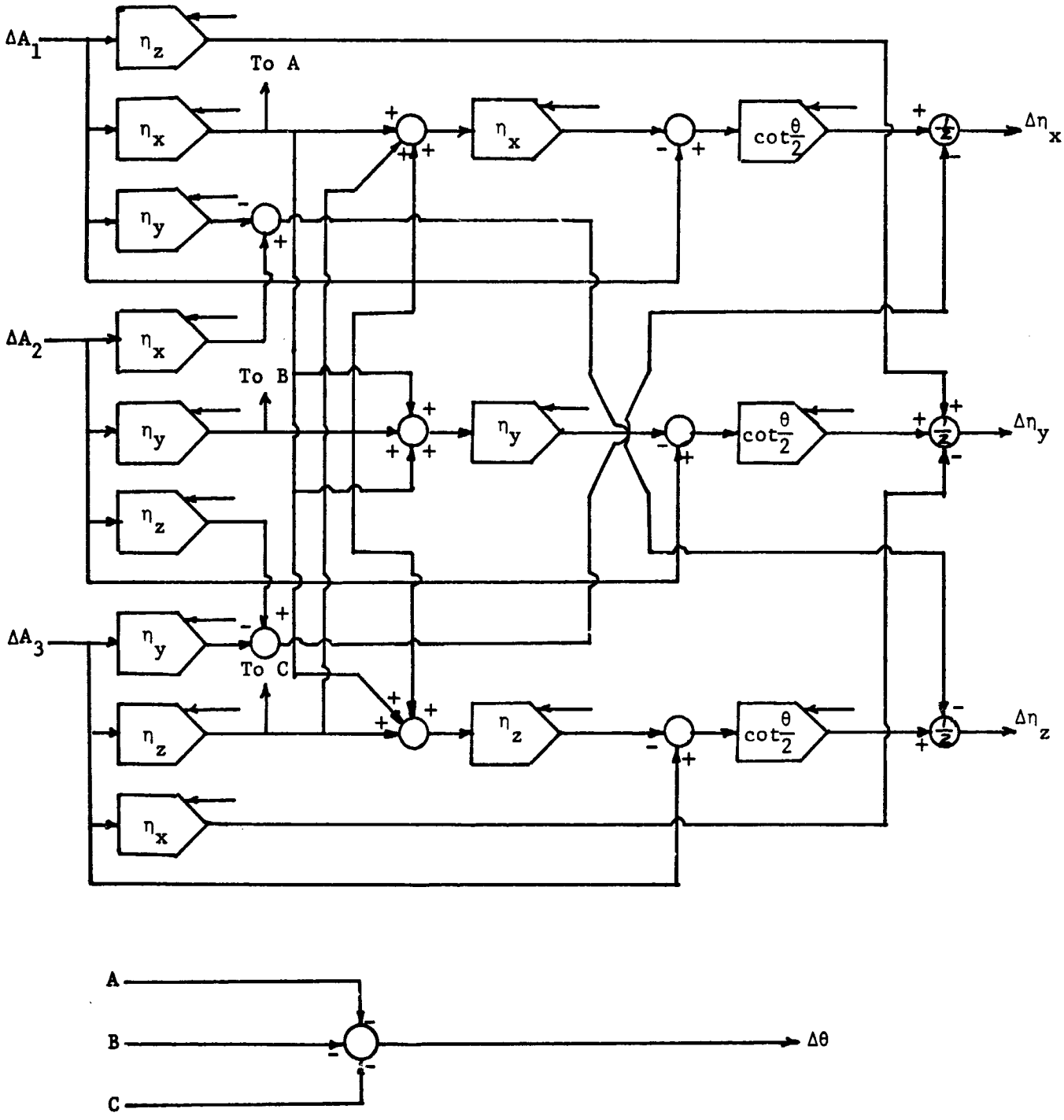

(c)

Figure 4-17. (Continued).

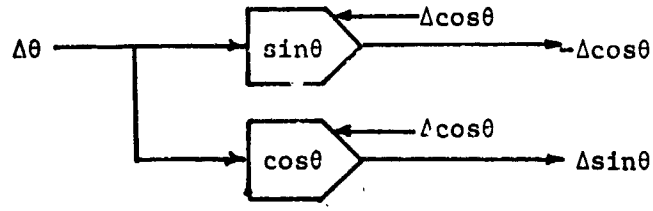

(d)

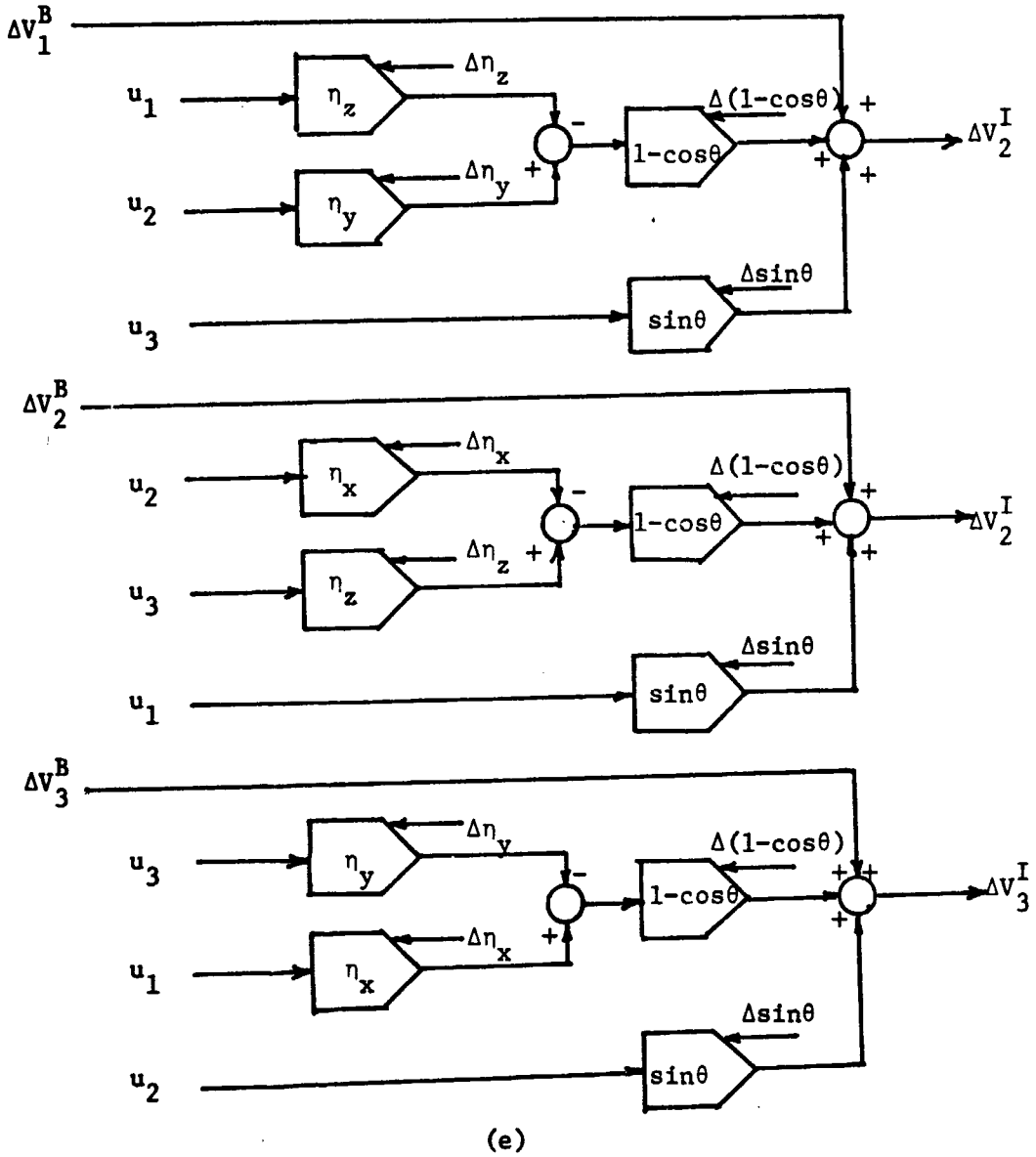

(e)

Figure 4-17. (Continued)

Quaternion or Cayley-Klein Algorithms

The DDA requirement for quaternion method or for Cayley-Klein method is the same due to the isomorphism of these two methods. The quaternion differential equations are expressed by

$$\begin{bmatrix} \dot{s} \\ \dot{v}_x \\ \dot{v}_y \\ \dot{v}_z \end{bmatrix} = \frac{1}{2} \begin{bmatrix} 0 & -\omega_x & -\omega_y & -\omega_z \\ \omega_x & 0 & -\omega_z & \omega_y \\ \omega_y & \omega_z & 0 & -\omega_x \\ \omega_z & -\omega_y & \omega_x & 0 \end{bmatrix} \begin{bmatrix} s \\ v_x \\ v_y \\ v_z \end{bmatrix} \tag{4-83}$$

In incremental form

$$\begin{bmatrix} \Delta s \\ \Delta v_x \\ \Delta v_y \\ \Delta v_z \end{bmatrix} = \frac{1}{2} \begin{bmatrix} 0 & -\Delta A_1 & -\Delta A_2 & -\Delta A_3 \\ \Delta A_1 & 0 & -\Delta A_3 & \Delta A_2 \\ \Delta A_2 & \Delta A_3 & 0 & -\Delta A_1 \\ \Delta A_3 & -\Delta A_2 & \Delta A_1 & 0 \end{bmatrix} \begin{bmatrix} s \\ v_x \\ v_y \\ v_z \end{bmatrix} \tag{4-146}$$

where

$$\Delta A_1 = \omega_x \Delta t$$

$$\Delta A_2 = \omega_y \Delta t$$

$$\Delta A_3 = \omega_z \Delta t$$

The transformation is given by

$$\begin{bmatrix} v_1^I \\ v_2^I \\ v_3^I \end{bmatrix} = \begin{bmatrix} 1 - 2(v_z^2 + v_y^2) & 2(-sv_z + v_x v_y) & 2(sv_y + v_x v_y) \\ 2(sv_z + v_x v_y) & 1 - 2(v_z^2 + v_x^2) & 2(-sv_x + v_z v_y) \\ 2(-sv_y + v_x v_z) & 2(sv_x + v_z v_y) & 1 - 2(v_y^2 + v_x^2) \end{bmatrix} \begin{bmatrix} v_1^B \\ v_2^B \\ v_3^B \end{bmatrix}$$

Multiplying the right hand side out and rearranging terms, we get

$$\left.\begin{aligned} v_1^I &= v_1^B + 2\left[(v_3^B v_x - v_1^B v_z)v_z + (v_2^B v_x - v_1^B v_y)v_y + (v_3^B v_y - v_2^B v_z)s\right] \\ v_2^I &= v_2^B + 2\left[(v_1^B v_y - v_2^B v_x)v_x + (v_3^B v_y - v_2^B v_z)v_z + (v_1^B v_z - v_3^B v_x)s\right] \\ v_3^I &= v_3^B + 2\left[(v_2^B v_z - v_3^B v_y)v_y + (v_1^B v_z - v_3^B v_x)v_x + (v_2^B v_x - v_1^B v_y)s\right] \end{aligned}\right\} \quad (4\text{-}147)$$

Let

$$\left.\begin{aligned} u_1 &= 2(v_1^B v_z - v_3^B v_x) \\ u_2 &= 2(v_2^B v_x - v_1^B v_y) \\ u_3 &= 2(v_3^B v_y - v_2^B v_z) \end{aligned}\right\} \quad (4\text{-}148)$$

Then, we have, from (4-147)

$$\left.\begin{aligned} v_1^I &= v_1^B - u_1 v_z + u_2 v_y + u_3 s \\ v_2^I &= v_2^B - u_2 v_x + u_3 v_z + u_1 s \\ V_3^I &= v_3^B - u_3 v_y + u_1 v_x + u_2 s \end{aligned}\right\} \quad (4\text{-}149)$$

The complete coordinate transformation is given by (4-146), (4-148) and (4-149). The DDA realization of (4-146) requires 12 DDA's as shown in Fig. 4-18a, the realization of (4-148) needs 6 DDA's as shown in Fig. 4-18b, and the realization of (4-149) requires 9 DDA's as shown in Fig. 4-18c. Therefore, the complete realization of (4-146), (4-148) and (4-149) for all coordinate variables requires a total of 12 + 6 + 9 = 27 DDA's

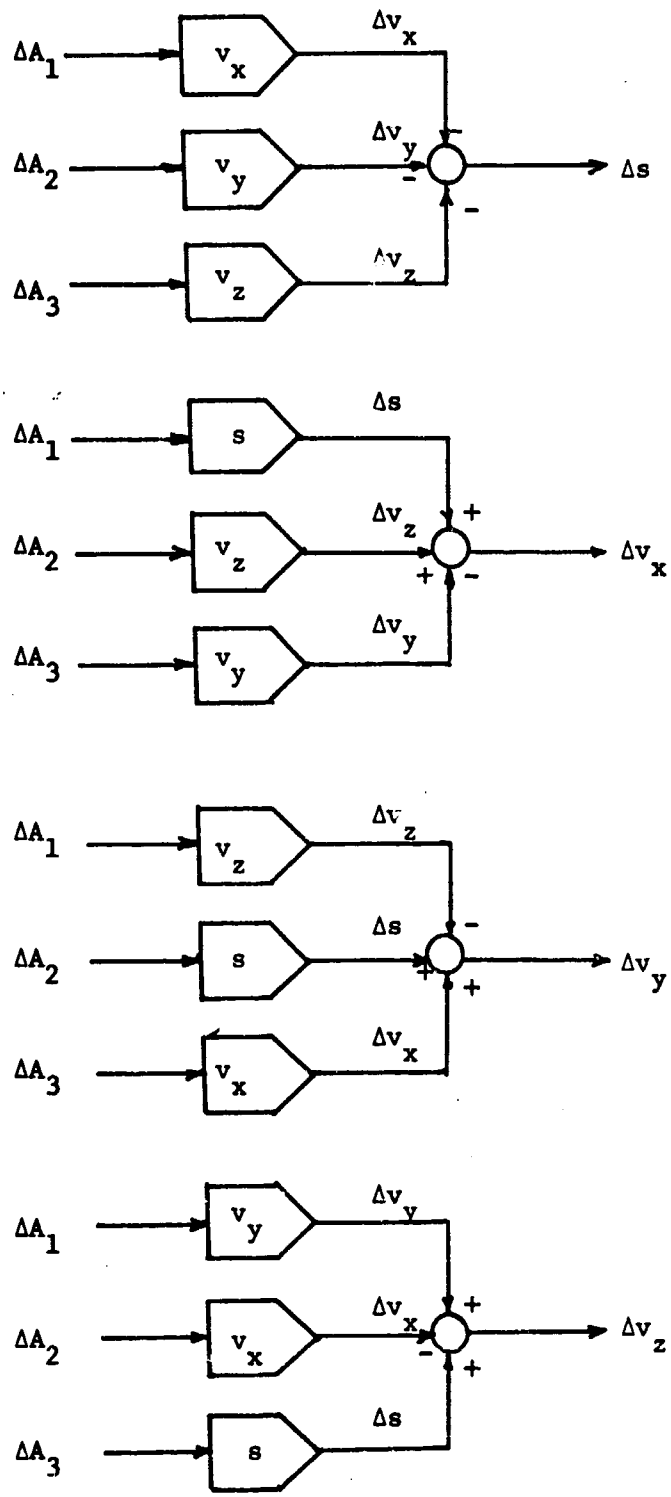

Figure 4-18. Realization of Quaternion Algorithm.

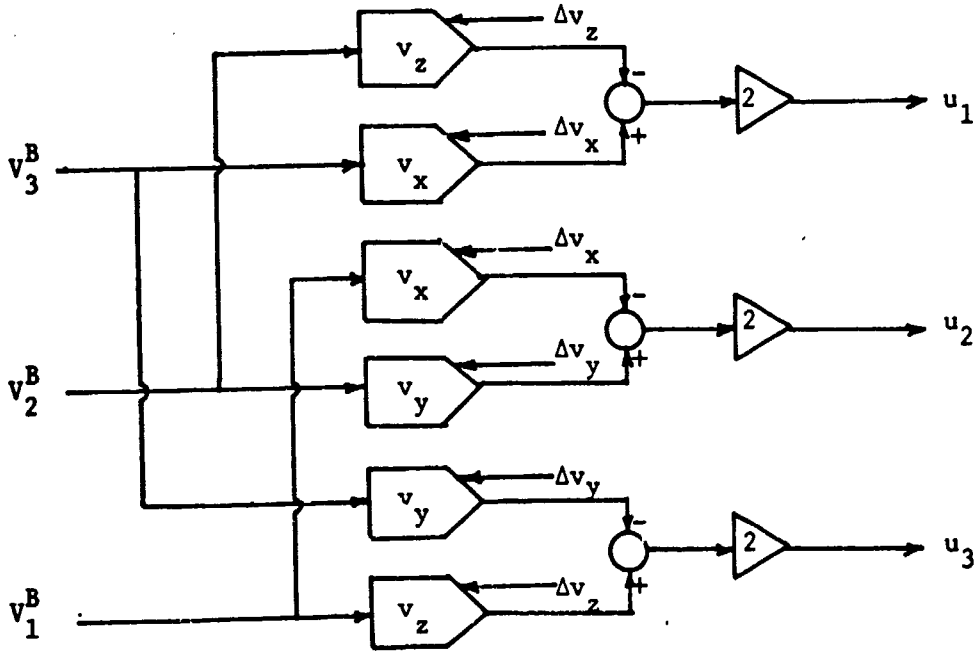

(b)

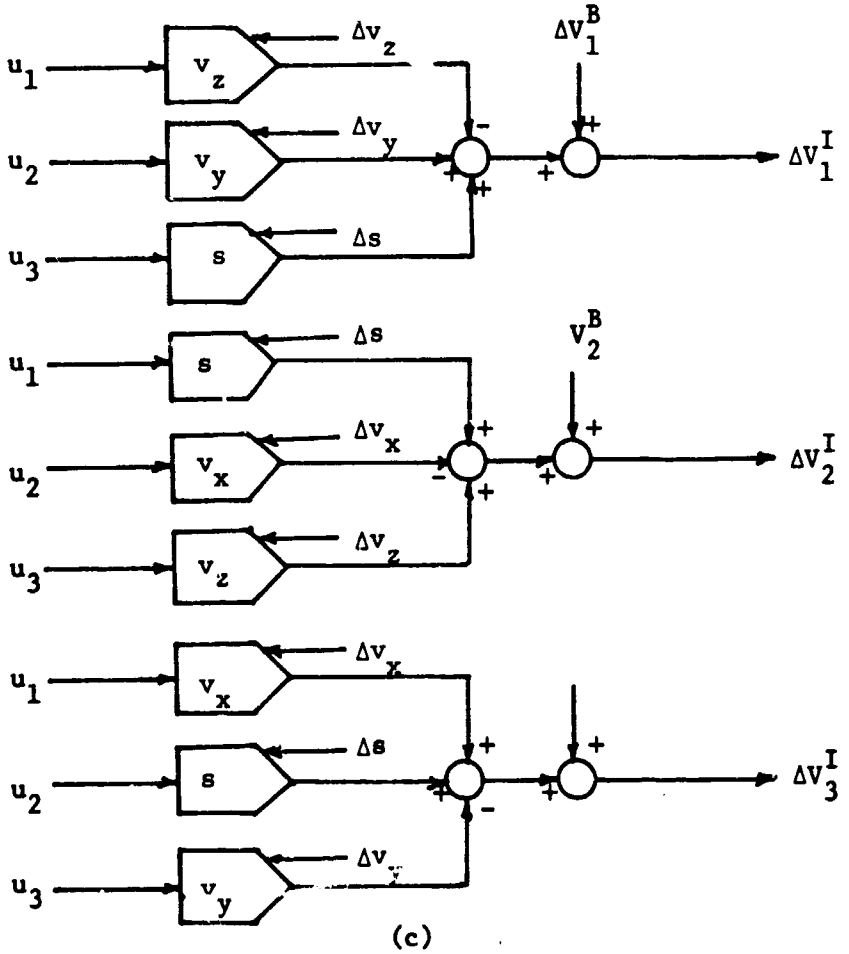

(c)

Figure 4-18. (Continued).

Vector Representation Method

Recall the equation

$$\dot{\Sigma} = \frac{1}{2}\left[\frac{1+\sigma^2}{2}\ \Omega + (\Sigma \times \Omega) + \Sigma \times (\Sigma \times \Omega)\right] \qquad (4\text{-}133)$$

Expanding (4-133) and then to put it into the matrix form

$$\begin{bmatrix}\dot{\sigma}_x\\ \dot{\sigma}_y\\ \dot{\sigma}_z\end{bmatrix} = \frac{1}{2}\begin{bmatrix}\frac{1}{2}(1+\sigma_x^2-\sigma_y^2-\sigma_z^2) & -\sigma_y+\sigma_x\sigma_y & \sigma_x+\sigma_x\sigma_z\\ \sigma_x+\sigma_x\sigma_y & \frac{1}{2}(1-\sigma_x^2+\sigma_y^2-\sigma_z^2) & -\sigma_x+\sigma_y\sigma_z\\ -\sigma_y+\sigma_x\sigma_z & \sigma_x+\sigma_z\sigma_y & \frac{1}{2}(1-\sigma_x^2-\sigma_y^2+\sigma_z^2)\end{bmatrix}\begin{bmatrix}\omega_x\\ \omega_y\\ \omega_z\end{bmatrix}$$

Letting

$$\Delta A_1 = \Delta_x \omega t$$

$$\Delta A_2 = \omega_y \Delta t$$

$$\Delta A_3 = \omega_z \Delta t$$

we then have

$$\begin{bmatrix}\Delta\sigma_x\\ \Delta\sigma_y\\ \Delta\sigma_z\end{bmatrix} = \frac{1}{2}\begin{bmatrix}\frac{1}{2}(1+\sigma_x^2-\sigma_y^2-\sigma_z^2) & -\sigma_z+\sigma_x\sigma_y & \sigma_y+\sigma_x\sigma_z\\ \sigma_z+\sigma_x\sigma_y & \frac{1}{2}(1-\sigma_x^2+\sigma_y^2-\sigma_z^2) & -\sigma_x+\sigma_y\sigma_z\\ -\sigma_y+\sigma_x\sigma_z & \sigma_x+\sigma_z\sigma_y & \frac{1}{2}(1-\sigma_x^2-\sigma_y^2-\sigma_z^2)\end{bmatrix}\begin{bmatrix}\Delta A_1\\ \Delta A_2\\ \Delta A_3\end{bmatrix}$$

or

$$\left.\begin{aligned}\Delta\sigma_x &= \frac{1+\sigma^2}{4}\cdot\Delta A_1 + \frac{1}{2}\left[(\Delta A_3\sigma_x-\Delta A_1\sigma_z)\sigma_z + (\Delta A_2\sigma_x-\Delta A_1\sigma_y)\sigma_y + (\Delta A_3\sigma_y-\Delta A_2\sigma_z)\right]\\ \Delta\sigma_y &= \frac{1+\sigma^2}{4}\cdot\Delta A_2 + \frac{1}{2}\left[(\Delta A_1\sigma_y-\Delta A_2\sigma_x)\sigma_x + (\Delta A_3\sigma_y-\Delta A_2\sigma_z)\sigma_z + (\Delta A_1\sigma_z-\Delta A_3\sigma_x)\right]\\ \Delta\sigma_z &= \frac{1+\sigma^2}{4}\cdot\Delta A_3 + \frac{1}{2}\left[(\Delta A_2\sigma_y-\Delta A_3\sigma_y)\sigma_y + (\Delta A_1\sigma_z-\Delta A_3\sigma_x)\sigma_x + (\Delta A_2\sigma_x-\Delta A_1\sigma_y)\right]\end{aligned}\right\} \qquad (4\text{-}150)$$

Letting

$$\left.\begin{aligned} u_1 &= \frac{1}{2}\,(\Delta A_1\sigma_z - \Delta A_z\sigma_x) \\ u_2 &= \frac{1}{2}\,(\Delta A_2\sigma_x - \Delta A_1\sigma_y) \\ u_3 &= \frac{1}{2}\,(\Delta A_3\sigma_y - \Delta A_2\sigma_z) \end{aligned}\right\} \qquad (4\text{-}151)$$

Then (4-150) becomes

$$\left.\begin{aligned} \Delta\sigma_x &= \frac{1+\sigma^2}{4}\cdot\Delta A_1 - u_1\sigma_z + u_2\sigma_y + u_3 \\ \Delta\sigma_y &= \frac{1+\sigma^2}{4}\cdot\Delta A_2 - u_2\sigma_x + u_3\sigma_z + u_1 \\ \Delta\sigma_{\ } &= \frac{1+\sigma^2}{4}\cdot\Delta A_3 - u_3\sigma_y + u_1\sigma_x + u_2 \end{aligned}\right\} \qquad (4\text{-}152)$$

The transformation equation is given by

$$V^I = V^B + \frac{4(1-\sigma^2)}{(1+\sigma^2)^2}\;(\Sigma \times V^B) + \frac{8}{(1+\sigma^2)^2}\;(\Sigma \times \Sigma \times V^B) \qquad (4\text{-}153)$$

Recognizing the similarity between (4-153 and (4-133) in their form, we can write (4-153) directly into the following form using incrementals,

$$\left.\begin{aligned} \Delta v_1^I &= \Delta v_1^B + \frac{1}{(1+\sigma^2)^2}\left[4(1-\sigma^2)u_3' + 8(u_2'\sigma_y - u_1'\sigma_z)\right] \\ \Delta v_2^I &= \Delta v_2^B + \frac{1}{(1+\sigma^2)^2}\left[4(1-\sigma^2)u_1' + 8(u_3'\sigma_z - u_2'\sigma_x)\right] \\ \Delta v_3^I &= \Delta v_3^B + \frac{1}{(1+\sigma^2)^2}\left[4(1-\sigma^2)u_2' + 8(u_1'\sigma_x - u_3'\sigma_y)\right] \end{aligned}\right\} \qquad (4\text{-}154)$$

where

$$\left.\begin{aligned} u_1' &= \Delta v_1^B\sigma_z - \Delta v_3^B\sigma_x \\ u_2' &= \Delta v_2^B\sigma_x - \Delta v_1^B\sigma_y \\ u_3' &= \Delta v_3^B\sigma_y - \Delta v_2^B\sigma_z \end{aligned}\right\} \qquad (4\text{-}155)$$

Since

$$\Delta(1+\sigma^2) = \Delta(1+\sigma_x^2 + \sigma_y^2 + \sigma_z^2) \cong 2\ (\sigma_x\ \Delta\sigma_x + \sigma_y\ \Delta\sigma_y + \sigma_z\ \Delta\sigma_z)$$

it needs 3 DDA's to realize as shown in Fig. 4-19a. The quantity

$$\Delta \frac{1}{(1+\sigma^2)^2} = -\ 2\frac{\Delta(1+\sigma^2)}{(1+\sigma^2)^3} = 2\ \frac{1}{(1+\sigma^2)}\ \frac{-\Delta(1+\sigma^2)}{(1+\sigma^2)^2} = 2\ \frac{1}{1+\sigma^2}\ \Delta\left(\frac{1}{1+\sigma^2}\right)$$

can be realized by 2 DDA's as shown in Fig. 4-19b. Equations (4-151), (4-152), (4-154) and (4-155) can be realized by 6, 9, 12 and 6 DDA's, respectively, as shown in Figures 4-19c, d, e and f. Therefore, a total of 3 + 2 + 6 + 9 + 12 + 6 = 38 DDA's are required. Notice that

$$\Delta(1-\sigma^2) = -\ 2\ (\sigma_x\Delta\sigma_x + \sigma_y\Delta\sigma_y + \sigma_z\Delta\sigma_z) = -\ \Delta(1+\sigma^2)$$

This operation is also included in Fig. 4-19.

Summary

The following is a table summarizing and comparing the numbers of required DDA's for each attitude algorithm, as obtained from this study and obtained by other research.[1]

Table 4-1. Summary of DDA Requirements.

Algorithm	Number of DDA's Required	
	Reference 1	This Study
Direction Cosine Algorithm	27	27
Euler Angle Algorithm	46	27
Euler 4-Parameter Algorithm	-	37
Quaternion or Cayley-Klein Algorithms	33	27
Vector Representation Algorithm	46	38

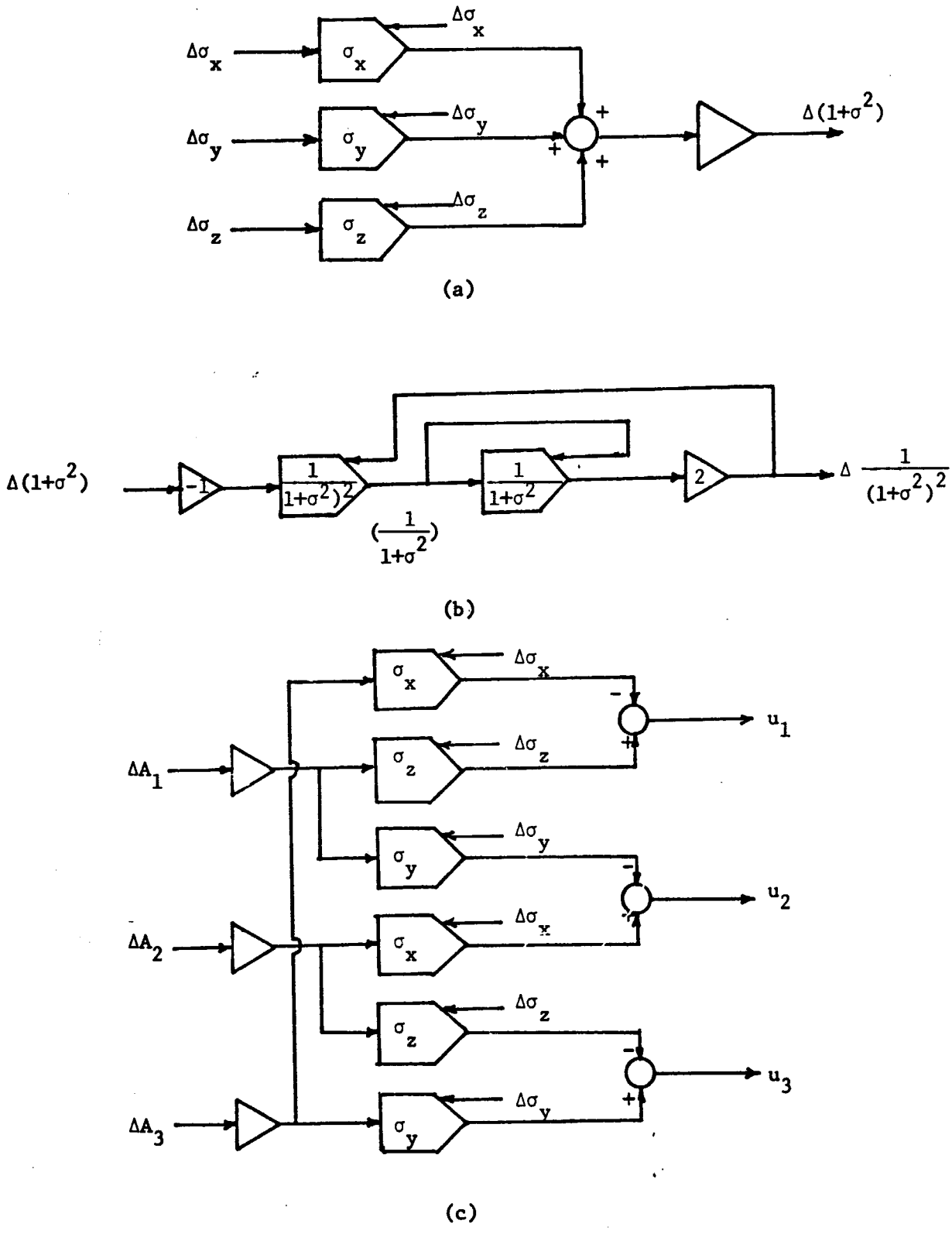

Figure 4-19. Realization of Vector Representation Algorithm.

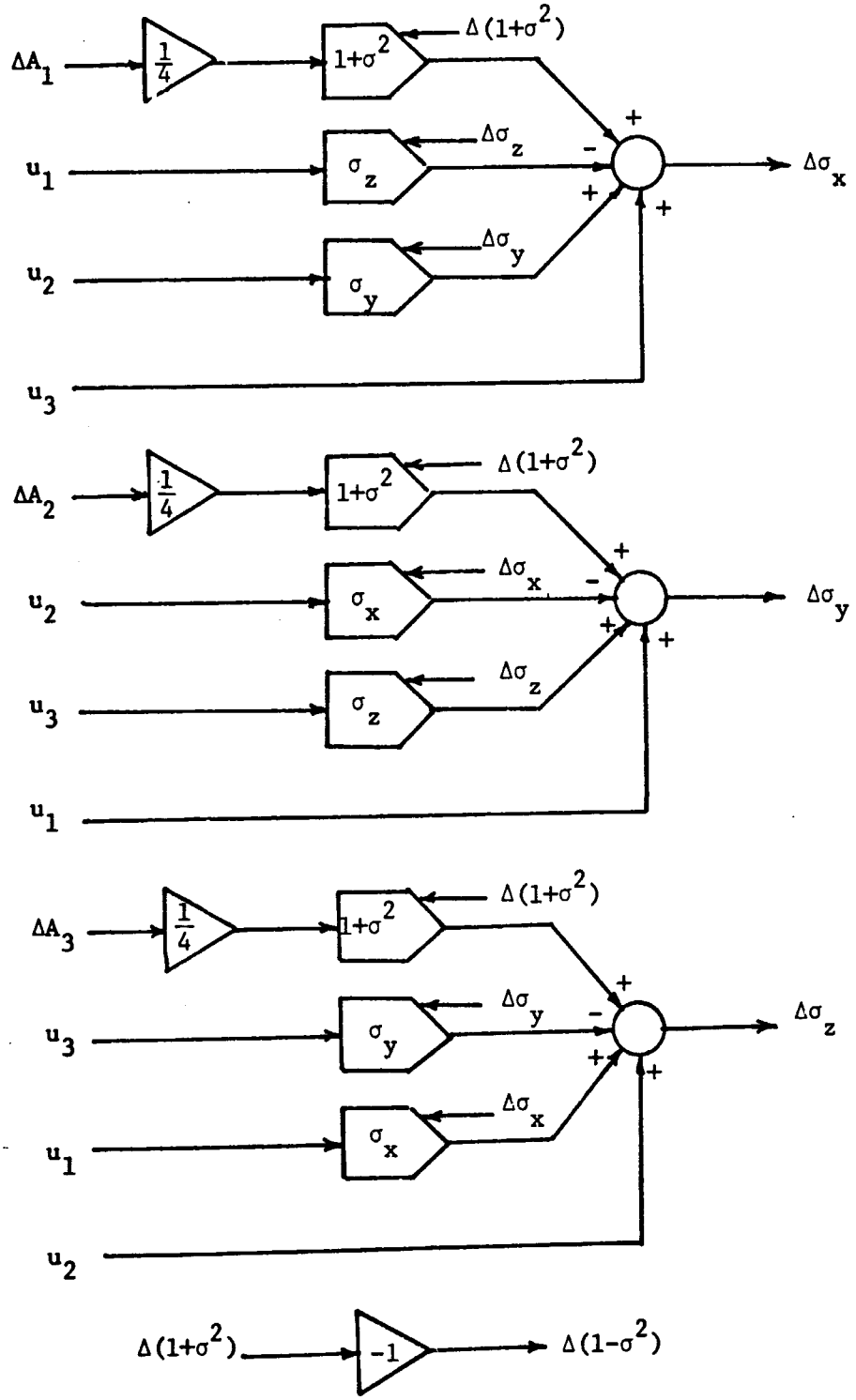

(d)

Figure 4-19. (Continued).

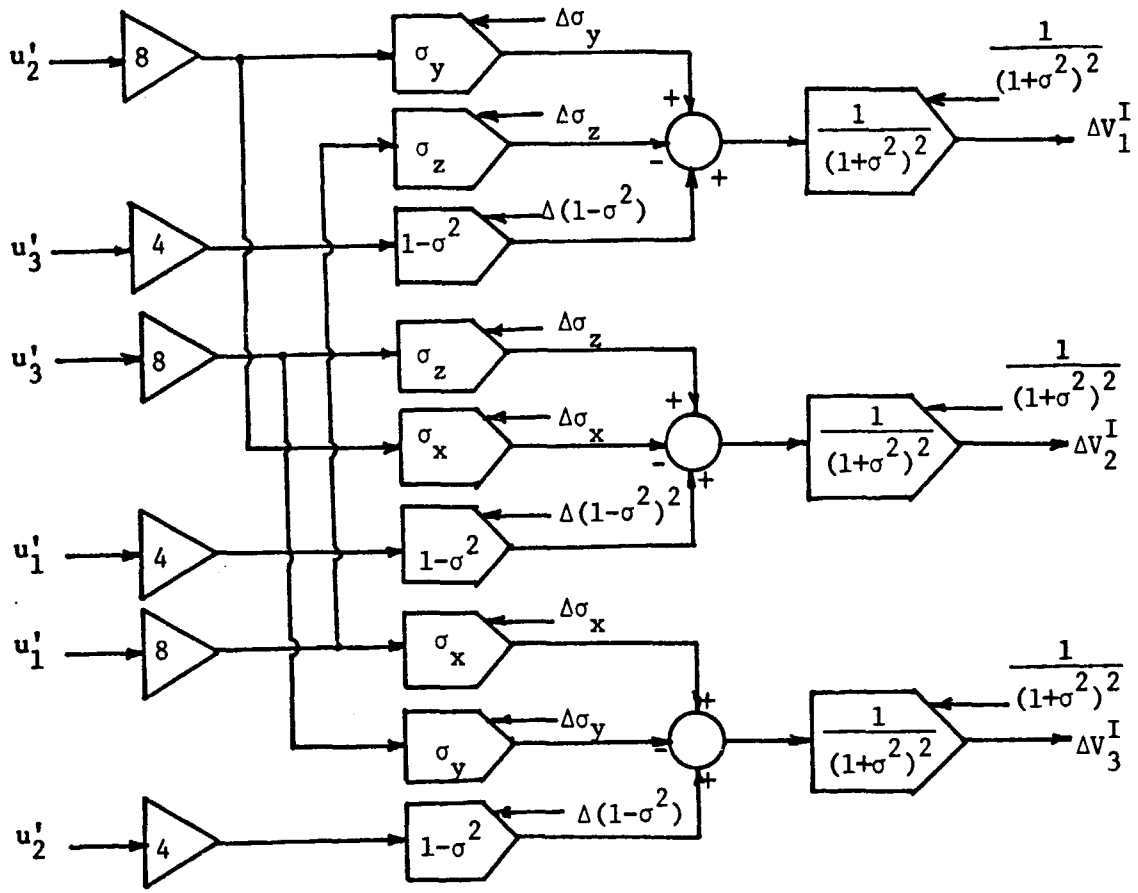

(e)

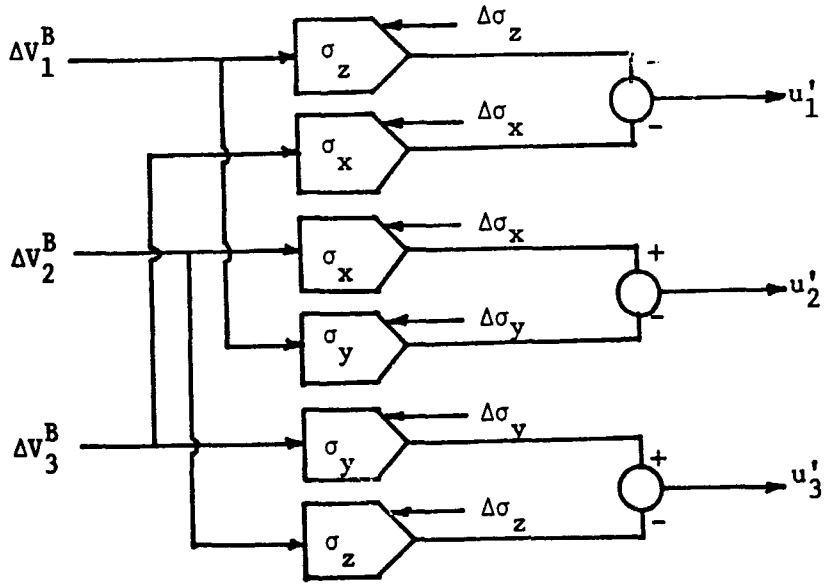

(f)

Figure 4-19. (Continued).

References

1. T.F. Wiener: Theoretical Analysis of Gimballess Inertial Reference Equipment Using Delta Modulated Instruments, Doctoral Dissertation, M.I.T., March, 1962.

2. K.C. Chu: Methods of Coordinate Transformations in Analytic Platform, M.S. Thesis, University of Tennessee, December, 1966.

3. H.B. Phillips: Vector Analysis, John Wiley and Sons, Inc., New York, N.Y., 1933.

4. F.R. Gantmacher: The Theory of Matrices, Volumes I & II, Chelsea Publishing Co., New York, N.Y., 1960.

5. H. Goldstein: Classical Mechanics, Addison-Wesley Publishing Co., Reading, Mass., 1950, Chapter 4.

6. P.M. Morse and H. Feshbach: Methods of Theoretical Physics, Volume I, McGraw-Hill Book Co., 1953.

7. Y. Yeh and J.C. Hung, "DDA Realizations of Attitude Algorithms", Proceedings of Fifth Hawaii International Conference on Systems Science, January 11-13, 1972, Honolulu, Hawaii.

CHAPTER 5

REBALANCE ELECTRONICS

T.V. Blalock and E.J. Kennedy

ABSTRACT

Two basic types of strapdown gyroscope rebalance-electronics were analyzed and compared. These two types were a discrete-pulse ternary system developed at the MIT Draper Laboratory and a width-modulated binary system developed at the Hamilton Standard System Center. In the analyses, major emphasis was placed on the logic sections, the H-switches, the precision voltage reference loops, the noise performance, common-mode rejection, and loop compensation. Results of the analyses were used in identifying specific advantages and disadvantages of system details and in making accuracy and resolution comparisons. Sound engineering principles were applied in the development of both systems; however, it was concluded that each system has some disadvantages that are amenable to improvement.

INTRODUCTION

A preliminary study of three different realizations of rebalance electronic loops for strapdown gyroscopes resulted in the selection of two of the three for the detailed analyses presented in this chapter. The three systems were (1) the Honeywell ternary[1], (2) the MIT Draper Laboratory ternary[2], and (3) the Hamilton Standard width-modulated binary[3].

After the preliminary study, the Honeywell system was eliminated as a candidate for the detailed analyses for two reasons, (1) the

preliminary study results indicated that the Honeywell system had several disadvantages not apparent in the other two systems, and (2) the allotted contract time would allow a detailed analysis of only one example of the two basic types of systems--ternary and binary.

In the second section of this chapter a description of the two systems analyzed will be given. In the third section, analyses of the logic blocks, H-switches, PVR loops, noise performance, common-mode rejection and compensation are presented. Resolution and accuracy are considered in the fourth section. The last section contains a summary of comparisons between the two systems analyzed and concluding recommendations.

DESCRIPTION OF SYSTEMS ANALYZED

A general description of the organization and operation of the Hamilton Standard and the MIT rebalance electronics will be presented in this Section.

Hamilton Standard System

The basic components of the rebalance electronics for the Hamilton Standard width-modulated-binary strapdown gyroscope system is shown in Fig. 5-1. The system can be divided into two sections, (1) the rebalance loop that surrounds the gyro, and (2) the digital control electronics (DCE) which generates the basic commands for system operation.

The rebalance loop senses movement of the gyro float from its quiescent position and then generates pulses of torque current to restore the float to its quiescent position. The DCE determines the error signal sampling frequency, determines the torquing mode and switches scale factor when necessary, and generates 256 kHz data pulses which give the amount of torque-current area (ampere-seconds) fed into the torquer.

The input to the rebalance loop is a 50 kHz sinusoidal error signal from a sensitive (1.39mv./arc-sec) capacitance bridge pick-off mounted in the gyroscope. The error signal is processed by a high-input impedance preamplifier which removes common-mode signals contaminating the error

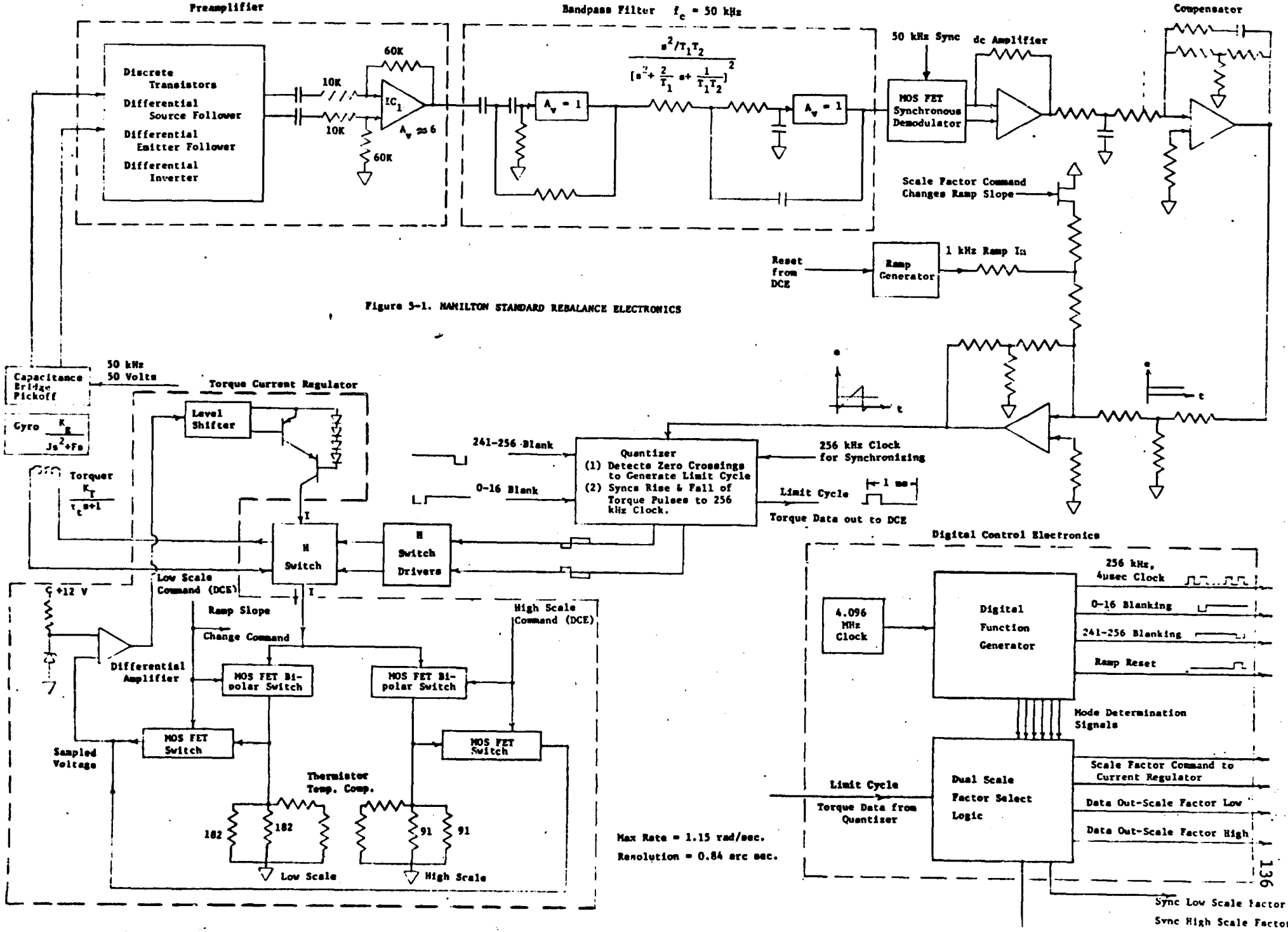

Figure 5-1. HAMILTON STANDARD REBALANCE ELECTRONICS

signal. The output of the preamplifier feeds a bandpass filter which further improves the signal-to-noise ratio of the amplified error signal. The bandpass filter feeds a synchronous demodulator whose dc output voltage can have positive or negative polarity depending on which of the two possible directions the gyro axis has moved. The dc error signal is amplified, compensated for system dynamics and then mixed with a 1 kHz ramp signal. The zero-voltage crossing point of this composite signal determines how the total torque applied to the torquer will be apportioned between positive and negative torques. The zero crossing is detected by a group of logic gates in the quantizer (Fig. 5-1). Detection of the zero crossing is indicated by a transition in the quantizer J-K flip-flop which feeds torque command signals to the H-switch drivers and a 1 kHz forced limit-cycle signal to the DCE for torque mode determination. The frequency (1 kHz) of the limit cycle is set by the ramp reset signal which is the inversion of the 241-256 blanking signal generated in the DCE. The blanking signals (0-16 blank and 241-256 blank) assure that for any torquing condition, both positive and negative torque will be applied for at least 16/256 msec.

The H-switch routes a precisely controlled current I to the torquer. The bilateral nature of the H-switch allows current to be driven in both directions through the torquer so that the net movement of the gyro float axis for each 1 msec torquing interval is proportional to the difference between the positive torque current area and the negative torque current area. Thus, a zero net torque requirement is fulfilled by equal positive and negative torque current areas.

The system scale factor is determined by the current level feeding the H-switch; consequently, a scale factor change is executed by switching the current level with a scale-factor change command from the DCE to the torque current regulator. The current level is changed in the regulator by switching the values of the current sensing resistors. The current I is about 143 ma in the high mode and about 71.5 ma in the low mode. The scale factor change command also changes the effective gain in the rebalance loop by varying the ramp signal slope.

The digital control electronics is fed by a 4.096 MHz clock signal. The DCE consists of two primary blocks; the digital function generator (DFG) and the dual scale-factor select logic (DSFS). The DFG generates (1) a 256 kHz, 1 μsec wide clock signal for logic synchronization and data output, (2) a 0-16 blanking signal, (3) a 241-256 blanking signal, (4) a ramp reset signal, and (5) a set of six mode-interrogation signals. All of these DFG signals are generated in each 1 msec interrogation period. Two of the mode interrogation signals determine the allowable high-mode limit-cycle range, two determine the low-mode range, and two are used to set the DSFS for scale factor change.

In the DSFS, the mode interrogation signals examine the 1 kHz limit cycle from the quantizer to ascertain in which torque mode (high or low) the rebalance loop should be operating. If the high mode is needed, the DSFS will generate a high scale factor command after 4 high torque-current pulses; if the low mode is required, the low scale factor command will be generated after 2048 low torque current pulses.

The DSFS also generates the 256 kHz data pulses which contain the torquing information. The DSFS selects one data line for high mode, and another for low mode. High and low mode sync pulses are transmitted out on two other lines to indicate the initiation of a data pulse train (a data train is produced for each 1 msec interrogation period).

MIT Draper Laboratory System

The MIT rebalance electronics is a ternary system that is composed of a rebalance loop and a logic block (Fig. 5-2). Pulses of torque current are routed to the torquer only when the error signal exceeds a pre-set positive or negative limit. The polarity of the error signal depends on which of the two possible motions of the gyro float axis has occurred, and therefore determines the polarity of the rebalance torque to be applied. The error signal is sampled at 104 μsec intervals (9.6 kHz rate). In each 104 μsec interval, a 6.5 μsec period is used to set up the torquing circuitry, and a 97.5 μsec torque command pulse is generated. The torquing circuitry is set up to (1) route the torque pulse to the torquer or to a dummy load, and (2)

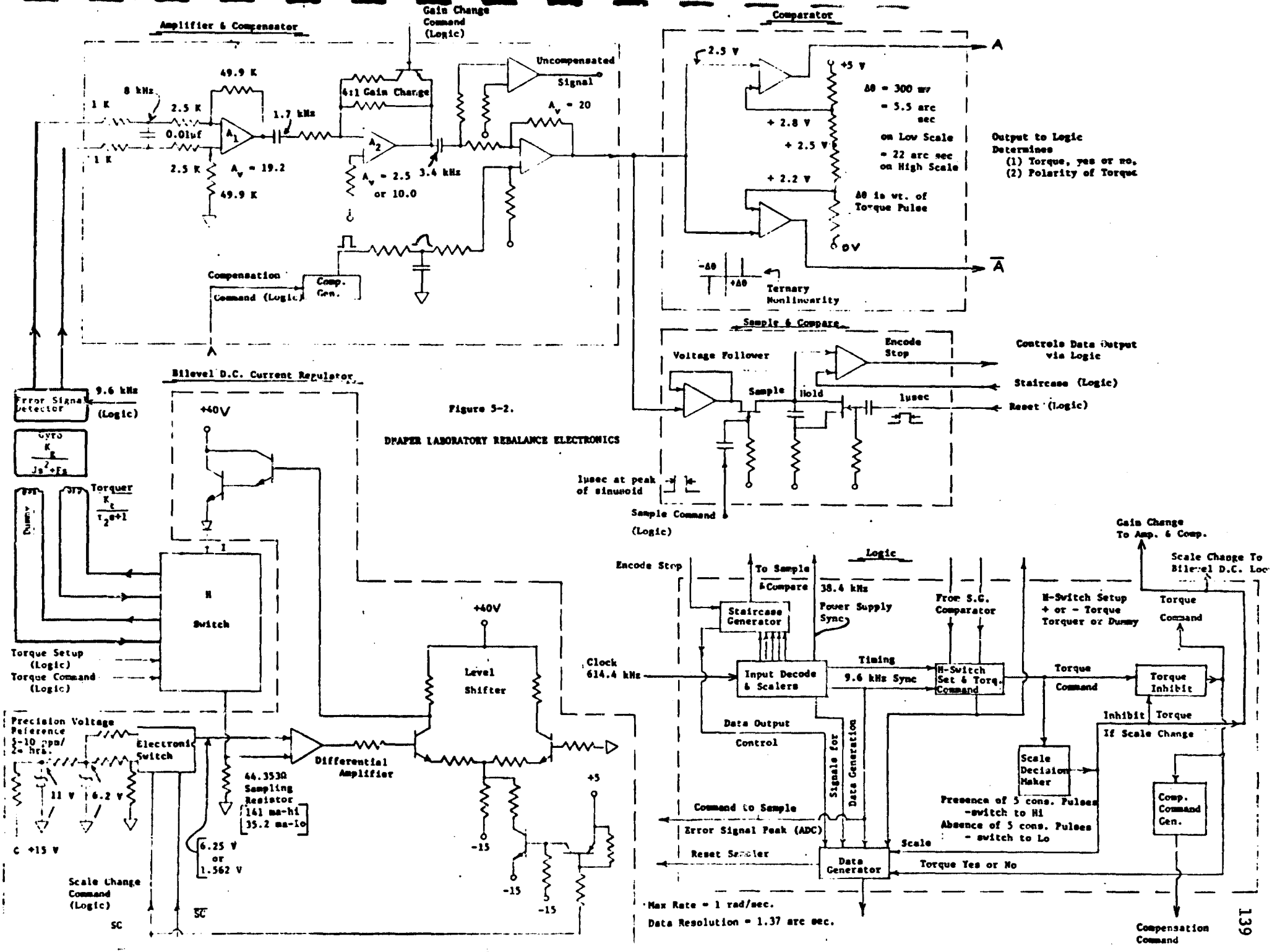

Figure 5-2.

DRAPER LABORATORY REBALANCE ELECTRONICS

to generate a negative or positive torque pulse.

The input of the rebalance loop is a 9.6 kHz error signal from the gyro float position pickoff which is fed by a 9.6 kHz signal generated in the logic block. Thus, the error signal phase is synchronized with the command signals generated in the logic block.

The error signal is first processed by the amplifier and compensation section (Fig. 5-2). In this section the error signal is amplified, filtered to reduce common-mode and electronic noise, and mixed with a parallel compensation signal. The compensation is applied only when the torque command pulse is present and causes that part of the rebalance loop from torquer input to amplifier output to have a response that closely approximates that of a pure integrator. The scale-factor command changes the gain of the amplifier by switching the value of a feedback resistor in an operational amplifier.

The amplified and compensated error signal (a 9.6 kHz sinusoid) is next fed to the comparator. At the comparator input the error signal is a sinusoid superimposed on a 2.5 volt dc level. The comparator reference signal (see Fig. 5-2) is also 2.5 volts. Since each interrogation period spans one cycle of the 9.6 kHz error signal, the polarity of the peak amplitude of the error signal at a fixed strobe time, which is set by logic synchronizing signals, determines the polarity of the required torque current pulse, and the amplitude of the error signal determines the need for a torque current pulse. That is, if the peak amplitude of the error signal is outside the comparator set points, 2.5 ± 0.3 volts, a torque current pulse of appropriate polarity will be routed to the torquer. The two outputs (one for positive and one for negative error signal polarity) are interrogated in the logic block by the strobe signal.

Connected in parallel with the input to the comparator is a sample-and-compare circuit. A sample command pulse from the logic block opens a field-effect transistor (FET) gate at the time of occurrence of the error signal peak. The peak value is then stored on a capacitor at one input to a comparator. The other input to the comparator is fed by a staircase

signal from the logic block. The number of steps necessary to reverse the comparator output is recorded in the logic block which generates a number of data pulses proportional to the number of stair steps, and thus, performs an analog-to-digital conversion (ADC) on the error signal peak amplitude. The resolution of the ADC operation is $\Delta\theta/4$ where $\Delta\theta$ is the 0.3 volt comparator set point. Thus, one data pulse corresponds to a 75 millivolt increment in the error signal amplitude at the comparator input. At the termination of the ADC operation, the logic block sends a reset command to the sample-and-compare circuit to return the sample capacitor voltage to its quiescent value in preparation for another interrogation period.

During the 6.5 μsec set-up interval, the logic block examines the comparator output and then (1) sets the H-switch to route a torque current pulse to a dummy load (no torque) or to the torquer, and (2) sets the H-switch to route a positive or negative torque current pulse to the torquer if torque is required. At the end of the 6.5 μsec set-up period, the logic block transmits a 97.5 μsec torque command pulse to the H-switch.

The H-switch torque current source is a precision regulated dc current I (Fig. 5-2). The current I is fixed in amplitude by a 44.353Ω precision resistor and a precision voltage reference. To change scale factors, the voltage reference is switched between 6.25 volt and 1.562 volt levels. Therefore, the scale factor can be changed by a factor of four.

The basic input to the logic block is a 614.4 kHz clock which determines all the system timing. The other inputs are (1) the two inputs from the error signal comparator, and (2) the encode stop signal from the sample-and-hold circuit. The outputs are the following: (1) a staircase voltage, (2) a 38.4 kHz sync signal to the power supplies, (3) H-switch setup signals, (4) torque command signal, (5) gain change command to the amplifier and compensator section, (6) scale change command to the bilevel dc current regulator, (7) compensation command to the amplifier and compensator section, (8) sample command to the sample-and-compare circuit, (9) a reset command to the sample-and-compare circuit, and (10) the data output train. The signals nos. 1, 3, 4, 7, 8, 9, 10 all occur in each 104 μsec interrogation interval. The signals nos. 5 and 6 occur only when a scale

factor change is demanded.

The scale decision maker in the logic block commands a scale change for the following conditions: the scale factor is switched to high if five consecutive torque current pulses are routed to the torquer; a switch to low occurs if five consecutive pulses are absent.

The data train is a sequence of pulses occurring at a 614.4 kHz rate. The first pulse occurs at the peak of the 9.6 kHz error signal; it is the data sync pulse and is 1 μsec wide. The second pulse contains scale factor information--pulse present means high scale, pulse absent means low scale. The presence of the third pulse indicates torque applied while the absence indicates the converse. The fourth pulse is present for positive and absent for negative torque. The next 1 to 31 pulses are data pulses, each with $\theta/4$ (75 mv) weighting. Consequently, the error signal dynamic range is $\pm 4\theta$ or $\pm$ 1.2 volts.

ANALYSIS OF SYSTEM BLOCKS

Logic Blocks

In this section, the detailed analysis of the operation of the Hamilton Standard and the MIT logic blocks will be presented and some comparisons of salient features will be made.

Hamilton Standard Logic[4]. The purpose of the digital function generator DFG is to produce in each millisec interrogation period the signals shown in Fig. 5-3. The 4.096 MHz clock input signal is counted down to produce the 256 kHz pulse train which is used for logic synchronization, data generation, mode interrogation signal generation, and basic command signal generation. Logic synchronization is accomplished simply by feeding the 256 kHz train into the clock inputs of each logic component so that logic signal excursions occur on the trailing edge of the sync signal. The logic components are standard-line TI SN5400-series devices.

In the DFG, the 256 kHz pulse train counts down a four-bit binary counter (TI SN5493). The 16 kHz output of this counter is used to count

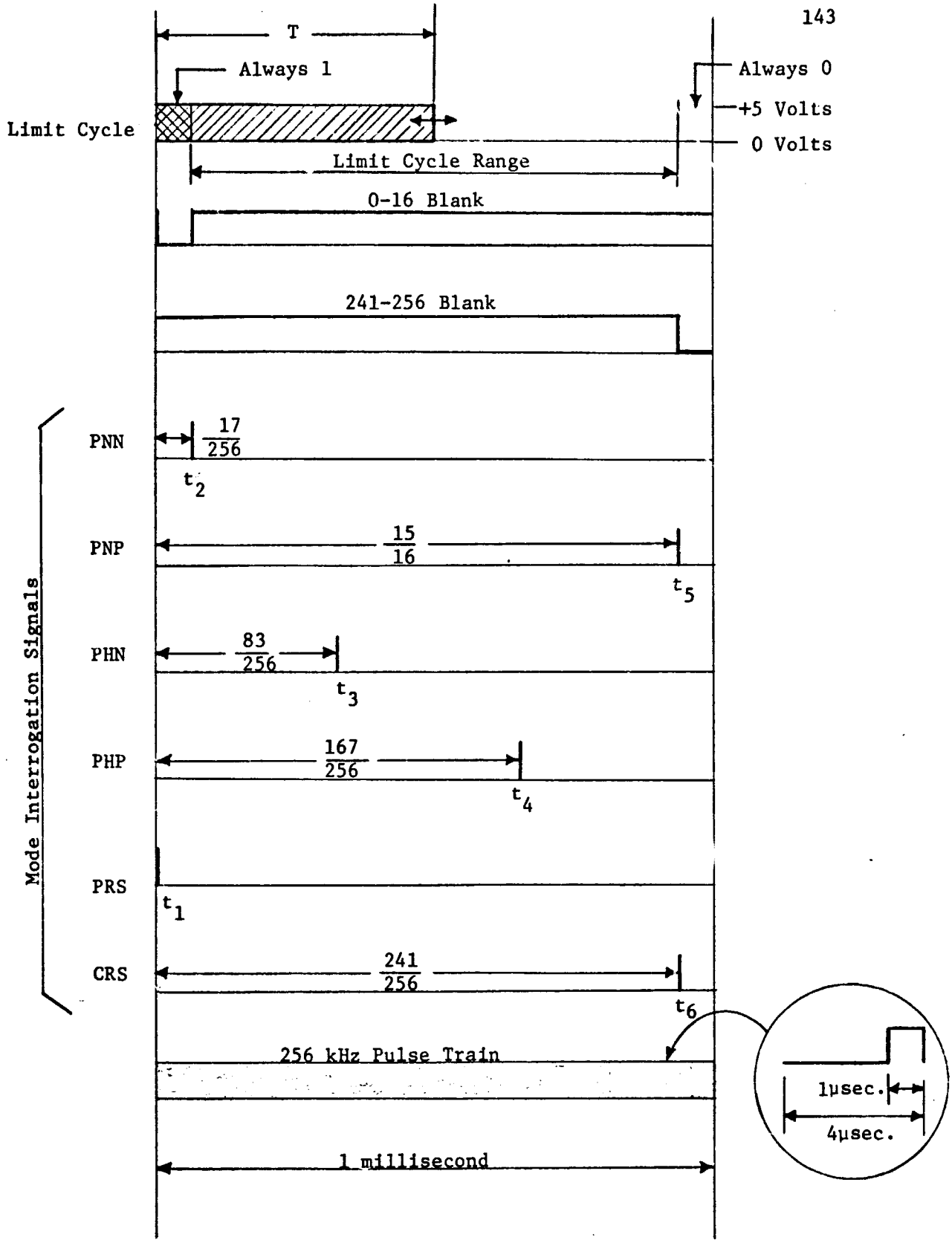

Figure 5-3. Signals Generated by the Digital Function Generator.

down a second four-bit binary counter. The outputs of the second counter feed two binary-to-decimal decoders (TI-SN5442) which provide the 0-16 blank, 241-256 blank, and a set of gating signals. The gating signals and the output signals from the first counter are fed into a set of positive nor gates (TI-SN5402) where the gating signals select certain of the first counter signals. These selected signals are then transferred through two 4-bit parallel-in, parallel-out storage registers (TI-SN5495) to the DFG output lines. These output signals are the mode interrogation signals PNN, PNP, PHN, PHP, PRS, and CRS shown in Fig. 5-3.

The blanking signals are sent to the quantizer where they limit the range of the limit cycle. The time T to the edge of the limit cycle (Fig. 5-3) is always at least 1/16 millisec, but never more than 15/16 millisec. This assures that the leading and falling edges of the torque pulses are never disturbed by limit cycle intrusion.

The dual scale factor selection (DSFS) logic can be divided into four basic sections as shown in Fig. 5-4. They are (1) the scale-factor-set J-K flip-flop which is in the "one" state for low scale factor and the "zero" state for high scale factor, (2) a nand gate group and J-K flip-flop that makes scale factor decisions, (3) a cascade of three four-bit binary counters and associated nand gates for providing delay before a scale factor change command is transmitted, and (4) a nand gate group for gating the 256 kHz data pulses and sync signals into the appropriate output lines.

Scale factor change requirements are decided in the following manner: The scale factor set signal (Fig. 5-4), the limit cycle, and the mode interrogation signals are fed into the "decide scale-factor group". The interrogation signals PNN and PNP (Fig. 5-3) determine the low mode range; the signals PHN and PHP determine the high mode range; the signal PRS sets the counter input gates to either count or not count; and the signal CRS either counts down the counter or resets the counter to zero. The signal CRS is also used as the data sync signal. If the system is in the low mode and $T < t_2$ or $T > t_5$, the counter will be set to count. After 4 counts (4 millisec) the scale factor set flip-flop will go to zero and high scale factor will be demanded. If the system is in low mode and $t_2 < T < t_5$,

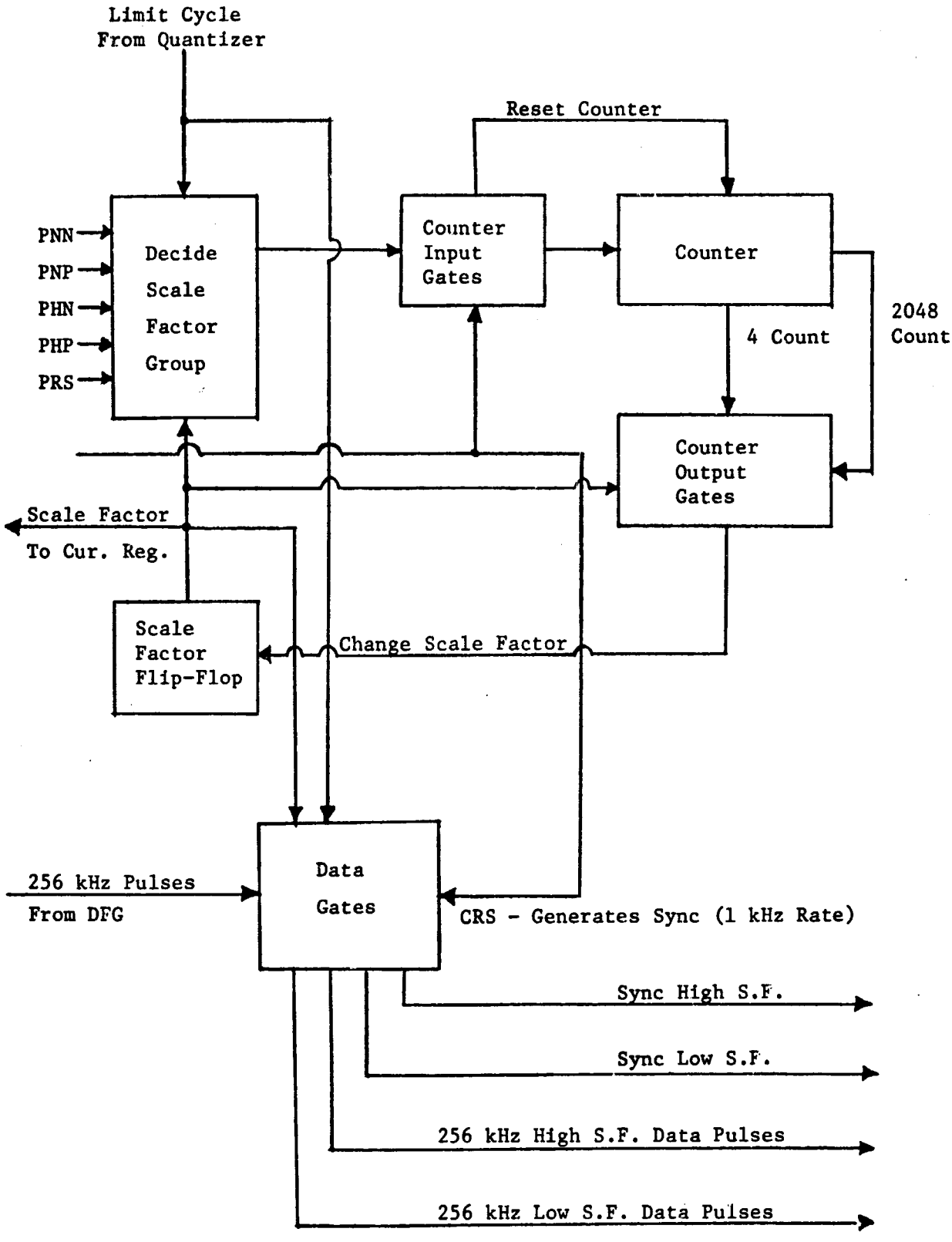

Figure 5-4. Organization of the Dual Scale Factor Select Logic.

the counter will only be reset by signal CRS during each 1 millisec interrogation period. If the system is in the high mode, and $T < t_3$ or $T > t_4$, the counter will be reset by signal CRS and no scale factor change will be demanded. If the system is in the high mode, and $t_3 < T < t_4$, the counter will be counted down. After 2048 counts (2.048 sec) the scale-factor set flip-flop will go to the "one" state and low scale-factor will be demanded. The delay is such that if high mode is needed, the system switches very quickly; however, low mode is not set until after considerable delay.

The scale factor signal (Fig. 5-4) selects the High or Low data line and the corresponding sync line in the output of the data gates. The limit cycle fixes the length of the 256 kHz data train. The length of the data train is always the time T, and an integral number of data pulses is always contained in the time T since the edge of the limit cycle is synchronized with the 256 kHz pulse train that generates the data pulses. Note also that the blanking signals in setting the limit cycle range as shown in Fig. 5-3 assure that there will always be a minimum of 16 data pulses and a maximum of 240 data pulses.

The results reported above have been experimentally verified on the Hamilton Standard logic breadboard constructed at MSFC. The scale factor switching was experimentally checked by feeding the logic with a variable-width limit-cycle generator which used the 0-16 blanking signal for synchronization.

MIT Draper Laboratory Logic*. The clock input to the logic section is a 614.4 kHz signal with a 1 μsec wide pulse that occurs every 64th pulse, with the other 63 pulses in the overall period having a width of 0.8 μsec. All inputs to and outputs from the logic section are coupled through differential line receivers and transmitters (NSC DM8820 and DM8830). These differential drivers and receivers retard ground loop problems often encountered in TTL logic, and further permit high level common-mode signals

*The diagram of this logic block is shown in Fig. 5-2. Circuit details are shown in Fig. XI, p. 23, of Reference 2.

to exist at the interfaces without disturbing signal processing. Standard TTL logic is utilized, with wide application of the newer low-power 74L series. Further, considerable use is made of MSI circuits to reduce component count.

The input clock is fed to a dual monostable RC-controlled multivibrator, with outputs of 0.8 μsec and 1.4 μsec wide pulses. The 1.4 μsec pulse serves as a count-down clock for a set of five J-K flip-flop scalars; thus, scaled frequencies of 307, 153, 76, 38, and 19 kHz are available to drive a simple (five-bit) staircase generator. Further, the 38 kHz output is fed to the drive circuit that controls the DC-to-DC converter power supply. The 0.8 μsec pulse from the monostable is Nanded with the 614.4 kHz clock to produce the synchronization signal (S) and its complement ($\overline{S}$). These signals are indicated in Fig. 5-5. Either S or $\overline{S}$ are utilized throughout the logic section to sync all commands at the 9.6 kHz rate, and to control the time at which interrogation of the sample-and-hold circuitry occurs.

If the compensated error signal from the inductive bridge pickoff on the gyro is sufficiently low so that the signal to the comparator circuit (CA 1 and CA 2 in the SG Processor block) is within the $\pm$ 300 mv zone, there is no torque applied to the gyro and the reference current is routed to the dummy load by the R-S logic which turns Q3B "on" and Q3A "off" in the lower part of the H-switch. The compensated error signal at the input to the comparator circuit is also fed to a JFET sample-and-hold circuit which samples the error at the peak. This signal is then compared to the signal from the staircase generator, so that with no error signal (zero error signal level is 2.50 v) the output from the A to D converter (Data Output Generator) is 16 bits. If the error is positive (error signal level at the input of the comparators CA1 and CA2 is > +2.50 volts) then the data output is between 17 and 31 bits, while for negative error signal (error output < 2.50 volts) the data output contains between 1 and 15 bits. Thus, each bit is equivalent to 1/4 of the torque pulse quantization for the scale (High or Low) in use (which is equivalent to $\Delta\theta/4$ = 75 mv, or a data resolution of 5.5 arc-sec/4 = 1.37 arc-sec on the low scale).

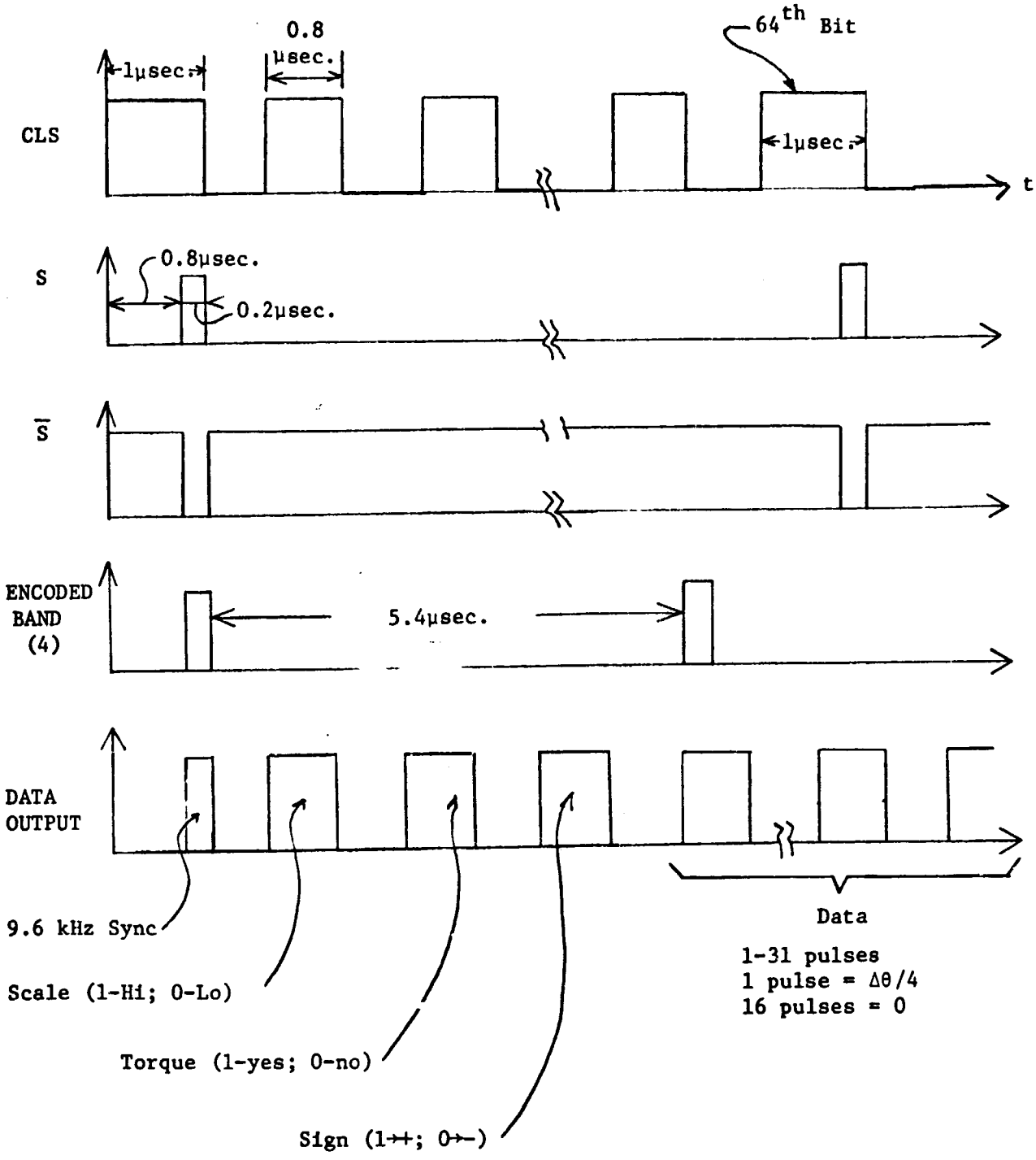

Figure 5-5. Control Signals and Data Output in the MIT Logic Block.

If the signal to the comparator circuit CA1 and CA2 is greater than the ± 300 mv zone, then output signals A and $\overline{A}$ (see Fig. 5-2) occur, with A in the "0" state and $\overline{A}$ in the "1" state for positive error, and reversed states for negative error. These signals from CA1 and CA2 drive Nand gates which provide the correct torque setup for the Upper and Lower parts of the H-switch, and also produce logic signals TM+ and TM- (and their complements) to obtain a logic command to order the Compensation Signal to be applied to the SG Processor, and further to generate the torque signal logic command (TM) to provide the presence of a bit in the data train. A real advantage of the ternary system occurs in this sequence, since Q_{1A}, Q_{1B}, Q_{2A} and Q_{2B} are set in their required state before the R-S signal is generated that switches the current from the dummy load into the gyro torquer winding. Hence, transients occurring during setup of the H-switch have no effect.

When a torque pulse is applied, the logic command TM (and $\overline{TM}$) also starts a four-bit binary counter (74L93) which acts as the decision maker for switching from Low to High torque mode. If five consecutive torque pulses are counted, a J-K flip-flop generates the Scale Change Command. This command is fed to the data train to establish a "1" indicating High Scale, and is coupled to the SG Processor to change the gain by a factor of four. An Inhibit pulse is also applied to the R-S switch that inhibits the next torque command to allow the H-switch and dc feedback loop to settle. Finally, the precision voltage reference (PVR) is switched from 1.6 V to 6.4 V, or the torquer current is increased by a factor of four. The scaling logic now continues to monitor the torque signal (TM) and when five consecutive torque pulses are absent, the various commands are again given, this time to switch back to low quantization.

As mentioned earlier, the initial four pulses (occupying 6.4 μsec) in the output data train indicate sync, scale (high or low), torque, and sign of the error signal. These pulses are separated from the data pulse by an encoding signal which is generated by combining scaled frequencies from the Input Scaler along with the 614.4 kHz clock and the output of a

16-bit binary counter. This timing signal produces a band 5.4 μsec wide immediately following the sync pulse, within which the encoding information appears in the data train (see Fig. 5-5).

H-Switch Comparisons

In the following section, a comparison between the Ternary H-Switch of MIT and the Binary H-Switch of Hamilton Standard is made. The H-Switch network is one of the most important blocks in the overall electronic rebalance loop, since not only the amount of the current through the torquer, but also the direction (or polarity) of the current is uniquely controlled by the H-switch and its associated error-sensing PVR network. Comparisons are made in terms of dc offset currents, plus also transient problems encountered in switching the direction of the current through the torquer winding.

MIT H-Switch. The schematic of the H-switch section is contained in the Howatt*report, and is shown in Fig. 5-6. The torque current I_{torque} is precisely controlled by the PVR reference and the negative feedback loop composed of R_p, A, the Error Amp, and the current-output transistors. Since the MIT system is a Ternary design, in the quiescent state (no torque) the current I_{torque} will flow through the dummy load, Q3B, and D7 into R_p, since the R-S logic will have Q3B "on" and Q3A "off". If torque in one direction is required, then logic command signals will turn Q1A and Q2B "on" while Q2A and Q1B are turned "off". However, this is an initial setup command and occurs before Q3A is turned "on" and Q3B "off". Thus, transient feedthrough currents in Q1 and Q2 have no appreciable effect. After setup occurs, logic signals turn Q3A "on" and Q3B "off". The switching transients in Q3 will furnish additional energy to R_p. However, if the pulse area is small, and further if the error-sensing network is slow in relation to the transient time, no appreciable transient error should result. In the MIT circuit, the dominant open-loop pole in the error-feedback circuit is in the input op-amp comparator A (LM 108) and is approximately 1 to 10 Hz.

*Reference 2, Fig. VI, p. 13, and Sec. 4 (pp. 14-17).

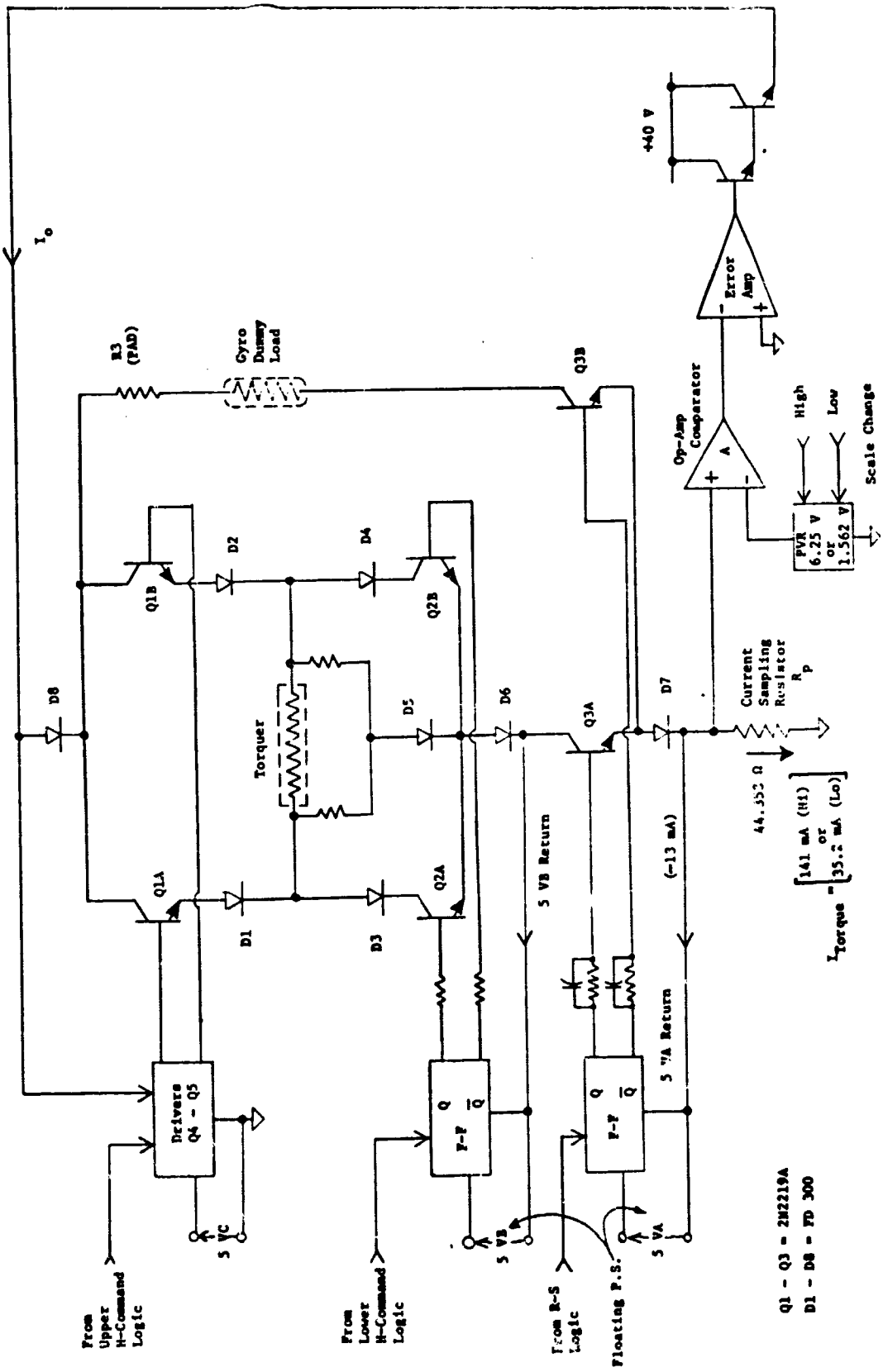

Figure 5-6. MIT H-Switch.

Further, diode D7 will help to decouple some of the transient feed-through from R_p. Although not indicated in the schematic for the MIT F-Switch, the use of the LM 108A for A does limit the differential input voltage (between + and - inputs) to 1 volt, because of the input protective network employed in this op-amp.

In the circuit of Fig. 5-6, not all of the output current I_o is used to drive the torquer, since some of the current feeds the Upper H-Command Driver circuit. This latter current splits, with the majority flowing as base current drive to the appropriate upper "on" transistor (Q1A or Q1B) and the remaining going to circuit ground (The base current does re-enter the loop to flow through the torquer). However, it is really not necessary that I_o be equal to I_{torque}; in fact, the only real requirement for minimum error is that the current through the torquer must <u>all</u> flow through the sampling resistor R_p. In effect, therefore, a basic theorem for H-switch operation is that whatever changes occur <u>above</u> the torquer winding creates insignificant error in the monitored current loop, whereas changes occurring <u>below</u> the torquer winding directly affect system accuracy.

When the torquer is in the quiescent state (no current flow), the current through R3 and the dummy load is the same as the current through the torquer in its active state.

The offset currents that can exist in the H-switch are those that occur in the lower H-switch transistors (Q2A and Q2B) and those that occur in the R-S switches (Q3A and Q3B). The model shown in Fig. 5-7 can be utilized to examine these offset errors. In this model, it is assumed that the requirement is to drive the torquer with a current such that Q1A and Q2B are "on" while Q1B and Q2A are "off". Also, Q3A must be "on" while Q3B must be "off". The resulting direction of current flow through the torquer is shown by heavy lines, with other currents indicated by dotted lines. The equation for the current sensed by R_p in terms of the actual current through the torquer I_t is

$$I_{sens.} = I_t - [I_1+I_4+I_5] + [I_{B2}-I_{B2}'] + [I_{B3}-I_{B3}'] \quad , \qquad (5\text{-}1)$$

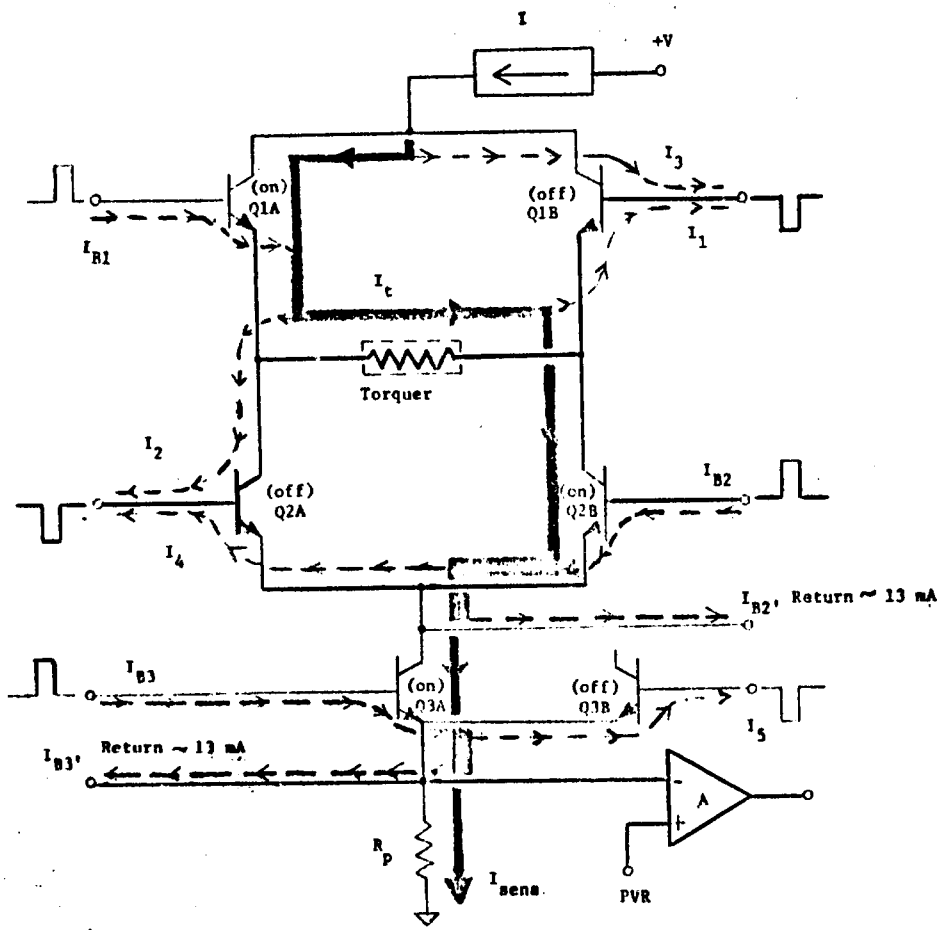

(a) Steady-State Currents

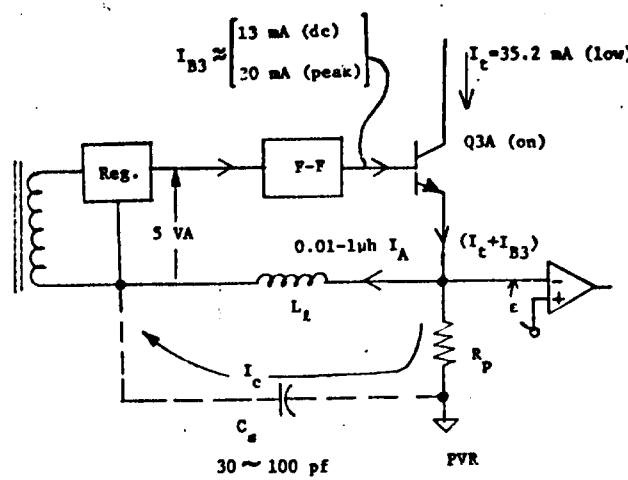

(b) Transient Turn-On Currents of Q3A

Figure 5-7. MIT H-Switch Model for Offset-Current Error Analysis.

where I_1, I_4, and I_5 are offset losses, while I_{B2} and I_{B3} are the base current drive for the "on" state switches Q_{2B} and Q_{3A}. Since the power supplies 5VA and 5VB are floating, these currents should return to the supplies and not show up in the output, or $I_{B2} = I_{B2}'$ and $I_{B3} = I_{B3}'$. Although this is true on a dc basis, it is not necessarily true for transient turn-on of Q3A. The transient turn-on problem is illustrated in Fig. 5-7b, where the lead inductance of the floating power supply return has been estimated as 0.1 - 1 μh, and the stray capacitance between the floating supply and circuit ground is probably in the 30-100 pf range. Since the current I_{B3} has two return paths ($I_{B3} = I_A + I_C$), this means that the actual current sensed through R_p is now I_{torque} plus I_C, and it would thus appear to the feedback network that the current through the torquer winding was greater than it actually was. This effect is certainly significant under Low Scale conditions, where the torque current is 35.2 mA, while the peak value of I_{B3} is approximately 30 mA. Thus, even if only 0.1% of I_{B3} returned to the power supply as the I_c current, this would be a peak transient error of about (0.001)(30mA)/35.2 mA $\approx$ 850 ppm. It would therefore certainly seem desirable to limit the bandwidth of the error-sensing feedback network for the H-switch to minimize transient error.

Under steady-state conditions, one need only consider the leakage current error due to the terms I_1, I_4, and I_5 in relation to I_{torque} in Eq. (5-1). For the 2N2219A transistor used for Q1-Q3, typical leakages at 50°C operating temperature of the torquer would be about 10 nA or less, with a temperature coefficient near 1 nA/°C. Thus, the error of these terms in comparison to I_{torque} on the low-scale is

$$\text{Static Error} \approx \frac{I_1 + I_4 + I_5}{I_{torque\ (low)}} = \frac{30 \times 10^{-9}}{35.2 \times 10^{-3}} = 0.9 \text{ ppm} \quad , \qquad (5\text{-}2)$$

and

$$\text{Drift Error} \approx 0.09 \text{ ppm/°C} \quad . \qquad (5\text{-}3)$$

For High-Torque conditions, these numbers would improve by a factor of four.

Hamilton-Standard H-Switch. A sketch of the Hamilton Standard H-Switch is shown in Fig. 5-8, with a more elaborate schematic contained in Ref. 5. The essential differences in implementation of the H-switch and PVR are (1) that for the Hamilton Standard system the precision reference resistor R_p is switched (by a factor of 2) whereas in the MIT design R_p is fixed while the precision voltage reference is switched, and (2) in the MIT H-Switch, the design is based on the use of all bipolar transistors with floating power supplies for the lower parts of the H-switch (as stated earlier, this was necessary to prevent unwanted currents from coupling into the sensed current), while in the Hamilton Standard circuit, the use of MOSFET pre-drivers for the switching transistors obviates the requirement for floating the power supplies.

A model for the HS circuit is shown in Fig. 5-9, where again the main torquer current is shown in heavy lines, with other offset currents indicated by dotted lines. Since the drive circuits are isolated from the torquer and switches Q5, Q6, Q9 and Q10 by insulated-gate FETS Q7, Q8, Q11 and Q12, there is no quiescent dc gate current present in the torque current. There will be transient feedthrough currents through the gate-source and gate-drain capacitance of the MOSFETS; however, these should be negligible in comparison with the currents encountered in the MIT design. It is assumed in Fig. 5-9 that Q5 and Q10 are "on" while Q6 and Q9 are "off". The main transient feedthrough will be I_6, I_2 and parts of I_4 and I_5. The dc offset leakage is due to I_4 and I_5 which gives

$$I_{sens.} \simeq I_{torque} + I_4 + I_5 \quad . \tag{5-4}$$

From data for the MOSFETS and 2N2219A switches, we obtain for the Low Scale torque current of 71.5 mA with maximum offset currents anticipated for both MOSFETS and bipolars of 10 nA,

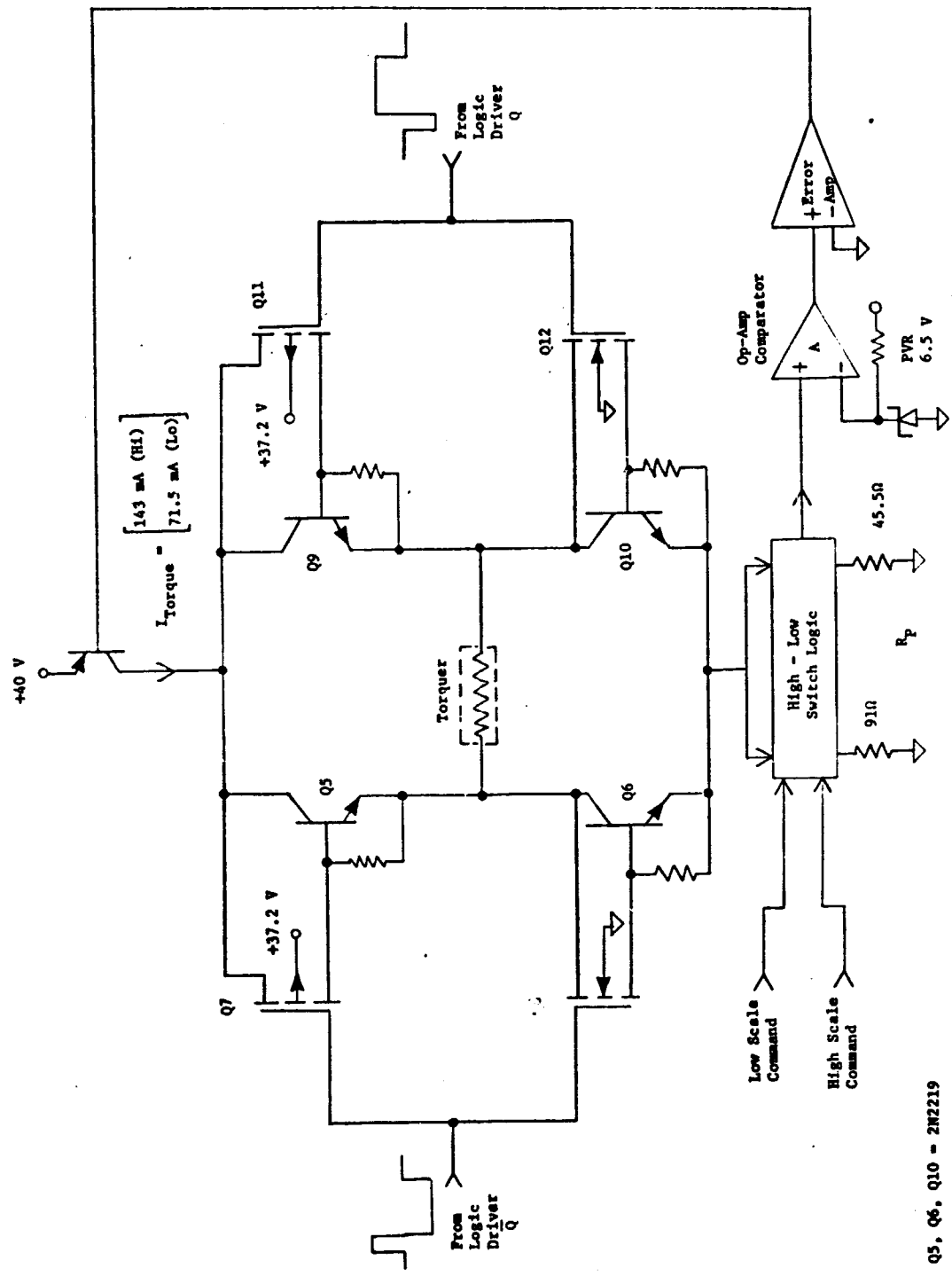

Figure 5-8. Hamilton Standard H-Switch.

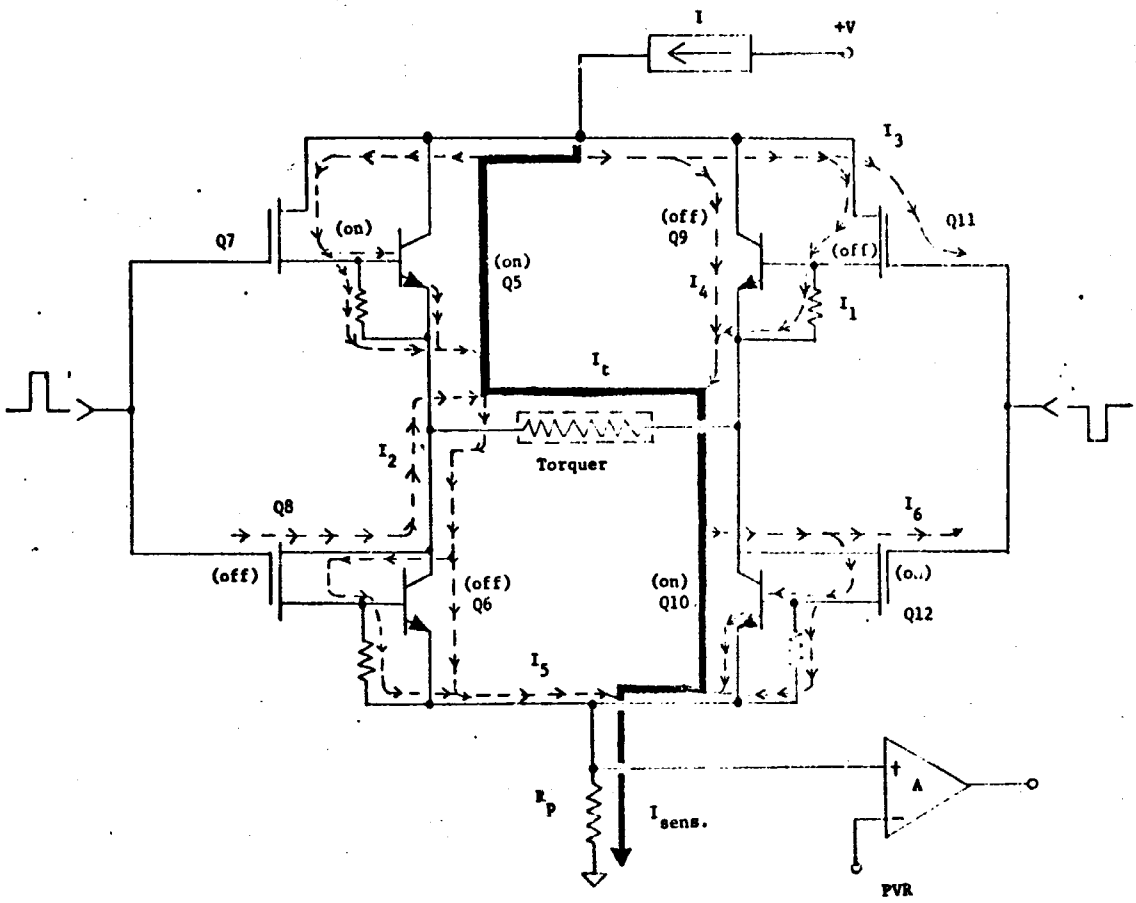

Figure 5-9. Hamilton Standard H-Switch Model for Offset Current Error Analysis.

$$\text{Static Error} \leq \frac{40 \times 10^{-9}}{71.5 \times 10^{-3}} \leq 0.6 \text{ ppm} \quad , \tag{5-5}$$

and

$$\text{Drift Error} \leq 0.06 \text{ ppm/°C} \quad . \tag{5-6}$$

Risetime Effects for the H-Switch. When the torque current is applied in the MIT H-Switch, the direction of the current is determined by whether the error signal from the gyro pickoff was positive or negative. The data shown in the Howatt* report indicates a torque pulse rise-time of 100 nsec and a fall-time of approximately 300 nsec. Thus, a 1% change in rise-time produces a change in torque pulse area of approximately 5 ppm, whereas a 1% variation in fall-time produces an area change of about 15 ppm. These changes are comparable to errors obtained elsewhere in the loop, and are therefore of considerable importance. Increasing the rise-and fall-times would decrease this error, but may well also increase transient feed-through problems. Since some of the same mechanisms control rise-and fall-times, there can be partially self-compensating changes produced.

In the Hamilton Standard H-Switch, since the circuit is operated in a Binary Loop, there must be both positive and negative torque pulses applied on a continuous basis. Thus, there is an inherent compensation in the Hamilton Standard H-Switch such that rise- or fall-time variations which would decrease the positive torque area would also decrease the negative pulse torque area as well, with a resultant small change in the overall net torque pulse area. This compensation will, of course, depend on the matching of cross-coupled pairs of drive transistors in the H-switch.

It would be expected in a low-rate torque environment that imperfect compensation in the Hamilton Standard H-Switch would accumulate more torque error than would occur in the MIT ternary design. However, in a high-rate torque condition, the inherent compensation in the Hamilton Standard design should be a significant advantage over the ternary design.

---

*Ref. 2, Fig. VIII, p. 17.

PVR Circuits

A comparison is made between the MIT and Hamilton Standard (HS) Precision Voltage Reference (PVR) Circuits. Basically, the requirement for the PVR is that it produce a scaled precision change in the torque current to drive the gyro. The approaches utilized are different for these two systems. In the Hamilton Standard PVR a precision resistor monitoring network is switched, while the voltage reference is held fixed, to produce a change of scale factor. Conversely, for the MIT PVR the precision resistor is held fixed, while the voltage reference is switched. Numerical values are obtained to enable a comparison between drift errors in these two methods.

Hamilton Standard PVR. A detailed schematic diagram of the PVR is shown in Ref. 3. A simplified model of the PVR is shown in Fig. 5-10. The terms suitable for drift error analysis indicated in this figure are the following:

I_{torque} - the precision current applied to the gyro torquer, and equal to V_{REF}/R_p

V_{REF} - the precision Zener diode reference voltage

R_p - the precision torque current monitoring resistor

I_Z - the Zener diode current

I_1, I_2 - input bias currents for the op-amp

V_o - the offset voltage for the op-amp

r_{on} - the "on" state channel resistance of the FET switches

r_Z - Zener diode dynamic resistance

ϵ - the error signal voltage in the feedback circuit

I_{off} - the "off" state channel leakage current of the FET switch.

The circuit of Fig. 5-10 has the same topological form irregardless of whether the system is in a Low or High torque region, hence parameters shown in brackets apply to the Low-Scale condition while un-bracketed

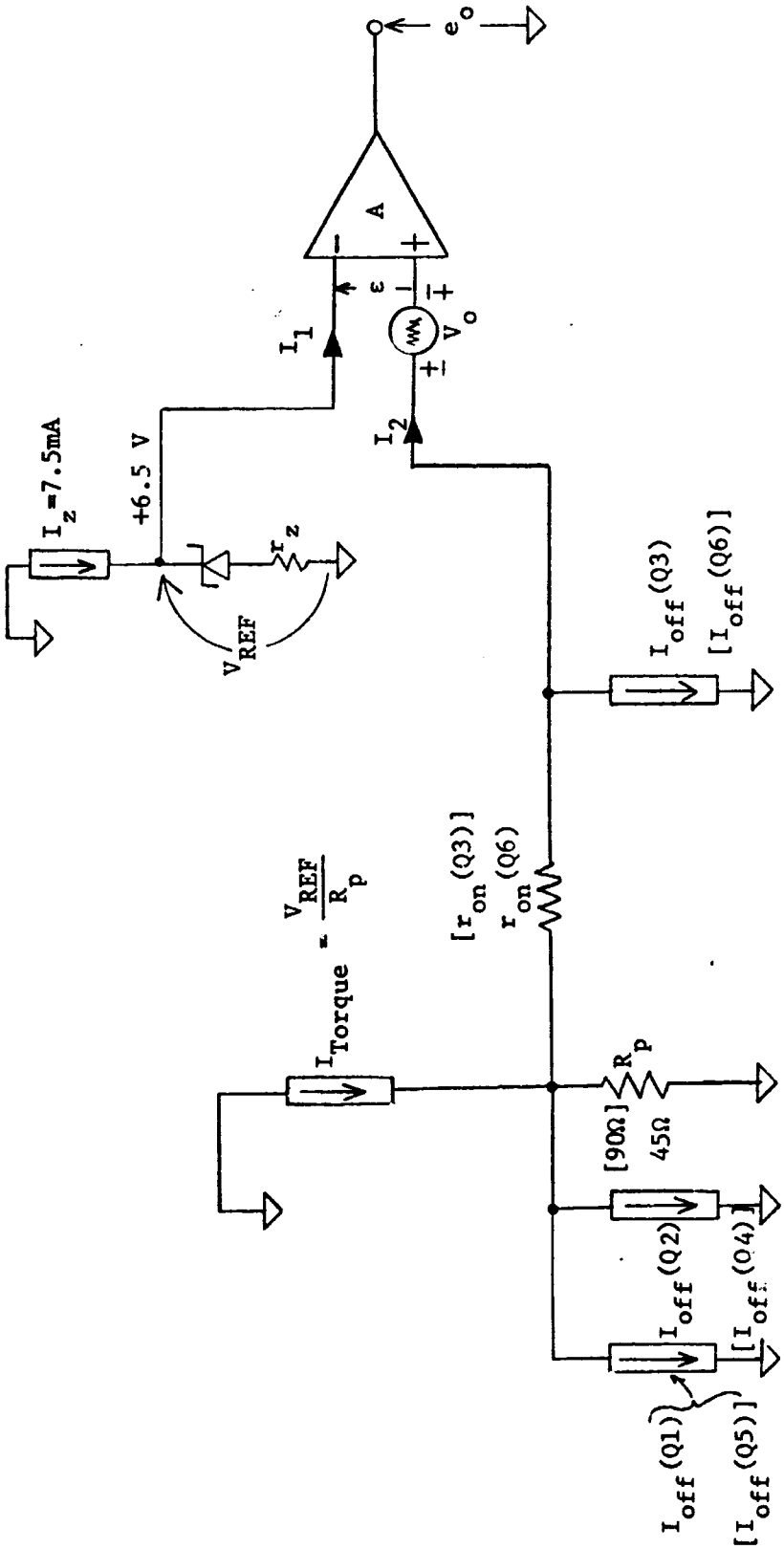

Figure 5-10. Hamilton-Standard Reference, High and Low Scale.

values indicate the High-Scale state. Transistor numbers refer to those indicated in Ref. 5.

Analysis of the circuit of Fig. 10 obtains the following equation for the error-signal, in the High Scale:

$$\varepsilon = \pm V_o + I_2[R_p + r_{on}(Q6)] - I_1 r_Z + (V_{REF} - R_p I_{torque})$$

$$+ R_p [I_{off}(Q1) - I_{off}(Q2)] + [R_p + r_{on}(Q6)] I_{off}(Q3) . \quad (5\text{-}7)$$

The drift due to temperature of the error signal ε can be estimated by a first-order linearization by computing $\Delta\varepsilon/\Delta T$ from Eq. (5-7), and using values substituted from the data sheets for the appropriate changes. Since the ultimate goal is to compare the HS PVR with the MIT circuit, the same typical drifts will be utilized for both circuits. Table I below indicates the data on drifts obtained from manufacturers data sheets, and values from both the HS and MIT reports.

Table 5-1.

Drift Data Used for a Comparison Between the Two PVR Circuits

$\frac{\Delta V_o}{\Delta T} = \pm 5\mu V/°C$

$I_1 = 75nA(max)$

$I_2 = 65nA(max)$

$(I_1 - I_2) = 10nA(max)$

$V_{REF} = 6.35V$

$\frac{\Delta V_{REF}}{\Delta T} \approx \pm 5\mu V/°C$

$r_{on} = 60\text{-ohm}$

$\frac{\Delta r_{on}}{\Delta T} \approx 0.4\Omega/°C$

$I_{off} = 2nA$

$\frac{\Delta I_{off}}{\Delta T} \approx 0.2nA/°C$

$r_z = 13\text{-ohm}$

$\frac{\Delta R_p}{\Delta T} = \pm 3ppm/°C$

$R_p = \begin{cases} 44.353\Omega & (MIT) \\ 31\Omega \text{ or } 45.5\Omega & (HS) \end{cases}$

Substituting values above and reducing obtains the following normalized drift equation for the Hamilton Standard PVR circuit, where only terms of significance have been retained.

$$\left(\frac{1}{V_{REF}}\right) \frac{\Delta\epsilon}{\Delta T} \simeq \pm \frac{1}{V_{REF}} \left[\frac{\Delta V_o}{\Delta T} + \frac{\Delta V_{REF}}{\Delta T} + \frac{V_{REF}}{R_p} \left(\frac{\Delta R_p}{\Delta T}\right)\right] , \qquad (5\text{-}8)$$

or, substituting values from Table I,

$$\left(\frac{1}{V_{REF}}\right) \frac{\Delta\epsilon}{\Delta T} \lesssim 8.8 \text{ ppm/°C} , \qquad (5\text{-}9)$$

for either High Scale or Low Scale. The long-term drift is also obtained similarly using values from the HS report for $\Delta V_o/\Delta t \simeq 23\mu V/1000$ hr, $\Delta V_{REF}/\Delta t \simeq 10$ ppm/1000 hr, and $\Delta R_p/\Delta t$ of 12 ppm/1000 hr, gives

$$\left(\frac{1}{V_{REF}}\right) \frac{\Delta\epsilon}{\Delta \text{time}} \lesssim 25 \text{ ppm/1000 hr} . \qquad (5\text{-}10)$$

MIT Draper Lab PVR. The schematic diagram for the PVR is shown in the Draper Lab report referred to earlier*. The model utilized for drift analysis is shown, for the High-Scale, in Fig. 5-11a and, for the Low-Scale, the replacement by the dotted portion of Fig. 5-11b is made. The same parameters are designated as for the HS system, with drift data of Table I utilized.

For the High-Scale circuit of Fig. 5-11a, the equation for the error-signal is

---

*Ref. 2, p. 13, and Appendix I (pp. 32-50).

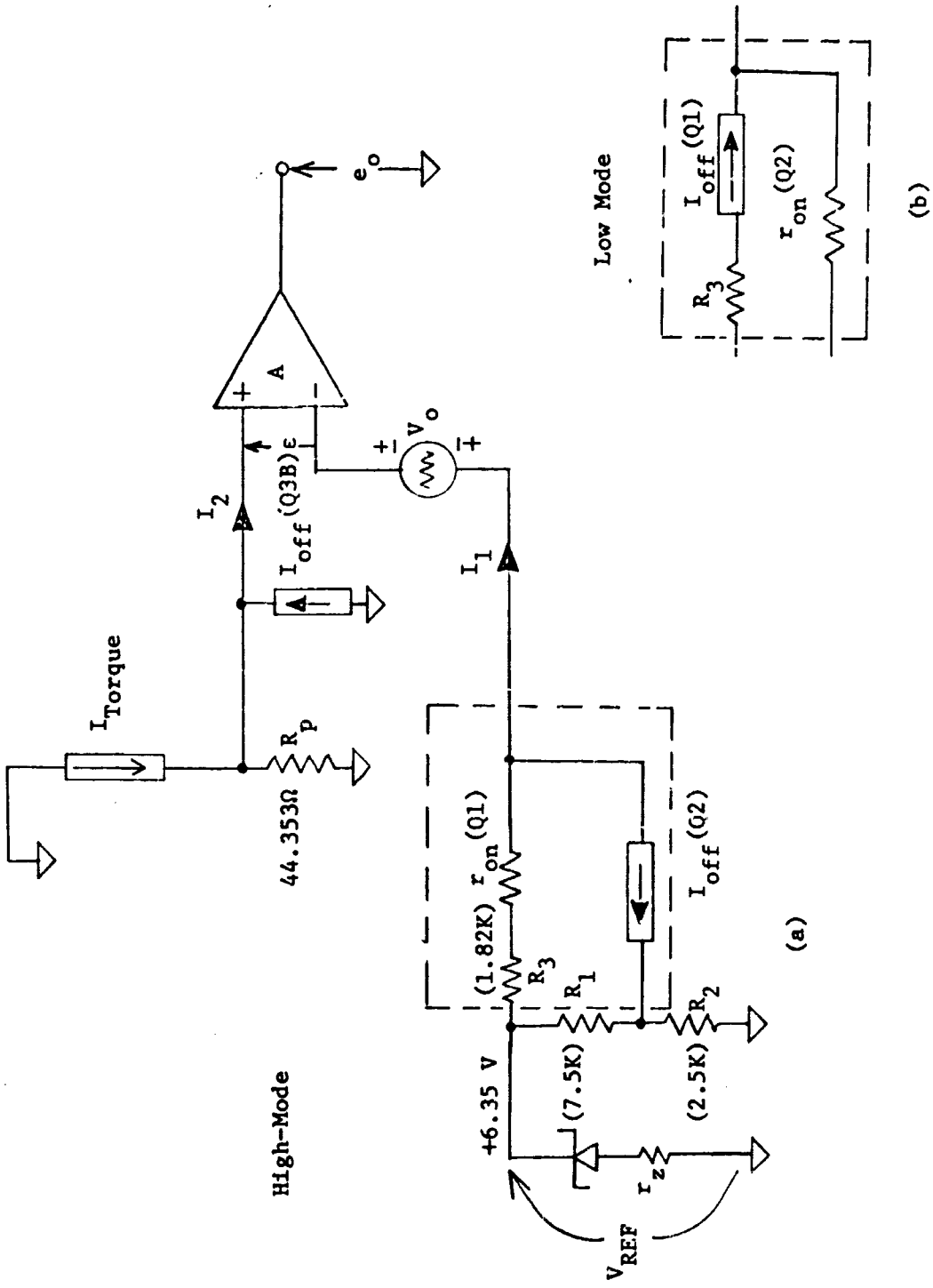

Figure 5-11. MIT Reference

$$\varepsilon \approx \pm V_o + R_p\,[I_{torque} + I_{off}(Q3B) - I_2]$$

$$- V_{REF} - [R_3 + r_{on}(Q1)][I_1 - I_{off}(Q2)] \quad , \qquad (5\text{-}11)$$

where R_1(7.5K) and R_2(2.5K) are precision resistors used to form a 4:1 voltage divider, and R_3 is a resistor chosen to offer the same impedance to the op-amp, regardless of the scale employed.

The computation of $\Delta\varepsilon/\Delta T$ from Eq. (5-11) is obtained as was that for the HS circuit. Substituting the values from Table I, and reducing, the following equation for drift is obtained for the MIT PVR circuit:

$$\left(\frac{1}{V_{REF}}\right)\left(\frac{\Delta\varepsilon}{\Delta T}\right)_{High} \approx \pm \frac{1}{V_{REF}}\left\{\frac{\Delta V_o}{\Delta T} + \frac{\Delta V_{REF}}{\Delta T} + \frac{V_{REF}}{R_p}\left(\frac{\Delta R_p}{\Delta T}\right)\right.$$

$$\left. + [R_3 + r_{on}(Q1)]\left[\frac{\Delta I_1}{\Delta T} + \frac{\Delta I_{off}(Q2)}{\Delta T}\right]\right\} . \qquad (5\text{-}12)$$

Substituting values from Table I,

$$\left(\frac{1}{V_{REF}}\right)\left(\frac{\Delta\varepsilon}{\Delta T}\right)_{High} \lesssim 9 \text{ ppm/°C} \quad . \qquad (5\text{-}13)$$

The long-term drift is similarly,

$$\left(\frac{1}{V_{REF}}\right)\left(\frac{\Delta\varepsilon}{\Delta time}\right) \lesssim 25 \text{ ppm/1000 hr} + \frac{1}{V_{REF}}[R_3 + r_{on}(Q1)] \times$$

$$\left[\frac{\Delta I_1}{\Delta t} + \frac{\Delta I_{off}(Q2)}{\Delta t}\right] \quad . \qquad (5\text{-}14)$$

For Low-Scale, using the circuit of Fig. 11b produces (with $k \equiv R_2/(R_1 + R_2)$]

$$\left(\frac{1}{k\ V_{REF}}\right)\ \frac{\Delta\varepsilon}{\Delta T} \simeq \pm\ \frac{1}{k\ V_{REF}} \left\{ \frac{\Delta V_o}{\Delta T} + \frac{k\ \Delta V_{REF}}{\Delta T} + \frac{k\ V_{REF}}{R_p} \left(\frac{\Delta R_p}{\Delta T}\right) + [k\ R_1 + r_{on}(Q2)]\ x \left[\frac{\Delta I_1}{\Delta T} - \frac{\Delta I_{off}(Q3)}{\Delta T}\right] + V_{REF} \left(\frac{\Delta k}{\Delta T}\right) \right\}, \qquad (5\text{-}15)$$

or

$$\text{Temp. drift (Low-Scale)} \lesssim 14.4\ \text{ppm/°C}\ . \qquad (5\text{-}16)$$

A similar equation for long-term drift for the Low-Scale can be obtained and is similar to Eq. (5-15).

The basic conclusion to be obtained from this analysis is that although the drift rates are comparable for High-Scale torque currents, under Low-Scale conditions it is better to leave the reference comparison voltage fixed and switch the precision resistor R_p. It is also apparent that switching the reference comparison voltage allows other drift terms in the circuit to be important, as evidenced by comparing the terms of Eqs. (5-8) and (5-15).

No comparison has been made of the switching transients involved in changing scale factor. However, it is apparent that in switching either resistors or voltage references, transient feed-through errors will result, unless the loop is given sufficient time to settle before torque is applied to the gyro. This can be done quite easily for the Ternary system, but not for the Binary loop. Further, the op-amp (A in Figs. 5-10 and 5-11) must have sufficient differential input rating so the switching transients do not cause junction breakdown.

Noise Considerations

The effect of electronic noise on system resolution will be considered in this section. The calculation details for obtaining a noise figure-of-merit for both the Hamilton Standard and MIT Systems will be presented and the noise performance of the two systems will be compared.

MIT System. The electronic noise contribution to the system uncertainty can be determined by computing the rms noise voltage at the input to the comparator block of Fig. 5-2. Since a voltage increment at the comparator input represents a known angular increment in gyro float position, the noise can be expressed as rms arc-seconds of uncertainty. At the comparator input, a 300 mv. voltage increment corresponds to 5.5 arc-seconds on the low scale and 22 arc-seconds on the high scale. This $\Delta\theta$ of 300 mv. is the weight of one torque pulse.

The white noise voltage at the comparator input is given by

$$e_{nw} = A_V \left[4kTR_n \Delta f\right]^{1/2} , \qquad (5\text{-}17)$$

where k is Boltzmann's constant, A_V is the voltage gain from the amplifier input to the comparator input, T is the absolute temperature, R_n is the equivalent input noise resistance of the amplifier and compensator block (Fig. 5-2), and Δf is the noise bandwidth from amplifier input to comparator input. Since the gain of the input stage of the amplifier is about 20, the noise should be controlled by this input stage. Assuming the error-detector output impedance is near zero, the equivalent input noise resistance should be about 8 kilohms (7 kilohms attributed to the input network and 1 kilohm attributed to the UC 4250 input op-amp). The dominant low-frequency 3 db point is about 3.4 kHz and is controlled by the coupling network between the second and third stages of the amplifier. The dominant high-frequency 3 db point is set by the input network and is about 8 kHz. Thus, a reasonable approximation to the noise bandwidth is 5 kHz. The gain A_V is about 4000 on the low scale. Using these values in Eq. (5-17) gives

$$e_{nw} = 3.3 \text{ millivolts rms.} \qquad (5\text{-}18)$$

Therefore, the noise referred to the gyro float motion is

$$\Delta\theta_n = (3.3 \text{ mv rms})\left(\frac{5.5 \text{ arc-sec}}{300 \text{ mv}}\right) ,$$

or

$$\Delta\theta_n = 0.06 \text{ arc-sec rms.} \qquad (5\text{-}19)$$

This value of $\Delta\theta_n$ should be considered a minimum value because low-frequency electronic noise and electronic noise generated by the error signal detector have been neglected; however, these two additional sources would not be expected to increase the noise of Eq. (5-19) by more than about 20%.

Hamilton Standard System. The sensitivity of the error-signal detector in the Ham. Std. System is given as 1.39 millivolts per arc-sec*. The white noise figure-of-merit can therefore be calculated by first finding the equivalent noise voltage at the preamplifier input (Fig. 5-1).

The IC_1 stage of the preamplifier will make a significant contribution to the input noise, since it is preceded by a unity-gain section. The IC_1 gain-of-6 should assure that only the preamplifier need be considered in the noise calculation.

The estimated total input-noise resistance R_n is composed of the following contributions: (1) differential source follower, 2K; (2) differential emitter follower, 2K; (3) differential inverter, 4K; and IC_1 circuit, 20K. These noise components sum to a value of 28K and are estimated to be caused primarily by circuit resistors.

Before a final value of R_n is determined, the noise contribution of the 1-meg gate resistors in the input source follower must be computed. The output ring capacitance of the error signal detector (a capacitance bridge) is 116 pf.* The 3db frequency associated with the gate resistance is

*Ham. Std. Report, Ref. 3, p. 125.

$$f_g = \frac{0.159}{(2 \times 10^6)(1.16 \times 10^{-10})} = 685 \text{ Hz} \quad . \tag{5-20}$$

the effective noise resistance at 50 kHz then becomes

$$R_{ng} = \frac{fg^2}{f_c^2}(2Rg) = \frac{(6.85 \times 10^2)^2}{(5 \times 10^4)^2}(2 \times 10^6) \quad , \tag{5-21}$$

or

$$R_{ng} = 360 \text{ ohms} \quad .$$

Thus, the contribution of the gate resistors is negligible.

Taking a value of R_n = 28K for the total white noise resistance, the input equivalent-noise-voltage density is

$$ENV = \sqrt{4kT\ R_n} = 21.7 \text{ nanovolts/Hz}^{1/2} \quad . \tag{5-22}$$

The noise bandwidth of the 50 kHz filter is about 5 kHz, thus, the equivalent noise voltage is approximately

$$ENV_T = 21.7 \quad \sqrt{5{,}000} = 1.54 \text{ microvolts rms} \quad . \tag{5-23}$$

Referring this to the detector signal gives

$$\Delta\theta_n = (1.54 \times 10^{-6}) \frac{1}{1.39 \times 10^{-3}} = 0.0011 \text{ arc-sec rms} \quad . \tag{5-24}$$

Comparisons. The electronic noise of the Ham. Std. rebalance electronics is much less then that of the MIT system. Yet, the equivalent noise resistance of the MIT system is less than that of the Ham. Std. system. The reason for the poorer signal-to-noise ratio of the MIT system is the much

lower sensitivity of the error-signal detector. This lower sensitivity is due not only to basic differences in the detectors (MIT is an inductance sensor; Ham. Std. is a capacitance sensor) but also to the higher frequency (50 kHz vs. 9.6 kHz) error signal employed by Ham. Std. Undoubtedly, the MIT detector could be made much more sensitive with a consequent system signal-to-noise ratio comparable to that of the Ham. Std. System.

The higher frequency error signal gives the Ham. Std. System a significant advantage if low-frequency electronic noise is a problem. For practically all modern semiconductor devices, a frequency of 50 kHz is well above the frequency range where low-frequency noise is important. Semiconductor devices must be selected to have negligible low-frequency noise at 9.6 kHz.

Neither the Ham. Std. nor the MIT preamplifier is a low-noise design. However, improving the noise performance of either preamplifier without sacrificing common-mode rejection and impedance requirements will not be a trivial exercise.

Common-Mode Rejection

Excellent common-mode rejection in the preamplifiers of both systems is essential for eliminating common-mode signals that could contaminate the error signal. Common-mode signals of several volts at the preamplifier input should have less effect on the preamplifier output than the millivolt-level differential signals from the detectors. Consequently, a common-mode rejection CMR of no less than 80 db would be indicated for the preamplifiers used in both the MIT and the Ham. Std. Systems.

No extensive detailed analysis has been completed on either system's preamplifier; however, preliminary results indicate that the CMR is probably adequate.

The Ham. Std. System has an elaborately designed preamplifier using discrete transistors and a monolithic differential amplifier with great emphasis placed on high CMR. The achievement of high CMR in the Ham. Std. System is greatly enhanced by having low-gain (about 6) before the bandpass

filter and by using a 50 kHz error signal which should be much higher in frequency than most expected common-mode signals.

The MIT preamplifier is a single monolithic differential amplifier which could possibly be selected to have a CMR of about 80 db at 9.6 kHz. The lower frequency bandpass (about 3 kHz to 8 kHz) of the MIT amplifier probably opens up this system more to CM signals; however, the much lower sensitivity of the error signal detector and the fact that monolithic operational amplifiers have maximum common-mode rejection at low frequencies may be partially compensating.

Compensation

The methods of compensating the rebalance loop used in the Ham. Std. and the MIT Systems are very different. In this section, the two types of compensation are described and their salient differences delineated.

Hamilton Standard Rebalance Loop Compensation. In the Ham. Std. System, a cascade compensation network was used to (1) provide a stable loop with sufficient phase and gain margins, (2) discriminate against gyro float angular vibrations that tend to saturate the loop amplifiers, and (3) attenuate signals arising from the gyro wheel rotation. For the gyro used in the Ham. Std report[3] the transfer function in the frequency domain for the gyro alone was approximately

$$G(jf) = \frac{K_g}{jf\left(1 + j\frac{f}{1050}\right)} \quad , \tag{5-25}$$

where f is the frequency in Hz. The transfer function for the compensation network (Fig. 5-1) used with this gyro was

$$C(jf) = \frac{K_c\left(1 + j\frac{f}{1.11}\right)}{\left(1 + j\frac{f}{0.016}\right)\left(1 + j\frac{f}{100}\right)} \quad . \tag{5-26}$$

Except for some poles at high frequencies that should be negligible, the overall frequency domain transfer function viewed by the torque current

pulses is the product -C(jf) G(jf). Clearly, the overall transfer function can not be approximated by that of a pure integrator. It appears that making the loop approximate a pure integrator was not a design goal for the Ham. Std. System as it was for the MIT System.

It may be difficult to achieve system stability for very high loop gains since the maximum phase shift of the -C(jf) G(jf) product is 450°. At a frequency of 5 kHz, where the bandpass filter begins to contribute phase shift, the frequency dependent part of C(jf) will have attenuated the loop transmission by a factor of about 3500. This attenuation in addition to that of the gyro dynamics should assure that the phase shifts of the high-frequency poles in the rebalance electronics will not cause system instability.

Even though the Ham. Std. compensator transfer function is more complex than that of the MIT compensator, the actual implementation can be rather easily achieved using standard operational amplifier networks.

MIT Rebalance Loop Compensation. The MIT compensator is simple and is designed to cause the effective transfer function from the torquer input to the comparator input (see Fig. 5-2) to approach that of a pure integrator. The detailed development of this method of compensation is presented in the M.S. Thesis by Lory[6]. The compensation technique is shown in Fig. 5-12.

The overall transfer function from point T to Point C in Fig. 5-12 is given by

$$T(s) = \frac{K + H_2(s)\,[s(\tau_1 s + 1)(\tau_2 s + 1)]}{s(\tau_1 s + 1)(\tau_2 s + 1)} \quad . \qquad (5\text{-}27)$$

Usually the gyro time constant τ_1 is much greater than the torquer time constant τ_2 (τ_1 is typically greater than 100 microseconds). For this usual case T(s) can be made equal to 1/s if (from Eq. (5-27))

$$H_2(s) = \frac{1}{\tau_1 s + 1} + \frac{1 - K}{s(\tau_1 s + 1)} \quad . \qquad (5\text{-}28)$$

The first term on the right side of Eq. (5-28) is a simple RC low-pass

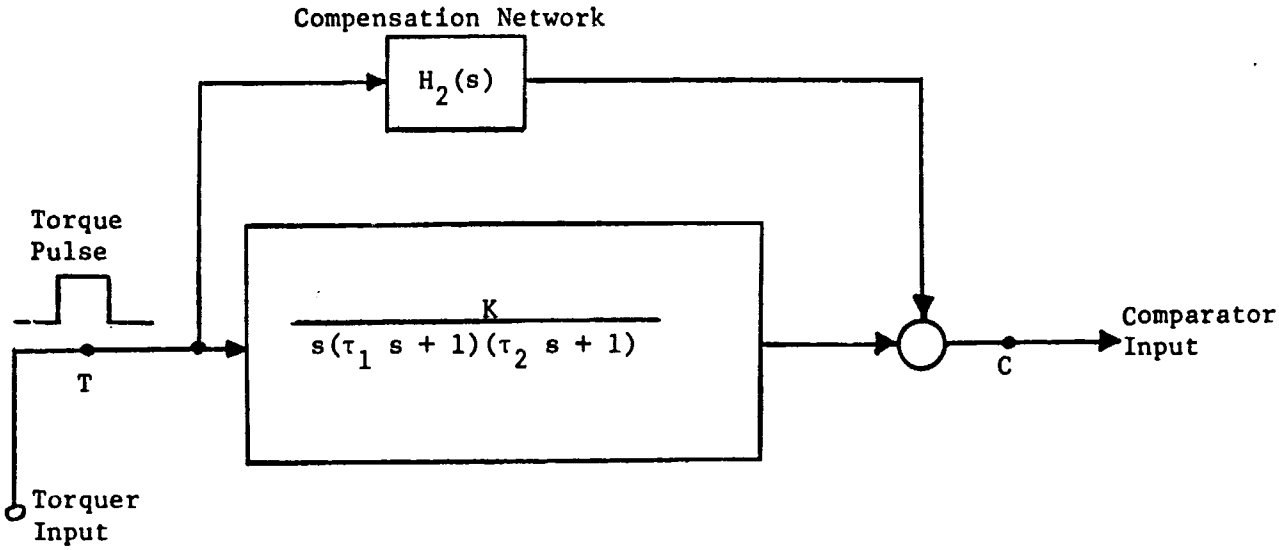

τ_1 = Gyro Time-constant

τ_2 = Torquer Time-constant

Figure 5-12. Compensation Technique for the MIT System.

network. The second term is a simple RC low-pass network cascaded with an integrator. The two terms can be realized, therefore, as the parallel combination of simple networks.

It is especially significant to note that the compensation only need be applied during the actual torquing and can be driven by any rectangular pulse with edges coincident with the actual torque current pulse and amplitude directly proportional to the torque command pulse generated in the logic. (Torque current pulse changes are accompanied by compensating loop-gain changes to hold the overall loop-gain constant.)

In the actual implementation of the MIT System, the compensation command generator is driven by the torque command pulse. The compensation network is a simple RC low pass circuit which provides accurate compensation only for the case K = 1.

It may appear a bit disturbing that the MIT compensation technique is equivalent to actually feeding a signal that is proportional to the torque current pulse around the gyro, detector, and error-signal amplifier. However, since the overall transfer function is nearly a pure integrator, the signal that appears at the comparator input is directly proportional to the area of the torque current pulses. Now, since the float angle increment $\Delta\theta$ is directly proportional to the area of the torque current pulses, then the signal at the comparator input is directly proportional to $\Delta\theta$. Thus, the sample-and-compare circuit will indeed generate data pulses proportional to $\Delta\theta$ which, of course, is the desired result.

The ease of implementation, the conceptual simplicity and the expected reliable performance of the MIT compensation technique make the technique an attractive way of compensating ternary systems with the consequent elimination of pulse bursting. One possible disadvantage of this compensation technique is the dependency of $H_2(s)$ on the gain K. If after $H_2(s)$ is implemented, either the gain of $H_2(s)$ or the gain of the preamplifier changes, then the compensation is no longer perfect. We have not yet determined the detailed effects of such gain drifts.

Another important consideration in compensation design is the effect of the width of the torque pulse on the system response. Since the MIT torque current pulse is only 97.5 microseconds compared to a maximum width of 15/16 milliseconds for the Ham. Std. System, it is much easier to make the loop appear to be an integrator for the MIT torque pulse. When the torque current pulse is sufficiently short relative to the gyro dominant time-constant (the pseudo-integrator), then several error-signal processor design constraints are relaxed. Among the relaxed constraints are those affecting the dynamic range and the spurious signal discrimination circuits (for instance, gyro float oscillations at the forced limit-cycle frequency) in the error-signal processor.

OVERALL SYSTEM CONSIDERATIONS

Three vital considerations in the comparison of all rebalance electronic schemes are resolution, accuracy, and reliability. Resolution and accuracy are usually interdependent and must be considered simultaneously in the design of rebalance electronics. For example, improvement in resolution at the expense of accuracy could result in a degradation of overall system performance. Also, reliability is obviously closely connected since reliability involves many alternatives not only in technique but also in selection of components. These choices of techniques and components must always be made carefully.

In this section, the resolution, accuracy, and reliability of the Ham. Std. and MIT rebalance electronics will be discussed and comparisons made where possible. The presentation will draw heavily on the results of the analyses given in the previous sections.

Resolution

To compare torque current-pulse area quantization and data pulse quantization, the gain of the system comprising the torquer, gyro, and error-signal detector can be removed by considering torque current-pulse area increments only at the input to the torquer. This normalization allows a direct comparison of the inherent quantization produced by the

rebalance electronics only.

The Ham. Std. System has a one-millisecond torque current pulse with both positive and negative area. The pulse can be changed in 3.9 μsec ($\frac{1}{256} \times 10^{-3}$ sec.) increments. Increasing the positive current width by 3.9 μsec also decreases the negative current width by 3.9 μsec. Thus, the smallest area increment ΔA is given by

$$\begin{aligned} \Delta A &= 3.9I - 3.9(-I) \quad , \\ \Delta A_H &= 7.8I \text{ nanoamp-seconds} \quad , \end{aligned} \tag{5-29}$$

where I is the amplitude of the torque current pulse in milliamperes. This increment in current-pulse area will produce a one pulse increment in the data train; thus, the data quantization ΔD_H is also

$$\Delta D_H = 7.8I \text{ nanoamp-seconds} \quad . \tag{5-30}$$

The finest quantization occurs in low-scale operation where I is 71.5 ma. Hence, the data quantization for the Ham. Std. System is

$$\Delta D_H = (7.8)(71.5) = 558 \text{ nanoamp-seconds} \quad ,$$

and also

$$\Delta A_H = 558 \text{ nanoamp-seconds} \quad .$$

The MIT torque current-pulse width is constant and is 97.5 micro-seconds. The torque current pulse quantization is therefore

$$\Delta A_M = 97.5I \text{ nanoamp-seconds} \quad , \tag{5-31}$$

if I is the amplitude of the current pulse in milliamperes. The data pulse weighting is such that four data pulses correspond to one torque pulse. Hence

$$\Delta D_M = 24.4I \quad . \tag{5-32}$$

The low-scale current amplitude is 35.2 ma; consequently, the numerical value of the MIT System data quantization is

$$\Delta D_M = (24.4)(35.2) = 860 \text{ nanoamp-seconds} \quad .$$

The difference in data quantization for the two systems is not very great - $\Delta D_M = 1.54\ \Delta D_H$ - but it is also not insignificant. There is an appreciable difference in torque current-pulse quantization - $\Delta A_M = 6.2\ \Delta A_H$. In conclusion, then, the data resolution of the Hamilton Standard System is somewhat higher than that of the MIT System, while the torque current-pulse resolution of the Ham. Std. System is much higher.

Another important resolution consideration for some strapdown gyro applications is how precisely the position of the gyro float angle is known as a function of time (time resolution). The MIT System has an apparent advantage in this case since the error signal is sampled at a well defined time and at a rate that is about an order of magnitude higher than in the Ham. Std. System. There is, however, some cause for concern if the MIT compensation is not perfect; that is, either too much (overcompensation) or too little (undercompensation) signal is fed through the parallel compensation feedback path into the comparator input. This imperfect compensation, which could arise from component change due to aging or temperature variations, may possibly cause short term error in data output with a consequent degradation in the time resolution of the system. If the compensator parameters drifted very much, perhaps new pulse bursting modes may be introduced. Further study of the MIT compensation technique is needed to provide definitive conclusions concerning the effects of imperfect compensation on time resolution of the system.

Accuracy

Assuming that the torquer has negligible non-linearity, the accuracy of both the MIT and the Ham. Std. Systems should depend primarily on the stability of the torque current-pulse amplitude regulator and on the performance of the H-switch. There are two secondary sources of inaccuracy that

could also be of significance. These are (1) instabilities in the analog-to-digital conversion for data generation and (2) spurious signal contamination of the error signal.

We will discuss the four sources of inaccuracy identified above, starting first with the secondary sources.

Analog-to-Digital Conversion. The analog-to-digital conversion, ADC, for data generation in the Ham. Std. System is accomplished by detecting the time t_c that a ramp signal crosses a slowly varying voltage level proportional to the error signal. The time t_c is sensitive to gain drifts in the error signal amplifiers and to the slope of the ramp. However, the entire ADC operation is accomplished inside the system loop so that for practical values of loop transmission, these inaccuracies should be made negligible by the feedback mechanism.

A very different situation exists in the MIT System. The ADC is connected parallel to the loop and is, therefore, not included in the loop. Thus, the stability of the calibration of the data output depends on the stability of the staircase generator. The critical resistors in the staircase generator should have stability comparable to that of the current sensing resistors in the torque current regulator. We are presently examining ways of eliminating this deficiency in the ternary system.

Spurious Signals. An important spurious signal is electronic noise superimposed on signals at points in the system where torquing decisions are made. Since this noise will be gaussian distributed about a zero mean value, its effect on system accuracy should be averaged to very small values over several torque pulses. Because of this averaging, the rms noise errors computed in the previous section on Noise Considerations are pessimistic.

The inaccuracies due to other spurious signals that are not correlated with the error signal should also be averaged over several torque pulses to negligible values. Correlated signals may possibly produce serious inaccuracies; thus, care in layout and attention to ground-loop elimination is essential in implementation of rebalance systems.

Effects of spurious signals on accuracy must usually be determined experimentally.

Current Regulator. The current regulator circuit is composed of the dc feedback loop containing the H-Switch, the Precision Voltage Reference, the comparator op-amp A and the error amplifier. This circuit was shown in Fig. 5-2, and in more detail in Figs. 5-6 and 5-8 for the two systems. It is absolutely essential for system accuracy that the weight of each torque pulse be precisely known; i.e., that the amplitude of the current pulse and its pulse width be accurately maintained, or more correctly that the area of the pulse be constant. The pulse width is basically controlled by the clock accuracy, and should contribute the same inaccuracies whether the system were binary or ternary. Calculations made earlier allow some comparison of pulse rise- and fall-time inaccuracy, and also inaccuracies in current amplitude. A worst-case comparison of the MIT and Ham. Std. current regulator designs can be made by adding these various inaccuracies, or

Overall Accuracy (worst-case analysis)

$$\approx \text{error (PVR)} + \text{error (Sensed Current)} + \text{error (rise- and fall-times)} \qquad (5\text{-}33)$$

Collecting results gives for the Low-Scale mode the following comparisons:

$$\text{Acc.}_{\text{MIT}}(\text{worst-case}) \leq (14.4\text{ppm}/^\circ\text{C and} > 25\text{ppm}/1000\text{ hr}) + (0.9\text{ppm and } 0.09\text{ppm}/^\circ\text{C, plus transient effects}) + (\approx 10\text{ppm for a 1\% change}), \qquad (5\text{-}34)$$

and

$$\text{Acc.}_{\text{HS}}(\text{worst-case}) \leq (8.8\text{ppm}/^\circ\text{C and } 25\text{ppm}/1000\text{ hr}) + (0.6\text{ppm and } 0.06\text{ppm}/^\circ\text{C}) + (<10\text{ppm for a 1\% change}) \qquad (5\text{-}35)$$

Reliability

No comparison has been made between the MIT and the Ham. Std. Systems regarding reliability, as this would involve considerable in-depth experimental analysis of the two. Qualitatively, there seems to be no reason one circuit should be any more reliable than the other. The considerable use of MOS transistors in the Ham. Std. design would cause problems if the circuits operated for an extended time in a radiation zone, since it has been found that the threshold voltages V_T of most enhancement-mode MOSFETs increase considerable in a radiation field.

SUMMARY AND RECOMMENDATIONS

The results of our analyses of the rebalance electronics of the two strapdown gyroscopes (MIT ternary and Ham. Std. binary) have not led to a conclusion that one system is clearly superior to the other. We have used our analytical results to produce a tabular comparison (Table II) of the two systems in seventeen important areas. Each system has a significant set of both relative advantages and disadvantages. We cannot distinguish an appreciable difference in the overall quality of electronic engineering design principles applied in the development of the two systems.

We recommend that the feasibility be explored of developing a system that would incorporate the best features of both the ternary and binary systems studied. Such a system perhaps would have the capability of operation in both ternary and width-modulated binary modes with built-in decision-making apparatus for causing the system to operate in the mode that is best for the rate environment in which the gyroscope finds itself. For example, a zero rate condition would probably require a ternary mode to eliminate cumulative torque-current bias errors; yet, a high rate environment may need a binary mode to take advantage of the inherent rise- and fall-time compensation in the binary H-switch.

Early in the development of a new system, an in-depth experimental

study of the two types of H-switch (binary and ternary) must be made since major design decisions will depend strongly on fundamental limitations in the performance of the H-switches. Also, of central importance are the loop transmission (which strongly influences system accuracy) system stability trade-offs and the design compromises among high interrogation rates, electronic implementation limitations, time resolution of data output, and accuracy.

Table 5-2.

Various salient features are indicated below comparing the ternary system design of Draper Labs with the width-modulated Binary system design of Hamilton Standard, Inc. Where a particular item is deemed to offer a very significant advantage for that particular system, it is underlined (_____); if judged to be only somewhat advantageous, dotted lines are shown (_ _ _ _ _), and if neither has a particular advantage over the other, no markings are used.

Item	TERNARY (MIT SYSTEM)	Item	WIDTH-MODULATED BINARY (HAMILTON-STD.)
1.	The error signal is sampled at a controlled, well-defined time, due to the synchronization. The error signal is sampled at a 9.6 kHz rate.	1.	The time of error signal sampling is determined by the level of the error signal. Hence, the error signal is not sampled at a well-defined time. The error signal is sampled at a 1 kHz rate.
2.	Torque is applied in coarsely quantized increment.	2.	Torque is applied in finely quantized increments.
3.	Data is obtained from an analog-to-digital converter which detects the magnitude of the error signal; hence, there is no direct connection between the data output and actual torque pulse. That is, the torque control circuits and the data output circuits are in parallel, but each of the circuits see the same error signal.	3.	Data is finely quantized and is directly determined by the torque pulse.
4.	Compensation is very simple and is applied only during the torque pulse. The compensation is connected in parallel with the error signal path.	4.	The compensation network is a complex active filter placed in series with the error signal path.

Item	TERNARY (MIT SYSTEM)	Item	WIDTH-MODULATED BINARY (HAMILTON-STD.)
5.	The error signal processing system is ac coupled and simple.	5.	Error signal must be rectified to obtain a dc signal for mixing with a ramp signal. The error signal processing system (ac amplifier, bandpass filter, rectifier, dc amplifier, compensator) is complex.
6.	There is a set-up time (6.5μsec) between interrogation of the error signal and torque command. Consequently, set-up switching transients in the Upper and Lower H-Switch cannot contaminate the system during the torque pulse.	6.	There is no set-up time to prohibit contamination of the system with switching transients. Consequently, the input stages of the error processing electronics must be carefully designed with special attention given to good common-mode rejection.
7.	The necessity for set-up time will probably limit interrogation frequency. Increasing interrogation frequency allows increase in data resolution.	7.	No set-up time requirement permits high data resolution.
8.	Since rise and fall times in the H-Switch are not determined entirely by the same mechanisms, a significant torque current pulse area error can occur due to changes in rise and/or fall times.	8.	By careful matching of certain sets of transistors in the H-Switch, both rise-time and fall-time errors in torque current pulse area can be compensated.
9.	Torque pulses are routed to either torquer or dummy load. Thus, torquer does not operate at constant input power; however, the dummy load can be placed near the torquer to give a nearly constant temperature profile.	9.	The H-Switch is driven continuously so that the torquer receives constant power.

Item	TERNARY (MIT SYSTEM)	Item	WIDTH-MODULATED BINARY (HAMILTON-STD.)
10.	Precision voltage reference (PVR) is switched for scale change. The required low-level voltage at low scale factor places a heavy stability burden on the comparison amplifier-PVR circuit.	10.	Reference resistors are switched instead of PVR for scale change. Thus, large PVR values can be used for high stability of comparison amplifier-PVR circuit.
11.	PVR switching is simple.	11.	Reference resistor switching is more involved due primarily to the necessity of making voltage offsets negligible.
12.	Pickoff is an inductive transducer (microsyn) with resolution of approximately 3.75 volts/rad.	12.	Pickoff is a capacitive bridge with resolution of approximately 260 volts/rad.
13.	Electronic White noise is determined by the preamplifier, and is about 0.06 rms arc-sec. This value could, however, be made comparable to the Hamilton-Std. design by using a more sensitive pickoff.	13.	Electronic White noise is about 0.001 rms arc-sec.
14.	Logic block complexity is comparable to that of the binary system. The mode determination logic is much simpler than that of the binary system, but the need for a staircase generator for the A-to-D Converter increases the overall logic complexity.	14.	Overall logic block complexity is comparable to that of the ternary system.
15.	Logic is low-power.	15.	Logic is standard but could possibly be designed with low-power components.

Item	TERNARY (MIT SYSTEM)	WIDTH-MODULATED BINARY (HAMILTON-STD.)
16.	Common-mode rejection in error signal processor is probably adequate.	Common-mode rejection is very high in error signal processor due to a specially designed discrete component preamplifier.
17.	The error signal is 9.6 kHz and could therefore be contaminated with low-frequency electronic or microphonic noise.	The ac error signal is 50 kHz and filtered by a bandpass filter before rectification. Thus, error signal should not be contaminated by low-frequency electronic or microphonic noise.

References

1. Digital Pulse Torque Electronics Development, Final Report, NASA Contract No. NAS9-9950, September 21, 1970.

2. Howatt, John R., A Gyroscope Bilevel Compensated Pulse Torque Rebalance Loop, NASA Contract No. NAS9-6823, Draper Laboratory, Massachusetts Institute of Technology, 1970.

3. Lawrence, A.W., et al, The Design of an Advanced Strapdown Gyroscope, NASA Contract No. NAS12-687, Hamilton Standard System Center, February 15, 1970.

4. Dual Scale Factor-Digital Control Electronics, Hamilton-Standard Drawing No. D-73030-31268, February 1970.

5. Strapdown Gyro Pulse Torque Servo Amplifier, Hamilton Standard Drawing No. J-73030-31283, February 1970.

6. Lory, C.B., Compensation of Pulse-Rebalanced Inertial Instruments, M.S. Thesis, Massachusetts Institute of Technology Instrumentation Laboratory, January 1968.

CHAPTER 6

PROBLEMS FOR FURTHER STUDY

Continued effort is needed to further develop the technology for the high reliability strapdown systems using TDF gyros. In particular, the following activities are recommended:

1. Development of optimum redundancy configurations for systems using more than six gyros.
2. Analysis of the system performance of the rebalance loops of a TDF sensor.
3. Further development of the sensor performance management concept to see if any more sophisticated detection and identification schemes can be employed to improve the overall system performance.

In the area of rebalance electronics, more work needs to be done to arrive at a design which is acceptable for NASA's applications. The following activities are desired.

1. Completion of the evaluation of MIT's and Hamilton Standard's electronic designs.
2. With the help of the background gained by evaluating the above designs, develop a better design of the rebalance electronic circuit.
3. Review of all applicable technology in the area of pulse rebalance electronics.

At present, various concepts are available for using SDF gyros as strapdown sensors. A study and evaluation effort is needed to extract and modify the best concepts so they can be incorporated together to form the best overall system. The following questions need to be answered.

1. Which gives a better system performance between the binary and the ternary pulsing concepts?

2. Among the known concepts of failure detection and faulty sensor identification, which one is the best?
3. What are the optimum sensor arrangements when more than six SDF sensors are used?
4. Can any better concepts be developed?